

Optimal gateway trajectory design for Earth-to-Mars missions

Master Thesis

Jasper Veen

July 19, 2021

Optimal gateway trajectory design for Earth-to-Mars missions

Master Thesis

by

Jasper Veen
July 19, 2021

to obtain the degree of Master of Science
at Delft University of Technology
to be publicly defended on Tuesday 31st of August at 14:30

Cover image: NASA Lunar gateway taken from the Lockheed Martin webpage titled *Moon to Mars* [1]

Student number:	4391829	
Project duration:	January 2021 – August 2021	
Chair:	Prof. dr. ir. P.N.A.M. Visser,	TU Delft
External examiner:	Ir. B.T.C. Zandbergen,	TU Delft
Supervisor:	Ir. R. Noomen,	TU Delft

An electronic version of this thesis report is publicly available at
<https://repository.tudelft.nl/>

Abstract

Half a decade after the original Space Age, we are at the dawn of another exciting period in spaceflight, already dubbed 'The New Space Age'. Fuelled by commercial interest and rapid technological improvements, the coming two decades are expected to have humans return to the Lunar surface and possibly set foot on Mars for the very first time. The gateway concept is likely to play a significant role in these missions. A gateway is a man-made structure in space that functions as an intermediate station in an interplanetary transfer. NASA's Artemis program relies on a gateway in an Halo orbit around the Earth-Moon L2 Lagrange point to facilitate sustainable Moon missions. This thesis will contain an extensive feasibility study into the application of the gateway concept to Earth-to-Mars travel. At the end of this work, an optimal trajectory design for a gateway concept that supports efficient and practical (crew) transportation from Earth to Mars will be presented.

The research will regard three distinct gateway trajectory design aspects: The gateway location, the gateway orbit and the transfers supported by the gateway. These three aspects can be combined to form a large number of different gateway trajectory designs. A total of three analyses were performed. In these analyses, the performance of the different gateway designs was researched. The goal of the first two analyses, Analysis A and Analysis B, was to investigate a specific set of design aspects, evaluate and compare the designs' performance and select a subset of design options to further investigate in the next analysis. As a result, Analysis C was able to perform a detailed study into a small number of designs and select a single optimal design.

Two types of gateway locations were identified: gateways orbiting a central celestial body and gateways in the vicinity of a Lagrange point. Analysis A focused on the Lagrange-point gateways only, so that the stationary-gateway assumption could be made. It was concluded that the equilateral Lagrange points are not suitable gateway locations. Additionally, it was determined that the remaining two analyses should focus on impulsive thrust transfers rather than their continuous thrust equivalent.

As a result, Analysis B could focus on a set of specific transfer trajectories and a selection of only seven gateway locations (both central-body and Lagrange-point locations). By modelling the gateway orbits and optimizing for ΔV requirements, it was found that the gateway orbit has a significant effect on the performance of the gateway concept. Both Halo orbits and vertical-Lyapunov orbits proved suitable gateway orbits for gateways stationed at the Lagrange points. Although central-body gateways significantly underperformed Lagrange-point gateways, a gateway orbiting the Moon at a high altitude was selected together with four Lagrange-point gateway designs.

Analysis C evaluated the consistency of the remaining five designs and investigated the TOF characteristics of the transfers supported by these gateways. By splitting a synodic year into ten separate launch windows and optimizing transfer trajectories for each, it was found that the Lagrange-point gateway designs allowed for more frequent travel from Earth to Mars than the gateway in Lunar orbit. Subsequently, it was found that a gateway at the Earth-Moon L1 location supports a better trade-off between TOF and ΔV compared to one at the Sun-Earth L2 point.

Through these three analysis, it was found that a gateway placed in a large Halo orbit at the Earth-Moon L1 point is the optimal gateway trajectory design for future Earth-to-Mars gateway missions. This design is capable of supporting multiple suitable transfer trajectories, of which the *EdG1 x G1mEM* is most efficient. The minimum ΔV transfer solution between Earth and Mars orbit in the synodic period starting January 1st 2033 is 5.99 km/s, but this would require a long TOF of 386 days. A TOF of 300 days is possible for a ΔV of 6.41 km/s, 250 days for a ΔV of 6.82 km/s and 200 days for a ΔV of 7.26 km/s. This gateway trajectory design scored good on consistency; allowing a transfer below a ΔV of 7km/s in five of the ten launch windows in which the synodic period was split.

A mission using this optimal gateway design was compared to a direct transfer between Earth and Mars (*EM*) and a flyby mission (*EmEM*), both traditional missions without gateway concepts. It was found that the inclusion of an intermediate gateway in the mission design both adds to the ΔV requirements and to the flight duration. The difference is a little over 1 km/s in ΔV for TOFs under 200 days and less than 0.2 km/s for a TOF of roughly a year. Mission planners will have to decide whether these differences are justified by the gateway concept's benefits, such as its function as a logistics hub in space and its ability to facilitate transfers between spacecraft.

Preface

The work that lies before you marks the end of my time as a student. With the completion of this thesis, I will be graduating from the TU Delft. Milestones such as this one evoke a feeling of pride and accomplishment. After seven months of hard work at the end of seven years of being a student, it is only natural that you feel content and satisfied with yourself. However, I am careful not to attribute this accomplishment to myself alone, for I have been lucky all my life. I would like to share my favourite metaphor, which has helped me to better understand the extent of my luck:

Anyone that has ever ridden their bike when its windy outside knows that riding in the direction of the wind instead of against it makes all the difference. Riding with the wind will let you go fast without putting in any effort, whilst you will work up a sweat riding against the wind without feeling like you are progressing at all. As a result, you are very aware of the wind when it is opposing you. However, it is easy to underestimate the effect of the wind when it is in your favour and attribute the extra speed to yourself.

To me, this metaphor describes the role that luck can play in life. When things go right, it is hard to see and acknowledge where you have been lucky. I have recently realized that I have been riding comfortably with the wind for my whole life. I would, therefore, like to thank some people that have blown the wind in my back or have shielded me from it during my life and, more specifically, during the last seven months of working on my thesis.

Starting with my parents, who have created the circumstances for me to be who I want and do what I want, with my happiness as their only interest. They have been the biggest source of wind in my back. I am grateful for my sister, Anabel, with whom I navigated through different kinds of weather. No matter the wind direction, I know she and I will always make a great team. I was lucky to have my girlfriend, Eleonor, by my side. After a turbulent period, she truly proved to be my shelter from the wind. Lastly, I would like to thank my supervisor Ron. In our weekly meetings we would often discuss actualities, sports and his cats before we'd realize the meeting was half-way done and we hadn't discussed any of the thesis content yet. Ron's personal touch and his warm involvement took away any stress before it could build up and made this thesis into a breezy experience. Thank you all!

Jasper Veen
July 19, 2021
Rotterdam

Contents

1	Introduction	1
I	Background	3
2	Research overview	5
3	Fundamentals	9
3.1	Gateway	9
3.1.1	Concept definition	9
3.1.2	Benefits and drawbacks	10
3.2	Mars missions	11
3.2.1	Basics.	11
3.2.2	Past and future Mars missions.	12
3.2.3	Future technologies	13
3.3	Astrodynamics.	14
3.3.1	Lagrange-point locations.	14
3.3.2	Orbits.	18
3.3.3	Transfers	22
4	Design considerations	31
4.1	Mission definition	31
4.2	Mission evaluation criteria	32
4.3	Mission characteristics	32
4.4	Gateway locations	34
4.4.1	Celestial body	34
4.4.2	Lagrange points	35
4.5	Gateway orbits.	36
4.5.1	Central orbit	36
4.5.2	Lagrange-point orbits	37
4.6	Transfers.	39
4.6.1	Impulsive transfers	39
4.6.2	Continuous-thrust transfers	39
II	Analyses	41
5	Analysis A - First filter	43
5.1	Introduction	43
5.2	Analysis methods	43
5.2.1	General method	44
5.2.2	IT method	46
5.2.3	CT method	48
5.2.4	Optimization method.	50
5.3	Verification.	51
5.3.1	Gateway locations	51
5.3.2	Impulsive-thrust transfers.	53
5.3.3	Continuous-thrust transfers	54

5.4	Results	55
5.4.1	G1 (Em-L1)	56
5.4.2	G2 (Em-L2)	57
5.4.3	G3 (Em-L4)	58
5.4.4	G4 (Em-L5)	59
5.4.5	G5 (SE-L2)	60
5.4.6	G6 (SE-L1)	61
5.4.7	Continuous-thrust results	62
5.5	Discussion	63
5.5.1	Impulsive-thrust	63
5.5.2	Continuous-thrust	66
5.6	Conclusions	67
5.6.1	Filtering of gateway locations	67
5.6.2	Selection of trajectories	68
6	Analysis B - Detailed Analysis	69
6.1	Introduction	69
6.2	Methodology	69
6.2.1	General methods	69
6.2.2	Gateway orbit model	71
6.2.3	Segment Timing Model	73
6.2.4	Optimization algorithm	74
6.3	Verification	75
6.3.1	LPO library	75
6.3.2	Central-orbit library	76
6.4	Results	76
6.4.1	G1 (Em-L1)	77
6.4.2	G2 (Em-L2)	78
6.4.3	G5 (SE-L2)	79
6.4.4	G6 (SM-L1)	80
6.4.5	G7 (Earth orbit)	81
6.4.6	G8 (Lunar orbit)	81
6.4.7	G9 (Mars orbit)	82
6.5	Discussion	83
6.6	Conclusions	91
6.6.1	Selecting gateway locations	91
6.6.2	Gateway orbit	92
6.6.3	Transfer options	92
6.6.4	Additional findings	93
7	Analysis C - Final selection	95
7.1	Analysis introduction	95
7.2	Methodology	95
7.2.1	General method	96
7.2.2	Analysis C-I: Consistency testing	97
7.2.3	Analysis C-II: Testing TOF characteristics	97
7.3	Verification	98
7.4	Results	99
7.4.1	G1 (Em-L1) - EdG1 x G1mEM	99
7.4.2	G1 (Em-L1) - EmG1 x G1mEM	100
7.4.3	G5 (SE-L2) - EdG5 x G5mEdEM	102
7.4.4	G5 (SE-L2) - EdG5 x G5mEM	103
7.4.5	G8 (Lunar orbit) - EdG8 x G8dM	105
7.5	Discussion	107
7.5.1	Analysis C-I	107
7.5.2	Analysis C-II	108

7.6	Conclusions	110
7.6.1	Single gateway trajectory design proposal.	110
7.7	Additional findings	110
III	Conclusions	111
8	Discussion - evaluation of optimal gateway trajectory design	113
8.1	Comparison to direct transfer (EM)	113
8.1.1	Best ΔV transfer	113
8.1.2	TOF characteristics	114
8.1.3	Consistency results.	115
8.2	Comparison to flyby transfer (EmEM)	115
8.2.1	Best ΔV transfer	115
8.2.2	TOF characteristics	116
8.2.3	Consistency results.	116
8.3	Evaluation of gateway concept	117
9	Conclusions	119
9.1	Answer to the research question	119
9.2	Main takeaways for gateway trajectory design	120
10	Recommendations for further research	121
A	All transfer trajectory options	129
B	Orbit ID mapping	131
C	Failed attempt at multi-objective optimization	135
C.1	Methodology	135
C.2	Results	137

Glossary

1DSM	Transfer using a single DSM.
AU	Astronomical Unit.
CB	Central-Body.
CR3BP	Circular-Restricted Three Body Problem.
CT	Continuous Thrust.
DC	Differential Correction.
DE	Differential Evolution.
DSM	Deep Space Manoeuvre.
DT	Direct transfer.
EG	Earth-to-Gateway (segment).
EOM	Equation Of Motion.
EP	Electric Propulsion.
ESA	European Space Agency.
GA	Genetic Algorithm.
GE	Gateway-to-Earth (segment).
GEO	Geostationary Earth Orbit.
GM	Gateway-to-Mars (segment).
GOM	Gateway Orbit Model.
GTOP	Global Trajectory Optimization Problems.
GW	Gateway (segment).
ISRU	In-Situ Resource Utilization.
ISS	International Space Station.
IT	Impulsive Thrust.
LEO	Low Earth Orbit.
LOAN	Longitude Of Ascending Node.
LP	Lagrange Point.
LPO	Lagrange Point Orbit.
MEO	Medium Earth Orbit.
MG	Mars-to-Gateway (segment).
MGA	Mars Gravity Area.
MGADSM	Multi-Gravity-Assist transfer using one DSM per leg.
MSL	Mars Science Laboratory.
NASA	National Aeronautics and Space Administration.
NC	Numerical Continuation.
NSGA	Nondominated Sorting Genetic Algorithm.
OCF	Orbit Cost Function.

PSO	Particle Swarm Optimization.
SEP	Solar Electric Propulsion.
STM	Segment Timing Model.
TOF	Time Of Flight.
TORA	Third-Order Richardson Approximation.
TRL	Technology Readiness Level.

List of Symbols

Greek symbols

α	Right ascension angle	[deg]
ΔV	Change in the spacecraft velocity	[m/s]
δ	Declination angle	[deg]
ϵ	Azimuth angle	[deg]
ϵ	Elevation angle	[deg]
ϵ_{req}	Desired maximum local truncation error	[m]
μ	Gravitational parameter	[m ³ /s ²]
Ω	Longitude of the ascending node	[deg]
ω	Argument of periapsis	[deg]
Φ	Terminal cost function	[m]
Ψ	Azimuth angle	[deg]
ρ	Density	[kg/m ³]
θ	True anomaly	[deg]
θ_t	Transfer angle	[deg]

Roman symbols

A	Area	[m ²]
a	Semi-major axis	[m]
B	Impact parameter	[km]
C_D	Drag coefficient	[-]
C_3	Characteristic energy	[km/s]
e	Eccentricity of orbit	[-]
E_t	Eccentric anomaly	[deg]
F	Force	[N]
G	Universal gravitational constant	6.67384×10^{-11} [N · m ² /kg ²]
g	Gravitational acceleration	[m/s ²]
g_0	Gravitational acceleration at Earth's surface	9.81, [m/s ²]
H	Hamiltonian	[-]
i	Inclination of orbit	[deg]
I_{sp}	Specific impulse	[s]

L	Running cost function	[–]
r	Radius	[m]
Sv	Sievert	[Sv]
V_{∞}	Hyperbolic excess velocity	[km/s]
V_{esc}	Escape velocity velocity	[km/s]
W	Power	[J/s]

1

Introduction

Ever since the Apollo 17 mission of 1972 left the last footprints on the Moon, humans have not left our front yard in space that is called Low-Earth Orbit (LEO). Although many significant milestones have been achieved by the National Aeronautics and Space Administration (NASA) and her partners in the fifty years that followed, the excitement and the astonishment of the space age era has so far been unrivalled. This, however, might soon change. Already in 2013, then NASA administrator Charles Bolden said: "Interest in sending people to Mars has never been higher" [2]. The increase in popular interest is matched by an increase in commercial interest in space. Collaboration between the traditional space agencies, such as NASA and the European Space Agency (ESA), and commercial space companies, such as SpaceX, has resulted in accelerating technological developments. As a result, the Moon is back on the table and this time it might serve as an appetizer for the highly anticipated Mars missions.

NASA is planning to send crew back to the Lunar surface as early as the mid-2020s. These Lunar missions will be vastly different from those over half a century ago, due to the incorporation of a new concept in the mission design: the Gateway concept. Much like one takes a bus to a station before boarding a train, the gateway will function as an intermediate station between two locations in space. In the case of the NASA gateway, this station is located close to the Moon to facilitate Lunar surface landings and scientific research focused on the Lunar environment. An artist impression of this Lunar gateway is depicted in Figure 1.1.

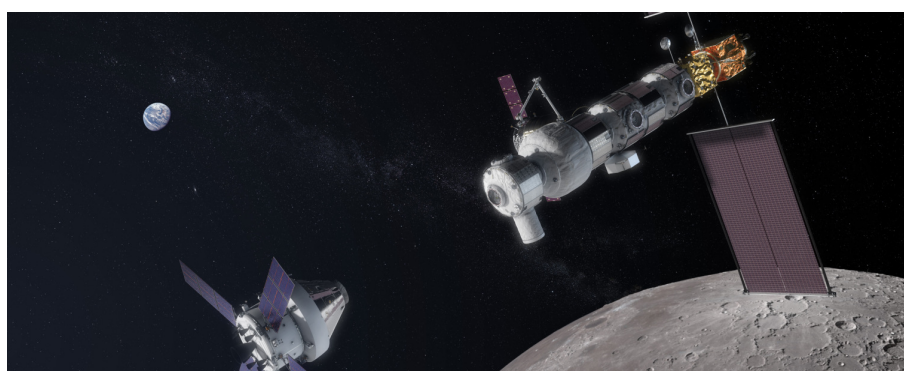


Figure 1.1: Artist impression of the NASA Lunar gateway [3].

In the future, NASA plans to utilize the existing Lunar gateway for missions to Mars. The design of this gateway, however, was optimized for Lunar missions. This sparked the following question: What if, in the foreseeable future, focus shifts away from the Moon and towards Mars? Would the proposed NASA Lunar gateway then still be the most suitable gateway design to support crew transportation between Earth and Mars? In the literature study that was conducted prior to this thesis work [4], no relevant research on the application of the gateway concept to Mars missions was found. Therefore, it was decided to dedicate the thesis work to investigating the applicability of the gateway concept to Earth-to-Mars transfers. The

following paragraph will introduce the research objective and the research questions. The research objective was formulated after having identified the research gap in the literature study [4]. It was surprising to find that little to no research could be found on the gateway concept. Individual elements of gateway design, such as Lagrange-point orbits or interplanetary transfers, have been thoroughly researched and documented, but the theory has never been applied to the gateway concept itself, let alone to its application in Mars missions. This thesis therefore sets out to fill this gap by fulfilling the research objective below:

Research objective *Perform an extensive feasibility study into the application of the gateway concept to efficient and practical Earth-to-Mars travel. The aim of this study is to provide a starting point for scientists and mission designers interested in incorporating the gateway concept into future Mars missions.*

The research objective will be achieved by providing answers to a set of questions linked to a single overarching question. This main research question is defined as follows:

Research question *What is the optimal trajectory design for a gateway concept that supports efficient and practical (crew) transportation from Earth to Mars?*

It must be emphasized that in the context of this thesis work, 'gateway design' will refer to trajectory design and not hardware design. In this thesis report, the term 'gateway trajectory design' will often be abbreviated to 'gateway design' or 'design' without loss of any meaning. This will be elaborated on in Chapter 2 *Design Considerations*. The research question above will be answered by providing answers to the following sub-questions:

Sub-question A *What is/are the gateway location(s) of the optimal gateway design?*

Sub-question B *What is/are the gateway orbit(s) of the optimal gateway design?*

Sub-question C *What transfer trajectories should the optimal gateway design support?*

Sub-question D *How does the optimal gateway design compare to a direct transfer?*

By searching for optimal gateway trajectory designs, this thesis will provide insights into what factors influence gateway performance and how the performance is influenced by these factors exactly. After one or more optimal designs are found, the gateway concept can be evaluated by comparing its performance against a direct transfer benchmark. Once all the sub-questions have been answered, an answer to the main question can be formulated and the research objective will be achieved. The next paragraph will introduce how the structure of this report was influenced by the structure of the research questions.

The main body of the report is divided into three parts. Part I, called *Background*, provides the necessary background for Part II *Analyses*. Both parts consist of several chapters. The first chapter of Part I, Chapter 2 *Research Overview*, aims to create an understanding of the framework and the context in which the chapters and analyses that follow will fit. As a result, the theory that will be covered in Chapter 3 *Fundamentals* can be understood within this new understanding of the framework. In turn, the theoretical fundamentals discussed in this chapter will help in comprehending the considerations in Chapter 4 *Design Considerations*. These chapters will clearly define the scope for the analyses in Part II. Part II consists of three analyses, each described in an individual chapter. The purpose of each analysis will be explained in the next chapter. Each analysis has its own introduction, methodology, results, discussion and conclusion section. After all analyses have been discussed individually, Part III will discuss the findings of the entire research globally. In the three chapters comprising part III the most significant findings of this work will be presented and the report will be brought to a conclusion.

I

Background

2

Research overview

This thesis report is built out of a variety of different elements that are tied together in a web of sequential and theoretical dependencies. Although the structure and its links are well-understood by the author of this report, it might not be so obvious for those for whom this thesis report is the first encounter with this project and its topic. This chapter is therefore dedicated to creating an understanding of the framework and context in which the coming chapters and analyses will fit. To this extent, this chapter will restate the research objective and then systematically go over the chapters and elements of this thesis report and discuss how they contribute to this objective and how they are linked among each other. A schematic illustration is used to give a clear overview of the research conducted in this thesis.

In its core, this research is a feasibility study into the application of the gateway concept to Earth-to-Mars transportation. It will set out to create, evaluate and compare a large number of different gateway trajectory designs. In a prior literature study, no other work into gateway designs for Earth-to-Mars transportation was found. Therefore, the goal of this study is to provide a recommendation whether or not the gateway concept should be further researched in the context of Mars missions. In the case that it is found that the gateway concept does have potential, this research aims to provide direction into what an effective design should look like. Ideally, the main take-away of this thesis is the recommendation of a single gateway trajectory design that was proven most suitable in the analyses of this work.

To this extent, it is important to understand what is meant by a 'gateway trajectory design'. In the context of this work, the trajectory design of a gateway concept encompasses three things:

1. **Gateway location** - Where is the gateway located?
2. **Gateway orbit** - In what orbit should the gateway be placed?
3. **Transfer options** - What transfer options between Earth, the gateway and Mars should be supported by the gateway?

A trajectory design therefore focuses on the dynamics of the gateway concept and not on its hardware. In this thesis report, the term 'gateway trajectory design' will often be abbreviated to 'gateway design' or 'design' without loss of any meaning. Through combination of the above-listed three design aspects hundreds of gateway designs can be created. In order to provide a better understanding of the various possibilities for the interpretation of these three design aspects and how they might influence design performance, the research is initiated with a chapter on the theoretical foundation of the thesis work (Chapter 3 *Fundamentals*). This collection of theory serves the purpose of supporting the design considerations made in the following chapter, Chapter 4 *Design Considerations*. This chapter will clearly define the scope of the research of this thesis. It will, among other things, provide a mission definition for the gateway concept's application to the Mars mission, define its evaluation criteria and characteristics and define a framework for the interpretation of the gateway trajectory design aspects. In this chapter it will be argued that the gateway trajectory design can either be located at a Lagrange point or around a central celestial body. Accordingly, it will propose the considerations that should be taken into account when designing gateway orbits at these locations. Furthermore, it will be explained that two transfer options should be considered in this research based on impulsive thrust and continuous-thrust propulsion.

As a result, the total number of gateway locations will be brought down to nine locations: six Lagrange-point locations and three central body gateways. For each, a single orbit family is selected along with a list of transfer options. This theoretical scoping will lay the groundwork for the analyses that followed.

A total of three types of analyses will be performed. In these analyses, the performance of the different gateway trajectory designs will be researched. The goal of the first two analyses, Analysis A and Analysis B, is to investigate a specific set of design aspects, evaluate and compare the designs' performance and select a subset of designs to further investigate in the next analysis. As a result, Analysis C is able to perform a detailed study into a small number of designs. This will lead to the selection of a single gateway trajectory design. This filtering of a large number of gateway trajectory designs to the selection of a single design is illustrated in Figure 2.1.

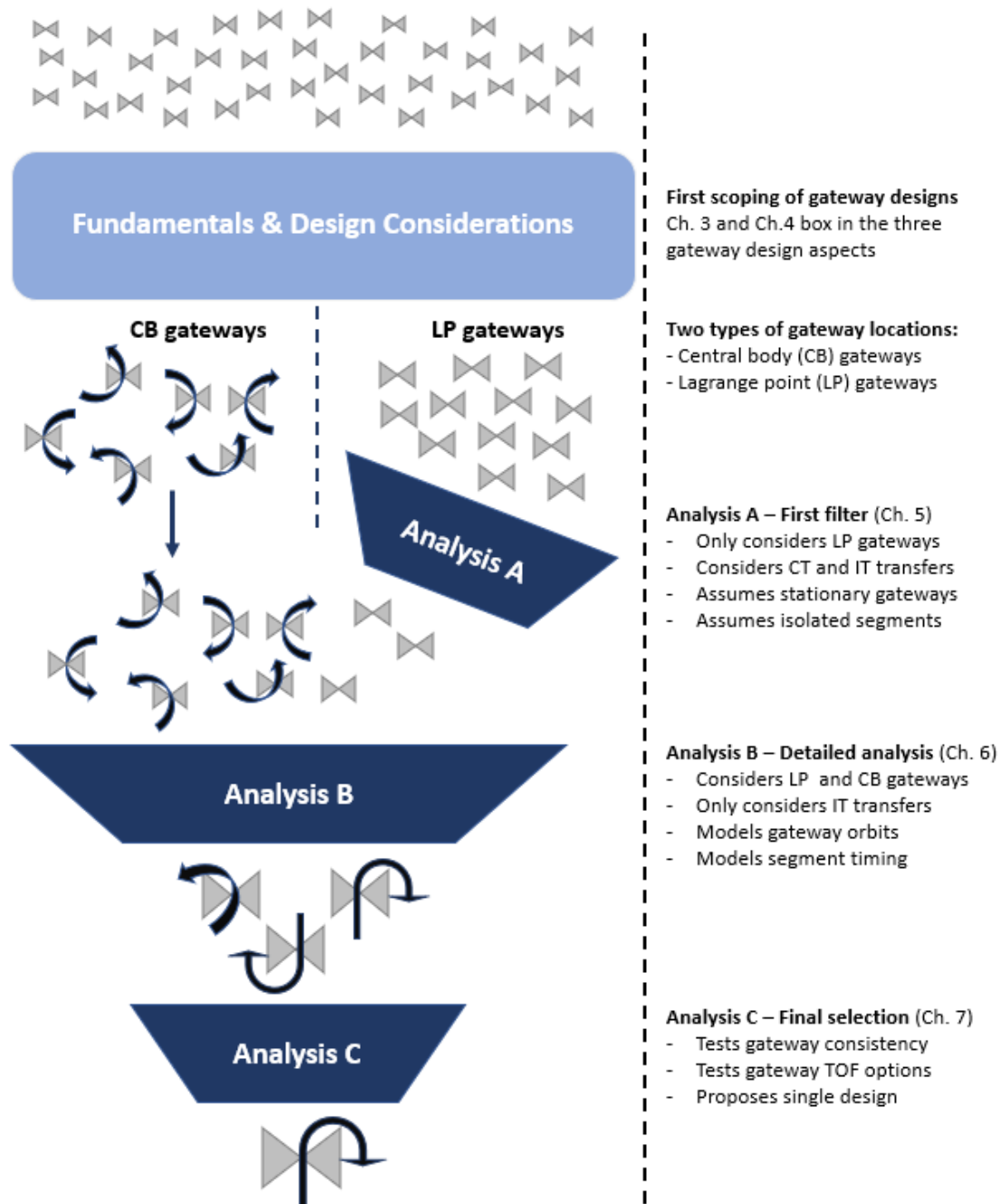


Figure 2.1: Schematic overview of the thesis research.

In this overview, a brief summary of each analysis is given. This paragraph will provide some more context to these analyses. As can be seen in Figure 2.1, Analysis A exclusively considers the Lagrange-point (LP) gateways. Since Analysis A assumes all gateways to be stationary, central-body (CB) gateways cannot be studied. CB gateways are by definition in orbit around the central-body. Analysis A is the only analysis that will consider continuous-thrust transfers. Enough insight into this transfer type will be created through this analysis, so that the subsequent analyses can focus on impulsive transfers exclusively. Analysis A will be able to filter out some LP gateway locations and transfer options, so that the scope for Analysis B can be narrowed. Analysis B will implement additional models to get rid of the simplifications and assumptions used in Analysis A. As a result, the CB gateways will now also be examined. Whereas Analysis A could only focus on the gateway location and on the transfer options, Analysis B will additionally search for gateway orbit solutions. As a result, Analysis B will produce a set of complete gateway trajectory designs that were selected because of their favourable ΔV transfer budgets. This set is then further studied in Analysis C. Whereas Analyses A and B focused on ΔV to evaluate the different designs, Analysis C will study two additional evaluation criteria: design consistency and TOF options. Analysis C will select a single gateway trajectory design.

All three analyses will be discussed in a stand-alone chapter. Each chapter will introduce the analysis, discuss its methodology, present and discuss its results and close with the conclusions of that analysis. After all analyses have been covered, a separate part (Part III) will discuss the main takeaways from the entire thesis work, present its conclusions and discuss recommendations for further research.

This chapter has shed light on the structure of the research conducted for this thesis. To further clarify this, each chapter will begin with an introduction that places the content of that chapter into the greater framework of this work. As will be evident when reading this report, the work performed in this thesis greatly benefits from work done in previous thesis works. If it were not for the work done by for instance Musegaas [5], Van der Ham [6], Melman [7] and Langemeijer [8], the goal set out in this thesis would never have been achievable within the seven-month period. These theses truly form the building blocks of this research, so that references to them will be found throughout the entire report.

3

Fundamentals

This chapter will lay the theoretical groundwork on which the next chapters will build. A reader that is familiar with interplanetary astrodynamics and mission design could consider skipping this chapter. Later sections will refer to the theory discussed here, so that the theoretical background can always be revisited.

This chapter has been structured in four sections, each discussing a distinct part of the theory used in this thesis. Section 3.1 will dive into what is understood by the gateway concept. The following section, Section 3.2, will lay out the very basics of Mars missions and discuss relevant prospects. Section 3.3 will finally cover the astrodynamics relevant to this thesis work.

3.1. Gateway

As the main focus of this thesis revolves around the concept of space gateways, it is important to clearly define this concept upfront. This will be done in the first subsection below. After this, the benefits of such a gateway can be put forward in the following section along with some potential drawbacks of using a gateway structure.

3.1.1. Concept definition

The concept of having (semi-)long term structures was the subject of academic and science-fiction writing long before NASA introduced its Lunar gateway plans. A variety of different terminology has been used in the past to refer to the concept, such as *Space hub* and *Spaceport*. In this thesis work, the word *gateway* will exclusively be used. Since no clear definition of the gateway concept can be found in literature, the definition used in this thesis was explicated in the literature study preceding this thesis work [4]. It can be found below:

A gateway is a man-made structure in space ...

- ... that is intended to be an intermediate station in an interplanetary transfer.
- ... that is not the transfer vehicle in the interplanetary transfer.
- ... that orbits a single celestial body or Lagrange point.
- ... that facilitates a crew transfer between two vehicles or the temporary accommodation of the crew before boarding the same vehicle by featuring an airlock.
- ... that is intended to be able to support a similar-style mission for multiple iterations and is therefore functional for a semi-long duration.

A space mission concept that is not in line with one or more of the points above, will not be classified as a gateway concept in this author's view. The exhaustiveness and exclusiveness of the definition can be validated by testing it against space structures that are similar but not the same as a gateway structure. A cyler spacecraft [9] is not a gateway since a cyler spacecraft would act as the transfer vehicle and as a

result orbits more than one celestial body. The SpaceX in-orbit tanker (discussed in Section 3.2) spaceship is not a gateway since it does not allow for temporary accommodation and is single-use. The ISS is not a gateway since it is not intended as an intermediate station in an interplanetary transfer. That being said, the concept definition does allow for a wide variety of different gateway designs. These can, for instance, vary in location, orbit and intended use. Apart from the NASA gateway concept, two commercial gateway proposals fit the definition. The Gateway Foundation's gateway, depicted in Figure 3.1, constitutes of a mega-structure in LEO [10]. The Gateway Earth plan [11] envisions two gateways, one in LEO and one in GEO.

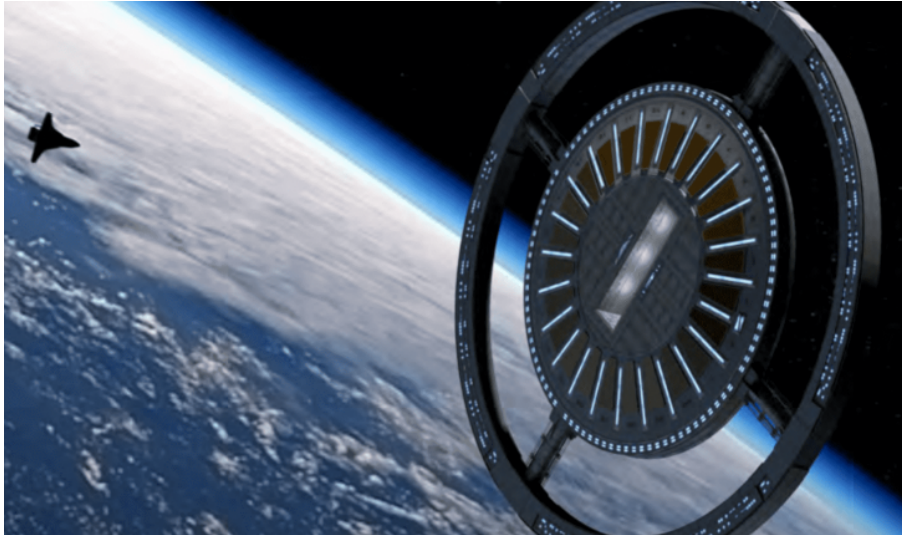


Figure 3.1: Render of what the proposed gateway would look like by The Gateway Foundation [10].

3.1.2. Benefits and drawbacks

The benefits and drawbacks of using a gateway structure in interplanetary space travel is a popular topic of discussion among academics and space enthusiasts. Some believe that a gateway is an important step in sustainable outer-space travel. Others advocate for direct transfers and believe the gateway concept is a waste of time and resources. The arguments of both sides have been studied and discussed into great depth in the literature study prior to this work [4]. A brief overview will be given below:

Benefits

- **Long-term characteristics** - Having existing infrastructure ensures some alleviation of the influence that politics, financing, public opinion and other factors have over decision-making in space.
- **Ability to transfer between spacecraft** - Different (reusable) spacecraft can be boarded for the different transfer segments.
- **Gateway can function as a hub** - Supplies, propellant and crew can arrive separately at the gateway before being integrated into one spacecraft.
- **Opening new transfer and return possibilities** - The gateway location might allow for a change in launch window and different transfer and return options. This will have to be researched further.
- **Contingency** - Interplanetary travel can be aborted at the gateway and a safe return can be guaranteed.
- **Position of gateway** - The position of the gateway could guarantee a continuous communication link between Earth and the destination planet. Research interests could also align with the gateway location.



Figure 3.2: The NASA lunar gateway concept functioning as a space hub [3].

Drawbacks

- **Time and costs** - Development of the gateway infrastructure are likely to be more time-consuming and expensive than development of direct transfer possibilities.
- **Environment** - Thermal, radiation and resource management is simpler on a surface than in space.

This analysis must be regarded as a preliminary analysis. It lists a number of benefits and drawbacks, but is not exhaustive and does not include any sound engineering data to support either side. This thesis work therefore sets out to provide scientific results that can be used in future discussions on the merits or shortcomings of the gateway concept.

3.2. Mars missions

The intended application of the above-discussed gateway concept is to support transportation from Earth to Mars. In order to get an understanding of the basics of Mars missions, this section will start with an overview of important orbital parameters that govern transfers between the two planets. Subsequently, a survey of a number of previous and future Mars missions is given to provide some insight into the current state affairs. Finally, this section will end with a discussion on enabling technology that will be available to Mars missions in the future.

3.2.1. Basics

Table 3.1 features the most relevant orbital parameters of the Earth-Mars system. It is important to highlight the physical meaning of some of these numbers. Firstly, as Mars orbits the Sun at a larger radius than Earth does, a spacecraft travelling from Earth to Mars needs to increase its specific energy, yet decrease its velocity about the Sun. Furthermore, Mars' orbit is slightly inclined with respect to Earth's orbital plane. As a result, a spacecraft will have to make an out-of-plane manoeuvre to arrive at Mars. Lastly, due to the difference in orbital period between the two planets, two successive identical configurations of the planets as seen from Earth, occur every 780 days. This period is called the synodic period. When being more precise by taking the eccentricity difference into account, this period is 15 years. This cycle gives rise to less and more favourable transfer windows. The next most optimal launch window will be in 2033 [12]. The last row lists the velocity an orbiter would have when orbiting the focus planet at an altitude of 250 kilometres.

Characteristic	Earth	Mars
Avg. distance to Sun [AU]	1	1.52
Avg. distance to Sun [10^6 km]	149.6	227.4
Eccentricity e	0.0167	0.0933
Inclination i [deg]	0.0	1.85
Orbital velocity [km/s^2]	29.78	24.07
Orbital period [Earth days]	365.26	686.98
Synodic period [Earth days]	780	
Synodic period [Earth years]	2.143	
Mass [10^{23} kg]	59.7	6.42
Planet radius [km]	6371	3390
Surface gravity [m/s^2]	9.81	3.71
Satellite velocity [km/s^2]	7.75	10.85

Table 3.1: Relevant orbital parameters of the Earth-Mars system [13].

3.2.2. Past and future Mars missions

Since the 1960's, 56 Mars missions have been launched of which 26 have been successful [14]. In general, Mars missions can be divided into three categories: flyby missions, orbiter missions and surface missions. Of these 26 missions, 12 missions landed on Mars. Since the purpose of this thesis is to acquire a better understanding of the role a gateway could play in future (crewed) Mars surface missions, it makes sense to go over a few significant past and future Mars robotic surface missions.

Table 3.2 lists four important Mars surface missions. All four have used a Type-I transfer from Earth to Mars, which is the category of all transfers that are faster than the classical, minimum-energy Hohmann transfer. An example of such a transfer is depicted in Figure 3.3.

Mission	Launch year	Trajectory	TOF [days]	Spacecraft Mass [kg]
Spirit	2003	Type-I	208	1062
Opportunity	2003	Type-I	201	1062
Curiosity (MSL)	2011	Type-I	254	3893
Insight	2018	Type-I	205	694

Table 3.2: Past Mars surface missions.

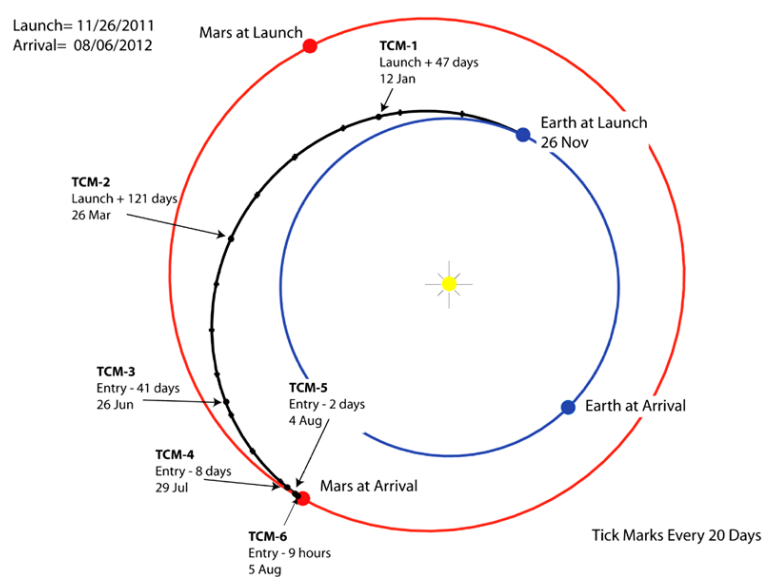


Figure 3.3: Earth-Mars Transfer Trajectory for the Mars Science Laboratory (MSL) [15].

Mars surface missions featuring robotic rovers, such as the missions in Table 3.2, will continue to play a role of importance in the future with missions such as ExoMars already planned. More relevant to this thesis are the plans to bring humans to Mars. Two of these plans should be studied: SpaceX's proposal for interplanetary travel using the Starship spacecraft and NASA's concept that uses the lunar gateway as the departure location for Mars transfers. No detailed proposals are available, so both can only be briefly discussed below.

SpaceX is currently developing a new launch system that will be the largest and most powerful rocket ever built. The spacecraft, dubbed Starship, will be launched into LEO, where it will be refueled in orbit by a up to three propellant tankers using milli-g accelerations. This means that small impulsive thrusts, in the order of one thousand of the gravitational attraction, will be used to guide the propellant from the tanker vehicle to the transfer vehicle. SpaceX claims this will add up to six km per second of ΔV budget to be used beyond LEO [16]. The concept's timeline seems to account for the synodic period. It seems likely that the Starship is envisioned to fly a Type-I transfer between Earth and Mars. The mission architecture is depicted in Figure 3.4 below, which was taken from the SpaceX Starship update slide deck [17].

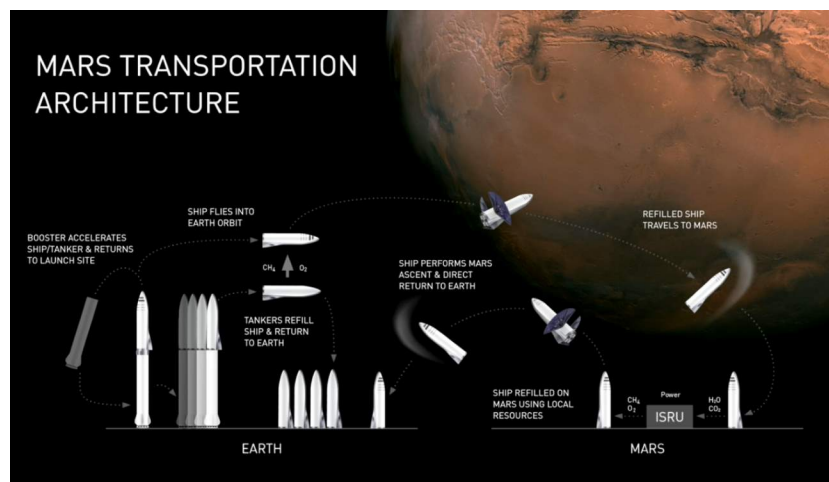


Figure 3.4: Mars Transportation Architecture by SpaceX [17].

No official plans or concepts have been published by NASA regarding future manned Mars missions. However, some of NASA's mission considerations are available [18]. High-power Solar Electric Propulsion (SEP) is regarded as one of the key enablers for its pioneering mission architecture. By harnessing the Sun's energy to accelerate ionized propellant to extremely high speeds, this propulsion method is capable of producing low levels of thrust for long periods of time (months to years). This enables two types of mission architectures that NASA is currently researching. Both architectures involve so-called split missions, which means that essential cargo is first pre-positioned in Mars orbit using SEP tugs. The two mission architectures differ in the use of pre-positioned chemical stages in Martian orbit. One of the missions uses a fully-SEP transfer vehicle, which rendezvous with a lander spacecraft and the chemical return stages in Martian orbit before landing on the red planet. The other mission architecture uses a hybrid transfer spacecraft, using both electric and chemical propulsion, which means the mission does not have to rely on the chemical return stages or lander spacecraft to be pre-positioned in Martian orbit. NASA documentation [19] suggests that crewed missions are planned to depart from and return to the Lunar Gateway using the reusable Deep Space Transport, which is the name of the proposed SEP hybrid tug. No more information is available at the time of writing.

3.2.3. Future technologies

The literature study performed prior to the thesis work [4] contains an in-depth survey of technologies that have the potential of playing a significant role in future Mars missions. The most important findings will be presented here. Readers interested in the theoretical background of the findings presented are referred to said literature study. The enabling technologies can be split into two categories: propulsion technologies and non-propulsion technologies. Both will be covered separately.

Propulsion systems

Three types of innovative propulsion systems are being developed: nuclear propulsion, electric propulsion and solar sailing. Solar sailing will not be useful for crewed transport in the near future, since the amount of mass needed to be transported in crewed missions is simply too high to be propelled using solar sailing technology. Nuclear propulsion systems, which are systems that produce propulsive force through nuclear processes, could play an important role of importance in the future. Two propulsion systems, different in the nuclear process they harness, seem to have the most potential: those based on nuclear fission and those based on nuclear fusion. Their potential and availability are featured in Table 3.3 below this section. If nuclear propulsion can be developed so that it can produce continuous-thrust for long time periods, it will unlock a wide variety of interplanetary transfer options.

Electric propulsive (EP) systems have been under development ever since the 1960's. However, recent breakthroughs on Hall thrusters have dramatically increased EP's potential for interplanetary missions. The information in Table 3.3 is based on the performance of the X3 Hall thruster developed by the University of Michigan and tested in October 2017 [20].

Technology	Availability	Pot. Exhaust velocity [km/s]	Pot. Thrust [kN]
Nuclear fission	early 2030s	8 - 70	1 - 1000
Nuclear fusion	late 2030s	70 - 6000	1 - 1000
Hall Electric Propulsion	early 2030s	10 - 50	~0.01

Table 3.3: Overview of future technologies with the potential to be used in future Mars missions.

Non-propulsion systems

Two technologies that do not involve ways of propulsion are important to mention: in-orbit refuelling and In-Situ Resource Utilization (ISRU). In a NASA article dated 2013 [21], it is stated that the TRL of in-orbit refuelling was raised to level 6. In July 2019, NASA announced that it would cooperate with SpaceX to develop in-orbit refuelling techniques [22]. It is therefore expected that the transfer of cryogenic (extremely low temperature) propellants in the low-gravity environment of deep space will be possible in the early 2030s. This would increase the ΔV budget of Mars missions drastically, opening up more transfer possibilities.

A different technique that also improves the ΔV budget, albeit mainly for return flights, is called ISRU. The most significant focus of ISRU research right now is harvesting propellants from Mars resources. Having such technology in place would allow interplanetary spacecraft to only carry the propellant needed for the inbound trip and not for the outbound trip. Currently, Mars Rover Perseverance carries the MOXIE payload [23]. This experiment will investigate the interaction between the ISRU system and the Mars environment.

3.3. Astrodynamics

The work done for this thesis has relied on a wide variety of different theory and concepts from the field of astrodynamics. The concepts used range from the quite simple, such as point-mass gravitational attraction, to extraordinarily complex, such as the Richardson third-order approximation used in Lagrange-point Orbit (LPO) generation. This section will only discuss the theory and concepts that tend to lie on the more complex side of the scale. For a more thorough description of all the astrodynamical concepts at the base of this thesis work, the reader is referred to the literature study supporting this thesis work [4] and the astrodynamics textbook written by Wakker [24].

The matter that will be discussed can be divided into three categories. First, the physics behind determining the locations of the Lagrange points will be covered. Subsequently, all relevant theory regarding orbits will be discussed. Finally, impulsive and continuous trajectory modelling methods considered in this research will be detailed.

3.3.1. Lagrange-point locations

Lagrange points are special points in space that could prove favourable gateway locations. This section will introduce the physics needed to find the locations of these points in the circular-restricted three-body problem (CR3BP) frame first. Afterwards, the frame transformation needed to denote these locations using cartesian coordinates with respect to a central origin is put forward.

Lagrange points in CR3BP frame

Lagrange points exist in three-body systems. Three-body systems comprise out of three bodies that undergo motion as a result of their mutual gravitational attraction. In interplanetary space travel, a spacecraft at some stage in its transfer is influenced by the gravitational attraction of the Sun and the Earth, for example. Interestingly, no analytical solution exists to describe the motion of the bodies in the three-body problem. However, a solution does exist under a set of specific assumptions. This simplified problem is referred to as the Circular-Restricted Three-Body Problem (CR3BP). It is based on the following assumptions:

- The mass of the primary (P1) and secondary (P2) is much larger than that of the third body (P3). As a result, the third body is influenced by the gravitational attraction of P1 and P2, but not the other way around.
- Bodies P1 and P2 move in strictly circular orbits about their collective barycenter.

These assumptions give rise to a special frame called the CR3BP frame, which is depicted in Figure 3.5 for the Sun-Earth system.

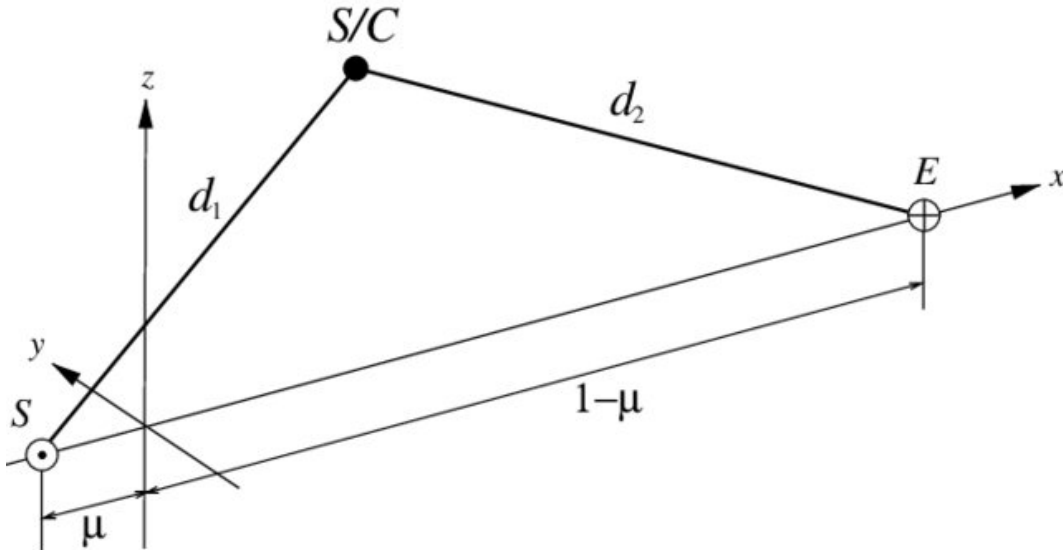


Figure 3.5: frame for the Sun-Earth three-body system [25].

This frame is defined as follows:

- **Origin** - The origin of the frame is placed in the barycenter of P1 and P2.
- **X-axis** - Along the line connecting P1 and P2. Positive in the direction of P1 towards P2.
- **Z-axis** - Along the angular momentum vector.
- **Y-axis** - Lies in the orbital plane, completing the right-hand system.

The parameter μ , seen in Figure 3.5, is the dimensionless mass ratio of P1 and P2:

$$\mu = \frac{m_2}{m_1 + m_2} \quad (3.1)$$

Using μ , the x-component of the position for P1 and P2 is $-\mu$ and $(1-\mu)$ respectively. Now that the parameterization and the frame has been laid out, the potential energy of the third body can be expressed as follows:

$$U = \frac{1}{2}(x^2 + y^2 + z^2) + \frac{1-\mu}{d_1} + \frac{\mu}{d_2} \quad (3.2)$$

where the first term represents the centrifugal force of the third body and the second and third term represent the contributions of the gravitational forces with respect to P1 and P2, respectively. A contour plot of this potential can be found in Figure 3.6.

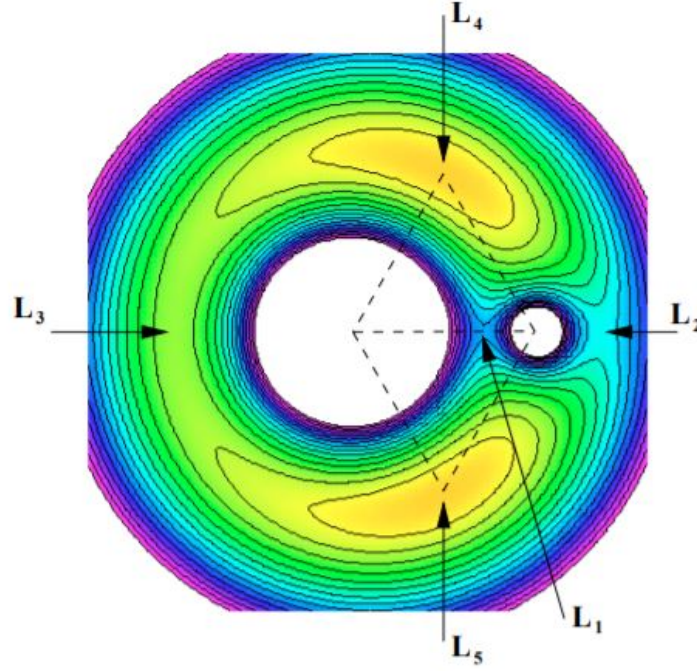


Figure 3.6: Contour plot of the potential expressed by equation 3.2 in the CR3BP [26].

Five points have been labelled L1 to L5 in Figure 3.6. These are the Lagrange points. At these locations, the derivatives of the potential with respect to x , y and z are zero: $\frac{\partial U}{\partial x} = \frac{\partial U}{\partial y} = \frac{\partial U}{\partial z} = 0$. Body P3 will as a result be stationary in the CR3BP frame when placed at these special locations. Three Lagrange points can be found in line with P1 and P2. These are the so-called collinear Lagrange points. The other two, L4 and L5, are at the apex of the equilateral triangles that have the bodies P1 and P2 at their vertices. These are called the equilateral Lagrange points. The collinear Lagrange points are unstable, whereas the equilateral points are dynamically stable.

The position of the Lagrange points in the CR3BP frame can be found by solving the systems of equation below. These follow from equating the equations of motion to zero, since \ddot{x} , \ddot{y} and \ddot{z} are zero at the Lagrange points. The equations of motion in the CR3BP will be listed later in this section.

$$\begin{aligned} x - \left(\frac{1-\mu}{d_1^3} \right) (\mu + x) + \frac{\mu}{d_2^3} (1 - \mu - x) &= 0 \\ y \left(1 - \frac{1-\mu}{d_1^3} - \frac{\mu}{d_2^3} \right) &= 0 \\ z \left(\frac{1-\mu}{d_1^3} + \frac{\mu}{d_2^3} \right) &= 0 \end{aligned} \quad (3.3)$$

Since d_1 and d_2 are positive and $0 \leq \mu < 0.5$, the third equation has a single solution: $z = 0$. The collinear Lagrange points can be found for:

$$x - (1 - \mu) - \frac{\mu + x}{|\mu + x|^3} + \mu \frac{1 - \mu - x}{|1 - \mu - x|^3} = 0 \quad (3.4)$$

A rootfinder algorithm can be used to solve the second equation. This will result in three solutions: L1, L2 and L3. The equilateral points can be found for $d_1 = d_2$. The coordinates of L4 and L5 therefore are:

$$\begin{aligned} x &= \frac{1}{2} - \mu \\ y &= \pm \frac{1}{2} \sqrt{3} \end{aligned} \quad (3.5)$$

Now that the locations of the Lagrange positions are known, it is time to briefly look at motion in the CR3BP frame. The equations of motion can be derived from the potential in Equation 3.2 and are shown below:

$$\begin{aligned}\ddot{x} - 2\dot{y} &= \frac{\partial U}{\partial x} \\ \dot{y} + 2\dot{x} &= \frac{\partial U}{\partial y} \\ \ddot{z} &= \frac{\partial U}{\partial z}\end{aligned}\quad (3.6)$$

Integration leads to finding Jacobi's Integral:

$$\dot{x}^2 + \dot{y}^2 + \dot{z}^2 = V^2 = 2U - C \quad (3.7)$$

where C is called the Jacobi constant. The Jacobi constant is the only known conserved quantity in the CR3BP. It will therefore later be used to characterize orbits about the Lagrange points.

Lagrange points in Cartesian frame

The interplanetary trajectories will not be represented in the CR3BP frame. A transformation between the CR3BP frame, seen in Figure 3.5, towards a Cartesian frame that is centred in P1 is therefore needed. This transformation can be split into two steps:

1. **Translation over x-axis** - A translation of $+\mu$ is performed to shift the origin to P1.
2. **Rotation over all axes** - This step will be further explained below.

One can regard a frame transformation as the effort of changing the original reference frame into the desired reference frame. The first step, the translation over $+\mu$, results in the coinciding of the origin at P1. Subsequently, all three axes have to be rotated so that they align with the desired reference frame. Using rotation matrices simplifies this process. A vector in the original frame multiplied by the rotation matrix will result in the vector's representation in the desired frame. This rotation matrix M_{rot} can be composed of the three separate rotation matrices for each axis:

$$\begin{aligned}M_x(\theta_x) &= \begin{bmatrix} 1 & 0 & 0 \\ 0 & \cos\theta_x & -\sin\theta_x \\ 0 & \sin\theta_x & \cos\theta_x \end{bmatrix} \\ M_y(\theta_y) &= \begin{bmatrix} \cos\theta_y & 0 & \sin\theta_y \\ 0 & 1 & 0 \\ -\sin\theta_y & 0 & \cos\theta_y \end{bmatrix} \\ M_z(\theta_z) &= \begin{bmatrix} \cos\theta_z & -\sin\theta_z & 0 \\ \sin\theta_z & \cos\theta_z & 0 \\ 0 & 0 & 1 \end{bmatrix}\end{aligned}\quad (3.8)$$

Rotation matrix M_x will result in a rotation over an angle θ_x rotated along the x-axis. These rotation angles θ depend on the position of P2 with respect to P1. The state of P2 with respect to P1 will be denoted by \vec{S} . The rotation angles θ_x , θ_y and θ_z can then be expressed as follows:

$$\begin{aligned}\theta_x &= \pm \cos^{-1} \left(\frac{\sqrt{\dot{S}_x^2 + \dot{S}_y^2}}{\|\dot{S}\|} \right) \\ \theta_y &= \mp \cos^{-1} \left(\frac{\sqrt{S_x^2 + S_y^2}}{\|S\|} \right) \\ \theta_z &= \text{atan2}(S_y, S_x)\end{aligned}\quad (3.9)$$

The \pm -sign depends on the sign of S_z : for $S_z > 0$ a plus sign is used. In the same way, the \mp -sign is dictated by \dot{S}_z : for $\dot{S}_z > 0$ a minus sign should be inserted.

The full rotation matrix, over all three axes, is simply the outcome of the matrix multiplication of the three separate rotation matrices. The order of multiplication is shown in Equation 3.10 below.

$$M_{rot}(\theta_x, \theta_y, \theta_z) = M_z(\theta_z) \cdot M_y(\theta_y) \cdot M_x(\theta_x) \quad (3.10)$$

A position vector in the CR3BP frame (\hat{r}_{cr3b}) can now be transformed into the Cartesian frame (\hat{r}_{cart}) by multiplying it with M_{rot} :

$$\hat{r}_{cart} = M_{rot} \cdot \hat{r}_{cr3b} \quad (3.11)$$

where the hat notation (\hat{r}_{cart}) is used to denote the dimensionless quantity of the state in the Cartesian frame. The velocity transformation is different, since it requires the derivative of the rotation matrix:

$$\hat{v}_{cart} = \frac{\delta M_{rot}}{\delta \theta} \cdot \hat{r}_{CR3BP} + M_{rot} \cdot \hat{v}_{cr3b} \quad (3.12)$$

The derivative of the rotation matrix with respect to all three angles θ can most easily be obtained using a skew-matrix. The product of a skew-matrix with matrix A gives the derivative of that matrix A. The skew-matrix is defined as follows:

$$S[A, B, C] = \begin{bmatrix} 0 & -C & B \\ C & 0 & -A \\ -B & A & 0 \end{bmatrix} \quad (3.13)$$

In this case, vector [A, B, C] should be substituted with the vector representing the rotation axis in the Cartesian frame. This axis can be found by multiplying the rotation axis in the CR3BP frame ([0,0,1]) with M_{rot} defined above.

Using Equations 3.11 and 3.12 a state in the CR3BP frame can be transformed into the Cartesian frame after translation of the frame's origin. However, this state will still be dimensionless (denoted by \hat{S}). Equations 3.14 and 3.15 should be used to convert the dimensionless position and velocity to their dimensional quantities, respectively.

$$\vec{r}_{cart} = \hat{r}_{cart} \cdot R_{12} \quad (3.14)$$

$$\vec{v}_{cart} = \hat{v}_{cart} \cdot \frac{\mu_1 + \mu_2}{R_{12}} \quad (3.15)$$

where R_{12} is the distance between the primaries and μ_1 and μ_2 are their respective gravitational parameters. Now that the dimensions have been converted, the state transformation is complete. Since this method was developed for this thesis work specifically, it will be validated in Section 5.3 later in this work.

3.3.2. Orbits

In this section, relevant theory regarding potential gateway orbits will be covered. As has been introduced in Chapter 2, two categories of orbits will be researched: orbits around a central body and orbits in the vicinity of a Lagrange point. Later in this work (in Chapter 4) it will be argued that for this research' purpose, central-body orbits can be modelled as simple unperturbed two-body Kepler orbits. The astrodynamics that underpins these orbits is assumed to be well-known to the reader and will therefore not be covered here. Readers that want to refresh their knowledge on this matter are advised to study the supporting literature study [4] or the textbook by Wakker [24].

Orbits around Lagrange points are more complex. This section will first cover what Lagrange-Point Orbits (LPO) are and will then describe the method used to generate these orbits.

Lagrange-Point Orbits (LPO)

Since the collinear Lagrange points are unstable, a Lagrange-point mission will need to be placed in some sort of orbit in the vicinity of the Lagrange point. The starting point for studying these orbits are the equations of motion in the vicinity of a Lagrange point, describing the distance away from the Lagrange point (denoted by $'$). These equations follow from Equation 3.6 and can be seen below:

$$\begin{aligned} \ddot{x}' - 2y' - x'U_{xx} - y'U_{xy} &= 0 \\ \ddot{y}' + 2x'' - x'U_{xy} - y'U_{yy} &= 0 \\ \ddot{z}' - z'U_{zz} &= 0 \end{aligned} \quad (3.16)$$

where $\frac{\partial^2 U}{\partial^2 x} = U_{xx}$, $\frac{\partial^2 U}{\partial x \partial y} = U_{xy}$ and $U_{xy} = U_{yx}$ since U_0 is continuous.

From studying Equations 3.16, it is evident that the motion in the Z-direction is completely decoupled from the motion in the XY-plane. For all five Lagrange points, so also the equilateral points, the motion in the Z-direction is described by Equation 3.17:

$$z' = C_1 \cos(\sqrt{|U_{zz}|}t) + C_2 \sin(\sqrt{|U_{zz}|}t) \quad (3.17)$$

A spacecraft in the vicinity of a Lagrange point will therefore describe a stable periodic oscillation with a period $T_z = \frac{2\pi}{\sqrt{|U_{zz}|}}$.

Motion in the XY-plane is coupled and thus more complex. After some derivations, which can be found in the literature study [4] and in Wakker [24], the following expressions are found:

$$\begin{aligned} x' &= A_1 e^{\lambda_1 t} + A_2 e^{-\lambda_1 t} + A_3 e^{\lambda_3 t} + A_4 e^{-\lambda_3 t} \\ y' &= \gamma_1 A_1 e^{\lambda_1 t} - \gamma_1 A_2 e^{-\lambda_1 t} + \gamma_3 A_3 e^{\lambda_3 t} - \gamma_3 A_4 e^{-\lambda_3 t} \end{aligned} \quad (3.18)$$

where λ_1 is a real values and λ_3 is imaginary. As a result, the terms $A_1 e^{\lambda_1 t}$ and $A_2 e^{-\lambda_1 t}$ represent exponentially increasing or decreasing motion whilst the terms $A_3 e^{\lambda_3 t} + A_4 e^{-\lambda_3 t}$ describe periodic motion about the Lagrange point. The values for A_i and γ_i are directly related to the initial conditions of the spacecraft. By controlling these parameters and parameters C_1 and C_2 in Equation 3.17, different Lagrange-Point Orbits (LPO) can be obtained. The most relevant families will be briefly listed below:

- **Horizontal-Lyapunov** - Periodic orbit in the XY-plane only
- **Vertical-Lyapunov** - Periodic orbit predominantly in the Z-direction
- **Lissajous** - Quasi-periodic orbit with motion in the Z-direction
- **Halo** - Periodic orbit with motion in the Z-direction (subgroup of Lissajous)

Similar to central orbits, a great number of different orbits exist for each orbit family. These orbits can best be categorized by their Jacobi Constant, which was given in Equation 6.3. Orbits of both Lyapunov families and the Halo family around L1 and L2 in the Earth-Moon system have been plotted in Figure 3.7 for $C = 3.100$. The cross symbols represent the L1 and L2 Lagrange points and the disk represents the position of the Moon.

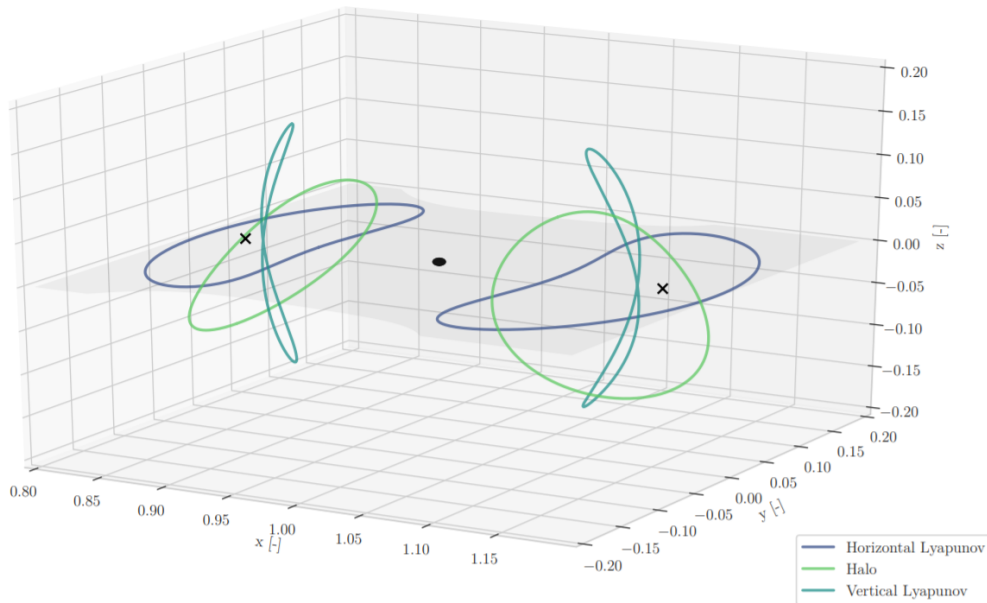


Figure 3.7: LPO in the Earth-Moon system for $C = 3.1$ [8].

Generation of LPO's

As was said in the previous section, different initial conditions lead to different motions around the Lagrange points. Finding the right conditions for a desired orbit is an extremely sensitive and complex process. This process was the subject of an entire thesis, written and performed by Koen Langemeijer [8] in 2018. Langemeijer's methodology and programs have been at the base of the LPO generation in this thesis. A brief summary of the methodology will therefore be given here, while Langemeijer's thesis work is recommended to readers interested in a more thorough description.

The methodology can roughly be described by the following four steps:

1. **Production of two initial guesses** - using Third-Order Richardson Approximation (TORA).
2. **Refinement of guesses** - using Differential Correction (DC).
3. **Validation of initial conditions** - using periodicity verification and Eigensystem validation.
4. **Expansion to other members of the orbit family** - using Numerical Continuation (NC).

In short, two guesses for appropriate initial conditions are generated using TORA. These do not yet produce the desired periodic orbits. Therefore, the guesses need to be refined by an iterative process called Differential Correction (DC), which stops when a specific periodicity is found. The results of the two produced orbits are then validated using periodicity verification and Eigensystem validation. When the two solutions are proven to be correct, they can be used to generate the next solution in the desired orbit family in a process called Numerical Continuation (NC).

Each of these processes will be discussed in the paragraphs below. Since orbit generation is not the core focus of this thesis work, this discussion will be very concise. Again, these processes have been described in more detail by Langemeijer [8]. The resulting orbit libraries generated for this thesis work will be presented and discussed in Analysis B of Part II.

Third-Order Richardson Approximation

In order to generate two initial guesses for the initial state of a LPO, an approximation method is used. More specifically, the third-order approximation method developed by Richardson (TORA) in 1980 [27] has been implemented. This method can find approximate solutions to nonlinear oscillators by using a form of perturbation theory. In his paper [27], Richardson arrives at the third-order estimate of the equations from the EOMs (Equation 3.16) after a "lengthy and tedious algebraic process" [27] that will not be repeated here. The equations below show the relation between the orbital amplitude in the x- and z-direction (A_x and A_z respectively) and the initial estimate of the state components. All other parameters, such as τ_1 , λ and a_{21} , are functions of the mass parameter of the three-body system and of the positions of the Lagrange point in the CR3BP frame.

$$x = -A_x \cos \tau_1 + a_{21}A_x^2 + a_{22}A_z^2 + (a_{23}A_x^2 - a_{24}A_z^2) \cos 2\tau_1 + (a_{31}A_x^3 - a_{32}A_xA_z^2) \cos 3\tau_1 \quad (3.19)$$

$$y = kA_x \sin \tau_1 + (b_{21}A_x^2 - b_{22}A_z^2) \sin 2\tau_1 + (b_{31}A_x^3 - b_{32}A_xA_z^2) \sin 3\tau_1 \quad (3.20)$$

$$z = \delta_n A_z \cos \tau_1 + \delta_n d_{21} A_x A_z (\cos 2\tau_1 - 3) + \delta_n (d_{32} A_z A_x^2 - d_{31} A_z^3) \cos 3\tau_1 \quad (3.21)$$

$$\dot{x} = \lambda A_x \sin \tau_1 - 2\lambda (a_{23}A_x^2 - a_{24}A_z^2) \sin 2\tau_1 - 3\lambda (a_{31}A_x^3 - a_{32}A_xA_z^2) \sin 3\tau_1 \quad (3.22)$$

$$\dot{y} = \lambda k A_x \cos \tau_1 + 2\lambda (b_{21}A_x^2 - b_{22}A_z^2) \cos 2\tau_1 + 3\lambda (b_{31}A_x^3 - b_{32}A_xA_z^2) \cos 3\tau_1 \quad (3.23)$$

$$\dot{z} = -\lambda \delta_n A_z \sin \tau_1 - 2\lambda \delta_n d_{21} A_x A_z \sin 2\tau_1 - 3\lambda \delta_n (d_{32} A_z A_x^2 - d_{31} A_z^3) \sin 3\tau_1 \quad (3.24)$$

The initial guess for the amplitudes A_x and A_z can be based on the quantities of known orbits from the desired orbit family. By choosing two slightly different values, two initial guesses are generated by Equations 3.19 to 3.24.

Differential Correction

The initial guesses generated by the TORA need to be refined until they describe a periodic orbit. This is done by a process called Differential Correction (DC). DC makes use of the symmetry of the Lyapunov and Halo orbits, which allows the initial conditions of any orbit to be expressed by only three of the six state components:

$$\vec{S}_{t_0} = \begin{bmatrix} x_0 & 0 & z_0 & 0 & \dot{y}_0 & 0 \end{bmatrix}^T \quad (3.25)$$

The initial state is then integrated until its estimated half-period, denoted by $\hat{T}/2$:

$$\vec{S}_{t_{\hat{T}/2}} = \begin{bmatrix} x_{t_{\hat{T}/2}} & y_{t_{\hat{T}/2}} & z_{t_{\hat{T}/2}} & \dot{x}_{t_{\hat{T}/2}} & \dot{y}_{t_{\hat{T}/2}} & \dot{z}_{t_{\hat{T}/2}} \end{bmatrix}^T \quad (3.26)$$

For a fully periodic orbit, the $y_{t_{\hat{T}/2}}$, $\dot{x}_{t_{\hat{T}/2}}$ and $\dot{z}_{t_{\hat{T}/2}}$ terms should be zero. The essence of the DC method is therefore to relate deviations in the half-period plane to a change in the initial state. This can be done using the state transition matrix (STM), which reflects the sensitivity of the final state to changes in initial orbital conditions. Figure 3.8 illustrates the process of Differential Correction (DC).

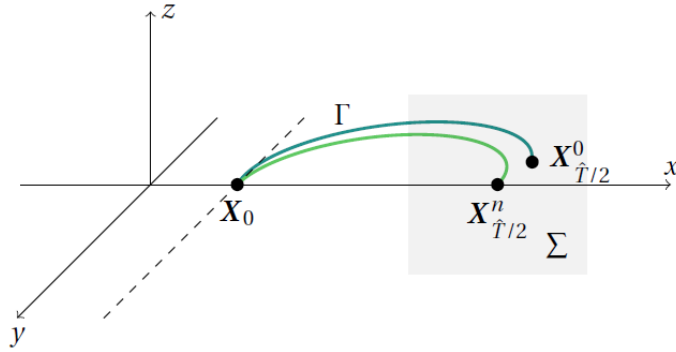


Figure 3.8: Refinement of initial conditions (X_0) by evaluating the orbital state in the half-period plane (Σ) [28].

Validation of initial conditions

It is important to validate the outcomes of the iterative DC process before they are used in the Numerical Continuation procedure to expand to new orbits. Two distinct steps are therefore to be performed:

1. Periodicity verification
2. Eigensystem validation

The periodicity verification was introduced in the paragraph on DC above. In order to check the periodicity of the orbit, the norm of the position and velocity deviation is checked against a threshold requirement at the estimated half-period. Additionally, the eigenvalue that denotes periodicity is checked against predetermined bounds.

The eigensystem validation will validate the orbit generation process by studying the monodromy matrix. A list of checks should be performed, which can be found in the work by Langemeijer [8]. The determinant of the monodromy matrix should be equal to zero, for instance.

Numerical Continuation

The two verified and validated initial conditions can now be used to approximate a third state. In principle, this can be done by simply adding the difference between the two states to either one to arrive at the third state. Langemeijer [8] used a slightly more complex method that includes a scaling factor with respect to the z-position of the initial conditions. This method, developed by Keller [29], allows for a better computation of the otherwise hard to find vertical-Lyapunov orbits. Both methods are Numerical Continuation (NC) methods and will result in a library of orbits for a specific orbit family (i.e. horizontal-Lyapunov). Each orbit in the library has a unique Jacobi constant. Different orbit family libraries can be created by altering the initial guesses in the TORA process.

3.3.3. Transfers

Now that the gateway concept has been defined and relevant theory regarding its potential orbit has been discussed, the theory involving transfer trajectories between the gateway and the planets of interest will be discussed. This section will discuss the physics that govern these transfers and will introduce the methods to model them effectively. The concepts that will be introduced can be separated into two distinct categories: impulsive transfers and continuous transfers.

Impulsive transfers

The most basic impulsive transfer consists of two burns, one at departure and one at arrival. Impulsive transfers can be further complicated by allowing the trajectory to include Deep Space Manoeuvres (DSMs) and flyby manoeuvres. This section will start off by discussing how the two-impulsive transfer is modelled. After that, flyby's and DSMs will be discussed separately. The theory and models used in this work were, to a large extent, based on the work done by Melman [7] and Musegaas [5] in their respective thesis work.

Lambert targeter

In interplanetary transfer design, one wants to design a trajectory that connects two points in space (i.e. planets). The position of these points in space are time dependent. This problem is the so-called Lambert problem, which was best described in a paper by Gooding [30]:

“An unperturbed orbit, about a given inverse-square law center of force, say F , is to be found connecting two given points, P_1 and P_2 , with a specified flight time $\Delta t = t_2 - t_1$.”

Figure 3.9 gives more insight into the geometry of the Lambert problem.

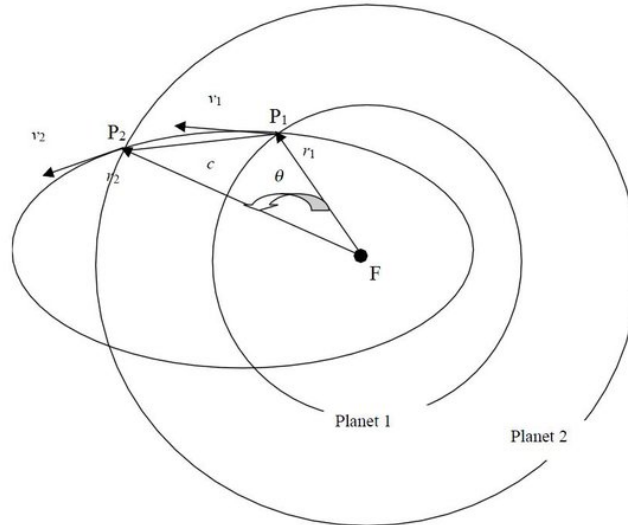


Figure 3.9: Representation of the Lambert problem for an interplanetary trajectory around the Sun [31].

The problem assumes that the spacecraft will only undergo gravitational attraction from the central body F . As a result, the spacecraft will describe part of the conical section that results from the two-body problem. In order to find the orbital elements that describe the solution of the Lambert problem, the time-of-flight equation below will need to be solved:

$$\Delta t = t_2 - t_1 = \sqrt{\frac{a^3}{\mu}} \left(E_2 - E_1 - e (\sin E_2 - \sin E_1) \right) \quad (3.27)$$

where E is the eccentric anomaly, which is defined as the angle between the periapsis direction and the spacecraft's position in orbit projected on a circle circumscribing the ellipse. The algorithms developed to solve for solutions of this problem are called Lambert targeters. Different targeters have been developed. The one used in this thesis work was developed by Dario Izzo while he was working on finding solutions to problems formulated in the GTOP library [32].

By rearranging Equation 3.27 using dimensionless variables and substitution of Equation 3.28 into the new TOF equation, Izzo's Lambert targeter ensures rapid convergence independent of the problem configuration.

$$x_0 = \log\left(1 + \cos\left(\frac{\alpha}{2}\right)\right) \quad (3.28)$$

The calculation scheme of the Izzo Lambert Targeter can be read into further detail in the thesis report by Leito Pinto Secretin [33]. Leito Pinto Secretin has also implemented the Izzo Lambert Targeter in Tudat and validated it using a rigorous verification process.

Powered Flyby's

When a spacecraft flies in the vicinity of a celestial body, the gravitational fields of the spacecraft and that body interact. Flybys are incorporated into trajectories to harness this effect in order to change the magnitude and the direction of the spacecraft cheaply. This section will first briefly discuss the fundamental physics of an unpowered flyby. Next, the mechanism behind a powered flyby is introduced along with a method to model them.

When a spacecraft (S) performs a flyby at target planet (t), the total momentum of the system is conserved. When assuming constant mass of the spacecraft (M_S) and of the planet (M_t), the flyby can mathematically be represented by:

$$M_S \cdot \vec{V}_{S,i} + M_t \cdot \vec{V}_{t,i} = M_S \cdot \vec{V}_{S,f} + M_t \cdot \vec{V}_{t,f} \quad (3.29)$$

where the subscripts i and f denote the initial and final values, respectively. From Equation 3.29, the change in the magnitude of the spacecraft's velocity can be deduced:

$$\Delta \vec{V}_S = \vec{V}_{S,f} - \vec{V}_{S,i} = \left(\vec{V}_{t,i} - \vec{V}_{t,f}\right) \frac{M_t}{M_S} \quad (3.30)$$

Since a planetary mass (approximately between 10^{24} and 10^{27} kg) is so much larger than that of a spacecraft (order of 10^5 kg and smaller), the planet's change in velocity will be negligibly small. The magnitude of the spacecraft's velocity before and after the flyby will therefore be equal in the planetocentric reference frame. However, the direction of this velocity can be different. This has important implications in the heliocentric reference frame, which will be evident after studying Figure 3.10.

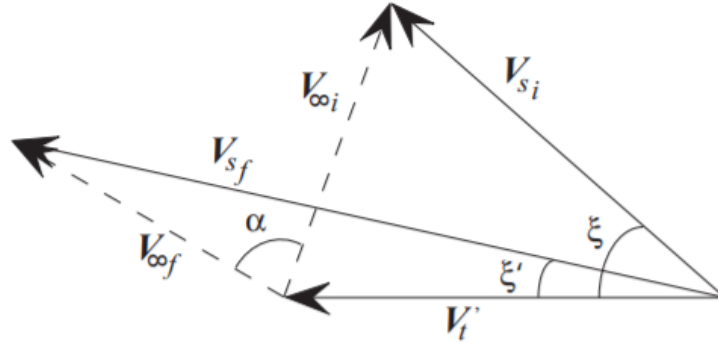


Figure 3.10: Schematic representation of the velocity change due to a flyby shown in the planetocentric and heliocentric reference frame [7].

In Figure 3.10, the V_∞ 's denote the spacecraft's velocity in the planetocentric reference frame. From this figure, it can be concluded that the magnitude of the velocity and thus the orbital energy of the spacecraft can be changed in the heliocentric frame as a result of a flyby. A flyby can be modelled using the parameters in Figure 3.11.

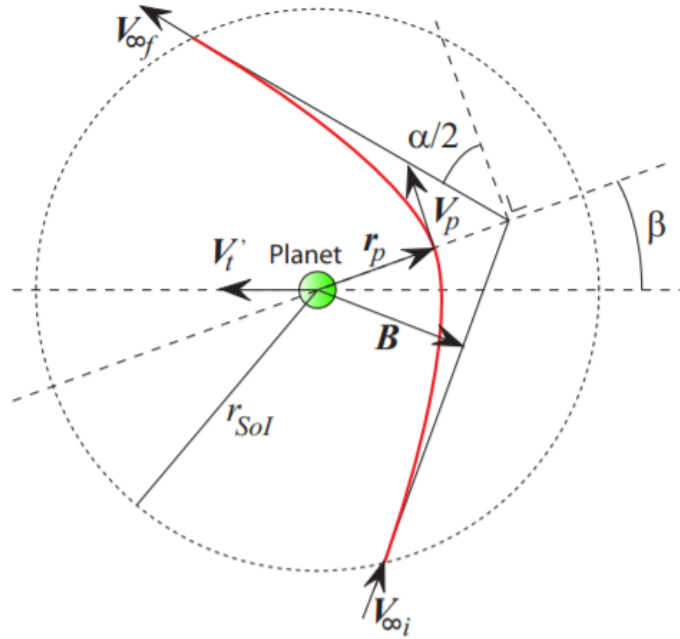


Figure 3.11: In-plane parameterization of a flyby in the planetocentric frame [7].

By controlling the impact parameter B , the velocity change in magnitude and direction can be regulated. Naturally, passing in front of a planet reduces the spacecraft's velocity, while passing it from behind will result in a velocity increase. The following equations that describe the spacecraft's motion during flyby have been derived by Cornelisse et al. [34]:

$$r_p = -\frac{\mu_t}{V_{\infty}^2} + \sqrt{\frac{\mu_t^2}{V_{\infty}^4} + B^2} \quad (3.31)$$

$$\sin \frac{\alpha}{2} = \frac{1}{1 + \frac{r_p V_{\infty}^2}{\mu_t}} = \frac{1}{\sqrt{1 + \frac{B^2 V_{\infty}^4}{\mu_t}}} \quad (3.32)$$

where r_p is the periapsis distance from the flyby planet and α is the deflection angle. As can be seen in Equation 3.32, the deflection angle is dependent on the impact parameter B , the hyperbolic excess velocity V_{∞} and the planet's gravitational parameter μ_t . From Equation 3.31, the minimum impact value for B to prevent impact on the target planet can be deduced:

$$B \geq R_{pl} \sqrt{1 + \frac{V_{esc_s}^2}{V_{\infty}^2}} \quad (3.33)$$

where V_{esc_s} is the local escape velocity at the planet's surface ($\sqrt{2\mu_t/R_t}$). In theory, this equation would produce the minimum pericenter radii to be used in this thesis work. However, it was decided to follow the example set by Melman and Musegaas and base the minimum pericenter radius on previous flyby missions. As a result, the pericenter values displayed in Table 3.4 were used throughout this thesis work.

Body	R_p [km]	r_{pmin} [R_p]	h_{pmin} [km]	Mission
Earth	6378	1.048	306	Galileo
Mars	3397	1.076	257	Rosetta
Moon	1737	1.01	17	-

Table 3.4: Minimum pericenter used for planetary flyby's relevant to this thesis work.

For a powered flyby, an impulsive thrust manoeuvre is added at the pericenter of the flyby. As a result, the deflection angle of the incoming leg is not equal to that of the outgoing leg anymore. This change in geometry can be seen in Figure 3.12.

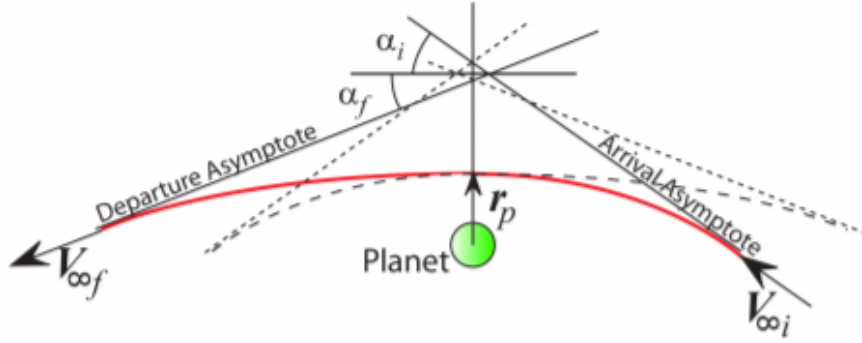


Figure 3.12: Change in geometry of a powered flyby [7].

Now the calculation scheme resulting in the outgoing heliocentric velocity of the spacecraft after flyby will be given. The subscript t denotes that the parameter is given in the planetocentric frame, the absence of an extra subscript means it is given in the heliocentric frame.

$$\vec{V}_{t,in} = \vec{V}_{in} - \vec{V}_t \quad (3.34)$$

where $\vec{V}_{in} = \vec{V}_{\infty_i}$. The incoming eccentricity (e_i) can then be calculated, which can then be used to find the incoming deflection angle (α_i):

$$e_i = 1 + \frac{r_p |\vec{V}_{t,in}^2|}{\mu_t} \quad (3.35)$$

$$\alpha_i = \sin^{-1} \frac{1}{e_i} \quad (3.36)$$

Then the pericenter velocity before and after the impulsive thrust ΔV can be calculated as follows:

$$V_{p,in} = \sqrt{|\vec{V}_{t,in}|^2 \cdot \frac{e_i + 1}{e_i - 1}} \quad (3.37)$$

$$V_{p,out} = V_{p,in} + \Delta V$$

Then the outgoing velocity in the planetocentric reference frame can be calculated:

$$V_{t,out} = \sqrt{V_{p,out}^2 - \frac{2 \cdot \mu_t}{r_p}} \quad (3.38)$$

Subsequently, the outgoing deflection angle (α_f) and the resulting total deflection angle (α) are expressed by:

$$\alpha_f = \sin^{-1} \frac{1}{1 + \frac{r_p \cdot |\vec{V}_{t,out}|^2}{\mu_t}} \quad (3.39)$$

$$\alpha = \alpha_i + \alpha_f$$

The outgoing velocity vector in the planetocentric frame is then:

$$\vec{V}_{t,out} = V_{t,out} \begin{pmatrix} \cos \alpha \\ \cos \beta \sin \alpha \\ \sin \beta \sin \alpha \end{pmatrix} \begin{pmatrix} \mathbf{i}_x \\ \mathbf{i}_y \\ \mathbf{i}_z \end{pmatrix} \quad (3.40)$$

where the angle β is defined as the angle the incoming velocity makes with \mathbf{i}_y (seen in Figure 3.11) and the directions \mathbf{i}_x , \mathbf{i}_y and \mathbf{i}_z are defined as:

$$\begin{aligned} \mathbf{i}_x &= \frac{\vec{V}_{t,in}}{|\vec{V}_{t,in}|} \\ \mathbf{i}_y &= \frac{\mathbf{i}_x \times \vec{V}_t}{|\mathbf{i}_x \times \vec{V}_t|} \\ \mathbf{i}_z &= \mathbf{i}_x \times \mathbf{i}_y \end{aligned} \quad (3.41)$$

Finally, the velocity of the spacecraft after the flyby in the heliocentric frame can be calculated as follows:

$$\vec{V}_{out} = \vec{V}_t + \vec{V}_{t,out} \quad (3.42)$$

These calculation steps have all been implemented in a single model by Musegaas. In his thesis work [5], the model is explained in great detail. The same work contains an extensive verification of the validity of the model and its results. This is the model that will also be used in this thesis work. The same model is also capable of calculating simple unpowered flybys. For these flyby's, the total deflection angle α is simply twice the incoming angle of Equation 3.36. The outgoing velocity can then be calculated using Equation 3.40, where $V_{t,out}$ is replaced by $V_{t,in}$. The magnitude of the outgoing velocity is then unaffected, but its direction will be able to change.

Inclusion of DSMs

Interplanetary trajectories often involve one or more DSMs. Apart from the advantage of ΔV reduction and broadening of the launch window, DSMs also allow for easier inclination changes and can bring the spacecraft at a more precise location close to the target planet in order to perform a flyby. Whereas the addition of a flyby requires additional physical theory and modelling, the addition of a DSM leverages existing theory and modelling to a large extent. This is best explained by Molenaar in his thesis work [35] and will be briefly summarized here.

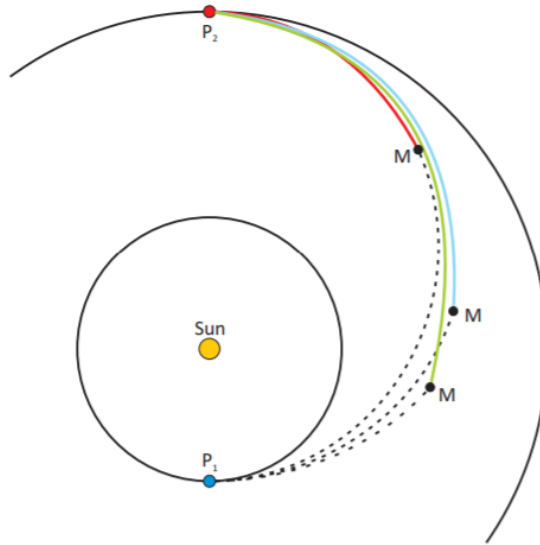


Figure 3.13: Sketch of three single-DSM trajectories between planet P_1 and P_2 [36].

Three options for a simple trajectory with one DSM are sketched in Figure 3.13 above. The DSM is performed at point M. Vasile and De Pascale proposed a parameterization of this problem in 2006 [36]. The standard 2-burn trajectory is parameterized by 2 parameters: Departure epoch (t_0) and Time of Flight (T). For a 3-burn trajectory, the parameter η is added so that the epoch of the DSM can be expressed as:

$$t_{DSM} = t_0 + T_{DSM} = t_0 + \eta T \quad (3.43)$$

Now the interplanetary trajectory is split into two parts: the part from P_1 to the DSM point M and the part from M to P_2 . Once the location of point M is known, the second part can be solved using the Lambert targeter discussed earlier. This targeter will use the locations of M and P_2 and a flight time of $(1 - \eta)T$. The first part cannot be described as a Lambert problem, since initially the location of the DSM point M is unknown, only its time is known. Therefore, the trajectory up to point M will be propagated along a Kepler orbit described by three design variables. Propagation stops at T_{DSM} and the final state is passed on to the Lambert targeter of the next leg.

Two different formulations for the initial Kepler orbit have been put forward by Musegaas [5]: the Position Formulation (PF) and the Velocity Formulation (VF). The Velocity Formulation was used in this thesis work, since the same formulation is used in most GTOP solutions and this allows for easier validation. VF uses three parameters to model the orbit up to a DSM. These parameters are different for a trajectory after departure and for a trajectory after a flyby. Both are listed below.

VF of orbit parameters after departure:

1. V_∞ : The magnitude of the relative velocity with respect to the departure planet.
2. θ : The in-plane angle of the relative velocity with respect to the departure planet.
3. Φ : The out-of-plane angle of the relative velocity with respect to the departure planet.

VF of orbit parameters after a flyby:

1. r_p : The pericenter radius of the gravity assist at the target planet (seen in Figure 3.11).
2. β : 3D rotation angle of the flyby (seen in Figure 3.11).
3. ΔV : Magnitude of the impulsive shot a pericenter of the flyby.

The theory described above has been implemented in a model by Musegaas. This model has been used in this thesis work. It will be verified in Section 5.3.2.

Continuous transfers

Whereas impulsive transfers rely on bursts of thrust at precisely timed intervals and locations, continuous-thrust engines allow for small, continuous acceleration over a long period of time. Due to the higher specific impulses of these engines the same ΔV can be achieved using less propellant according to Tsiolkovsky's rocket equation. Furthermore, the ability to continuously accelerate opens up new trajectory possibilities.

Two categories of continuous-thrust trajectory design exist: linked-conics and shape-based methods. Similarly to the DSM trajectories discussed earlier, the linked-conics approach divides the complete trajectory in a number of *legs* that begin and end at *nodes*. Legs are further divided into *segments*, which embody a small ΔV impulse each. As a result, the linked-conics approach models a continuous-thrust transfer as a collection of small impulsive bursts. This approach is depicted in Figure 3.14.

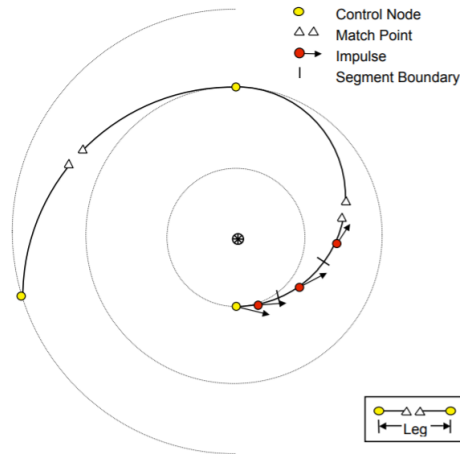


Figure 3.14: Trajectory structure of the linked-conics approach for continuous-thrust trajectories [37].

Alternatively, shape-based methods design transfers by assuming spacecraft trajectories to be of a certain shape. This shape is made to satisfy the boundary conditions of the trajectory problem. At the same time, it must adhere to the equations of motion that govern a continuous-thrust transfer:

$$\ddot{\vec{r}} + \frac{\mu}{r^3}\vec{r} = \frac{\vec{T}}{M} = \vec{f} \quad (3.44)$$

After a suitable shape is found, the thrust profile and time evolution of the spacecraft can be computed. In his thesis [38], David Gondelach set out to study and compare a number of different shaping methods on top of developing a method himself. From this thesis work, two potentially interesting shaping methods will be considered for the purpose of this thesis work and will therefore be briefly discussed here: spherical shaping and hodographic shaping. For a more detailed discussion of both methods, an interested reader is referred to Gondelach's thesis work [38].

Spherical shaping

This shaping method, as the name gives away, makes use of spherical coordinates (r , θ and ϕ). The trajectory is parameterized using an angle θ , so that the shaping functions are:

$$\begin{aligned} r &= R(\theta) \\ \phi &= \Phi(\theta) \\ t &= T(\theta) \end{aligned} \quad (3.45)$$

The geometry of the trajectory is modelled by R and Φ , whilst the function T determines the evolution of time along this shape. A wise choice for the functions R and Φ would be one for which the boundary conditions can be computed analytically, but otherwise they can be chosen freely. Naturally, the time evolution is provided by the expression of $\dot{\theta}$. For a suitable selection of functions, an interested reader is referred to a paper by Novak and Vasile in 2011 [39].

The thrust profile can be found using the equations of motion for θ :

$$\dot{\theta} \frac{d^2 \vec{r}}{d\theta^2} + \ddot{\theta} \frac{d\vec{r}}{d\theta} = -\mu \frac{\vec{r}}{r^3} + \vec{f} \quad (3.46)$$

A total of 10 boundary conditions need to be satisfied: four on position and six on velocity. The functions R and Φ should therefore have at least ten parameters. Novak's suggested functions use 11 parameters, so that the extra parameter can be used to satisfy constraints on Time of Flight (TOF). The TOF and ΔV of the trajectory can be found by integrating $\frac{\delta T}{\delta \theta}$ and $|\vec{f}| \frac{\delta T}{\delta \theta}$ over θ respectively. Of all the existing shaping methods, Gondelach found the best solutions with regards to ΔV using the spherical shaping method. However, a clear disadvantage is the lack of free parameters, which leads to a loss of design flexibility.

Hodographic shaping

Gondelach therefore set out to design a shaping method with high accuracy and with high flexibility due to the use of free parameters. The method relies on velocity hodographs, which give a representation of velocity change over position or time. Instead of 'drawing' a trajectory between the positions of two orbits, the hodographic shaping method connects the velocity hodographs of the two orbits. This is best depicted in Figure 3.15.

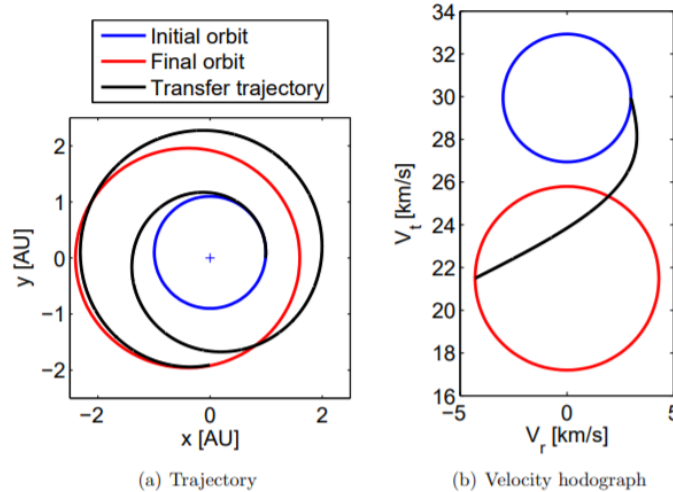


Figure 3.15: Hodographic shaping method connecting orbits in position graph and velocity hodograph [38].

In order to shape the trajectory in the velocity hodograph, this method makes use of velocity functions in the radial (r), normal (θ) and axial direction (z). These functions, V_r , V_θ and V_z , express the velocity components either as a function of time t or of polar angle θ . Both formulations result in slightly different calculations of TOF and ΔV and result in different definitions of the boundary conditions. In his thesis, Gondelach has done an extensive analysis into suitable base functions for the velocity functions. These have been implemented in the method and are readily available in the computer program.

In short, the hodographic shaping method works with a total of nine boundary conditions. The method allows for easy implementation of additional free parameters, which enables flexible trajectory design. A drawback is that the base functions should be tailored to the trajectory of interest for optimal results.

4

Design considerations

With the theoretical building blocks of this thesis in place, this chapter will go over all the aspects that need to be considered before moving onto the analysis phase of the research. The goal of this design phase is to clearly lay out the scope of the analyses that will follow and define all the relevant components. To this extent, this chapter will start with a mission definition, followed by a section on mission evaluation criteria. Subsequently, some important mission characteristics will be covered. Afterwards, three separate sections will each narrow down the scope of the research. First, an assessment on what gateway locations to include will be made. Second, a consideration of orbital types the gateway could be placed in is laid out. Third and last, the different transfer and trajectory types that will be evaluated will be listed. All these aspects will be covered in individual sections.

4.1. Mission definition

In this feasibility study different designs of the gateway concept will be compared and analysed. To this extent, the basis on which they will be evaluated should first be defined. This basis will be referred to as "the mission". The mission will be defined in this section through a discussion of the mission goal, the mission timeline, the mission boundaries and the mission architecture.

- **Mission goal** - "Establish the gateway trajectory design for an efficient and practical crew transportation system between the parking orbits of Earth and Mars." [4]
The next section will discuss the criteria used to evaluate the efficiency and practicality of this system. The mission goal clearly states that its intended use is for crew transportation. It is further focused on transportation between Earth and Mars only. To further narrow the scope, it was decided to focus on one-way travel between Earth and Mars, from Earth to Mars. This direction is especially significant since Earth departure is more demanding than Mars departure.
- **Mission timeline** - The mission will be considered to be in operation in the 2030s. The first epoch considered will be January 1st, 2030, on 00:00 (10958 MJD2000).
- **Mission boundaries** - The mission will focus on transfers from Earth orbit to Mars orbit. It will therefore not include surface departure and parking orbit insertion at Earth, nor will it include re-entry at Mars. The parking orbit altitudes around Earth and Mars, therefore the boundaries of the focus mission, are given in Table 4.1 below. The parking orbits are assumed to be circular orbits.

Parking orbit planet	Altitude [km]
Earth	250
Mars	250

Table 4.1: Definition of the parking orbits around Earth and Mars, which act as the mission boundaries.

- **Mission architecture** - The mission architecture consists of a single gateway. As a result, the mission will always be split into two segments: Earth-to-Gateway (EG) and Gateway-to-Mars (GM). The mission architecture is depicted in Figure 4.1.

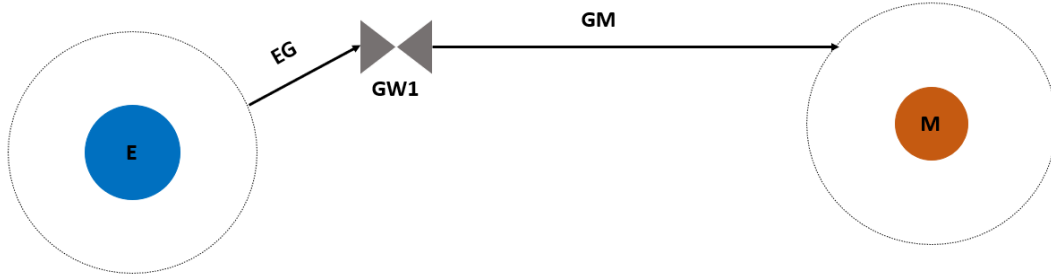


Figure 4.1: Schematic overview of the single-gateway architecture and the resulting mission segments.

4.2. Mission evaluation criteria

Now that the mission has been defined, it is clear what will be evaluated. Next, the evaluation criteria need to be defined. Different gateway mission concepts can be compared by how they rank on each evaluation criterion. A list of criteria to be used in the following analyses is included below.

- **ΔV requirements** - This is the most straightforward and, therefore, most widely used metric in assessing trajectories. The ΔV budget quantifies the total velocity change needed over the entire trajectory. This is of importance since a spacecraft uses propellant to change its velocity. There is a direct relation between the propellant mass needed for a transfer and the ΔV budget of that same transfer.
- **Orbit Cost Function** - The relation between propellant mass and ΔV does depend on the specific impulse (I_{sp}), which is a characteristic of the propulsion system. When comparing trajectories flown by different spacecraft, comparisons based on ΔV alone are not representative. To this extent, Wertz [40] has introduced the Orbit Cost Function (OCF), which expression can be found below:

$$OCF = (1 + K)e^{\frac{\Delta V}{V_0}} - K = (1 + K)e^{\frac{\Delta V}{g_0 I_{sp}}} - K \quad (4.1)$$

The parameter K is a measure for the fraction of the propellant mass assigned to tankage and other propellant hardware. Table 4.2 further below in this chapter lists the values of K and I_{sp} for the different propulsion systems used in this research. OCF is a useful measure since it can be used to estimate the total mass for a mission concept.

- **Time Of Flight** - Each mission design is associated with a time it takes to complete the Earth to Mars transfer, henceforth referred to as TOF. A lower TOF is favourable, since it means less exposure to radiation, less demands on life-support systems and a more comfortable flight for the crew. The TOF will be expressed in days.
- **Consistency** - When a mission design ranks highest on all three criteria above, this does not necessarily mean it is the most practical design. A design that is able to support a highly efficient transfer once every 20 years, will not be considered more suitable than a design that is able to support a slightly less efficient transfer every month. This criterion evaluates the consistency with which a design can support an efficient transfer. Section 7.2.3 will discuss how exactly this criterion is put into practice.

4.3. Mission characteristics

This section will dive into some relevant mission characteristics, such as transfer vehicle mass and propulsion system characteristics.

- **Spacecraft mass** - In the supporting literature study [4], an estimation of the mass of the transfer vehicle was made. In Landau and Longuski [41] it was found that an estimated 5 kilograms per day per crew member should be used as supply mass. By studying a number of Mars concept missions, it was found that a reference mass of 2.5 tonnes per crew member should be used for the spacecraft construction mass. This resulted in a very rough estimate of the mass relation in tonnes:

$$M_{TV} = 2.5N_c + 5 \cdot 10^{-3}N_c TOF \quad (4.2)$$

where N_c denotes the number of crew members and TOF represents the TOF in days. The great uncertainty in this relation is legitimized since the outcome will not be used in simulations but will only be used to provide insight in the propulsion systems effectiveness in the section below. For this purpose, a simple order of magnitude suffices. As an example, a crew of 100 on a transfer with a 200-day trip time, would require a spacecraft of at least 350 metric ton. Of this total mass, 100 metric tons is the supply mass.

- **Propulsion systems** - To be able to compute the OCF, some metrics of the propulsion systems need to be known. Table 4.2 lists all the relevant parameters for the propulsion systems considered. The specific impulse (I_{sp}) and maximum thrust level (T) for the nuclear and electric propulsion were taken on the conservative side of the range deduced from the sources used in Section 3.2. The SpaceX Raptor Engine was used as a reference for the impulsive propulsion systems. This engine can produce 2 MN of thrust at an I_{sp} of 383 s today and is expected to improve considerably over the next few years. The tankage parameter K is also listed in Table 4.2. It has not been calculated for the electric propulsion system, the reason for which will be given below.

Propulsion system	I_{sp} [s]	T [kN]	K [-]
Impulsive	400	2200	0.1
Nuclear	5000	1000	0.21
Electric	2500	0.01	n/a

Table 4.2: Mission characteristics of the relevant propulsion systems.

To get a feel for what the differences in propulsion systems mean, they are compared by studying their implementation on the NASA design reference mission 5.0 [42]. The ΔV budget of this mission is 4 km/s and the TOF is roughly 180 days. Some mass and acceleration characteristics of the propulsion systems for this reference mission can now be calculated using the rocket equation and simple mechanics. The results are shown in Table 4.3 below. The results shown have been calculated for a single propulsion system, which will be the case for electric and nuclear systems. Transfer vehicles most often incorporate multiple chemical rocket engines in their design, so that the total thrust force and as a result the acceleration must be multiplied by the total engine number. The transfer vehicle mass relation of Equation 4.2 was used for N_p is 100.

Propulsion system	$\frac{M_{beg}}{M_{end}}$	M_0 [mt]	M_{prop} [mt]	$a_{min} - a_{max}$ [$\frac{m}{s^2}$]
Impulsive	2.77	942	602	2.33 - 6.47
Nuclear	1.08	369	29	2.71 - 2.94
Electric	1.18	400	60	0.000025 - 0.000029

Table 4.3: Mass and acceleration characteristics for the three propulsion systems implemented on NASA DRM 5.0 [42].

Two important conclusions must be drawn from the table above. First, the nuclear and electric propulsion systems require far less propellant than the chemical impulsive system. This is explained by the difference in I_{sp} between the systems. Second, the impulsive and nuclear systems can provide accelerations of similar order of magnitude. Electric propulsion systems are far less powerful and can only provide fractions of the accelerations provided by the other two systems. In fact, this acceleration is so low that it would take over 4 years to accomplish the ΔV budget required in this mission.

Therefore, the electric propulsion systems available in the 2030s will not be capable of supporting the focus mission of this thesis work. The electric propulsion system will therefore not be considered in the remainder of this research.

4.4. Gateway locations

As has been discussed in the mission definition (Section 4.1), the mission architecture involves a single gateway structure positioned in space. This section will discuss which gateway locations should be considered in this research. A clear distinction can be made between two location types: locations around a central body and locations in the vicinity of Lagrange points. Each will be studied individually. It is important to note that this section will address the locations only, the next section (Section 4.5 *Gateway Orbits*) will go into the motion of the gateway at these locations.

4.4.1. Celestial body

Like the ISS, the gateway can be positioned in orbit around a central body. The type of orbit is not the subject of discussion in this section since this section will solely focus on the celestial body at the center of the orbit. At first thought, four celestial bodies seem to offer an appropriate gateway location to support Earth-Mars transfers: Earth, the Moon, Mars and the Sun. These locations have been depicted in Figure 4.2, which was taken from the literature study [4]. In this figure, the locations are denoted by the first letter of the celestial body at the center of the orbit (lowercase 'm' for the Moon) followed by the 'O' for orbit. At this stage, any type of orbit is still possible, but for the sake of simplicity only circular orbits have been depicted.

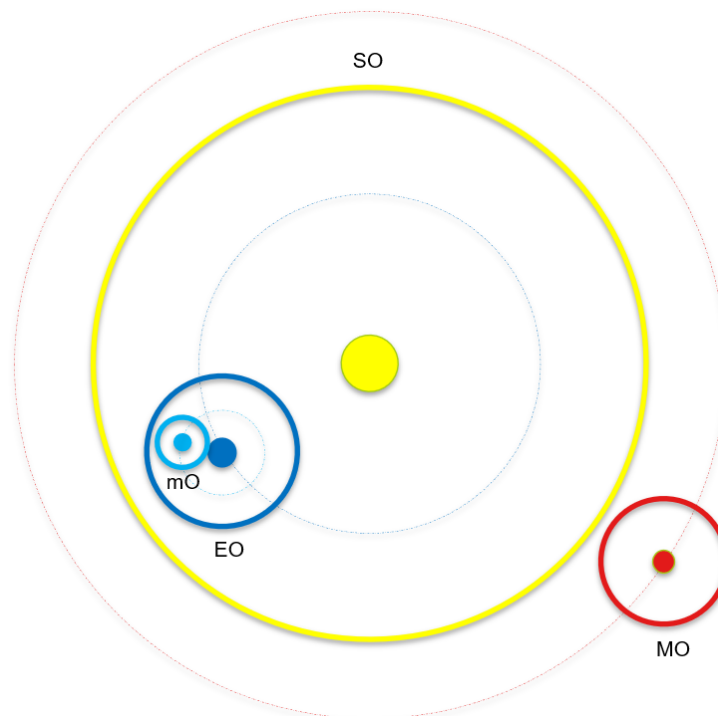


Figure 4.2: Gateway location options around a celestial body [4].

Of these four potential locations, only three will be considered in the research. The gateway location around the Sun (SO) was eliminated for practicality reasons. For a gateway to support Earth-Mars transfers frequently, the gateway should be positioned in between the departure and arrival location. A gateway in orbit around the Sun, will by definition have an orbital period different from that of at least one planet. As a result, the gateway would be positioned at impracticable distance to at least one planet. In short, three gateway locations around a celestial body will be considered in the remainder of this thesis work. They have been listed in Table 4.4, classified by their closest planet.

Gateway locations around a celestial body	
Earth vicinity	Mars vicinity
Earth Orbit (EO)	Mars Orbit (MO)
Lunar orbit (mO)	

Table 4.4: Overview of the gateway locations around a celestial body that will be considered in this research.

4.4.2. Lagrange points

Alternatively, the gateway can be positioned in the vicinity of a Lagrange point. Figure 4.3 depicts all Lagrange points that at first thought might be relevant in supporting Earth-to-Mars transfers. The locations have been labelled using the letters for the primary bodies in the three-body problem along with the respective Lagrange-point number. As can be seen, all Lagrange points of the Sun-Earth (SE), Sun-Mars (SM) and Earth-Moon (Em) system are displayed, except for the SE-L3 and SM-L3 points.

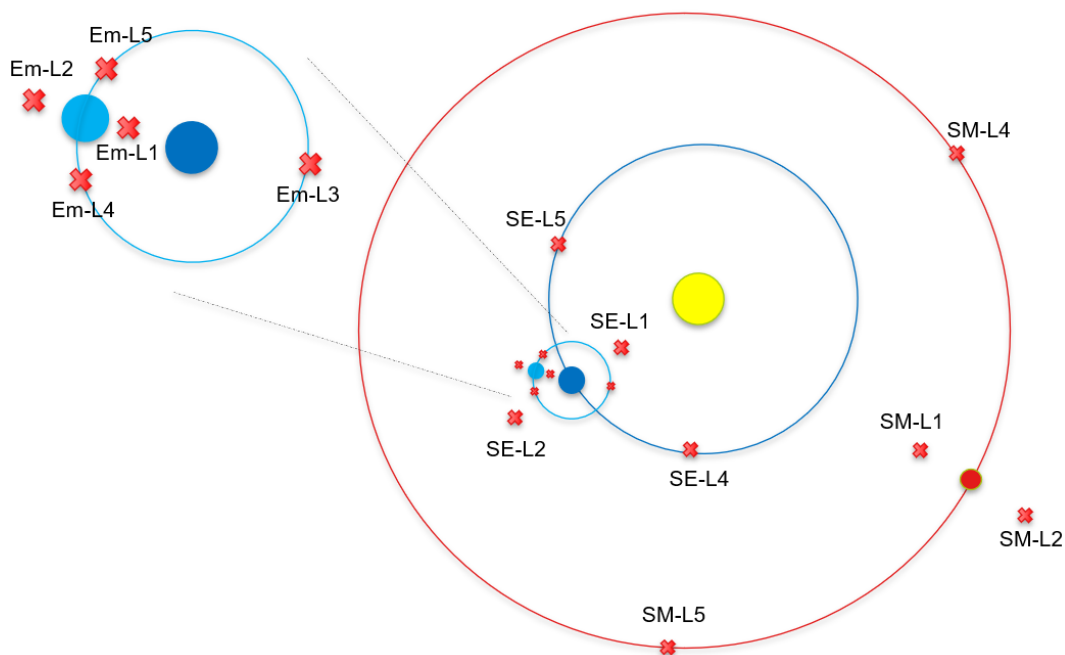


Figure 4.3: Gateway location options in the vicinity of a Lagrange point [4].

A total of 13 positions are shown in Figure 4.3 above. These can be filtered down to six options using the reasoning below:

- **SE-L4, SE-L5, SM-L4** and **SM-L5** can be eliminated because their positions are simply too distant with respect to either the departure or arrival planet. A gateway at SM-L4 or SM-L5 will be positioned in the same orbit as Mars. The transfer from Earth to this gateway would therefore be similar to a transfer to Mars. Instead, the spacecraft will have to use additional phasing orbits to travel from the gateway to Mars, which would simply be very inefficient. The same arguments can be made to eliminate the SE-L4 and SE-L5 locations.
- **Em-L3** will not be considered on account of better alternatives. Since the Em-L3 location approximately is the mirrored position of the Moon, it would make more sense to station the gateway in Lunar vicinity. This would allow for research, resource utilization and flyby opportunities.
- **SE-L1** and **SM-L2** will finally also be excluded from the research. It does not make sense to decrease the spacecraft's orbital radius by accelerating to reach SE-L1 to then, subsequently, decelerate to increase the orbital radius and reach Mars. This would not be an effective use of ΔV . Similarly, it would be irrational to target SM-L2 before transferring to Mars.

This results in a total of six locations in the vicinity of a Lagrange point to be considered in this research. All six have been listed in Table 4.5.

Gateway location at Lagrange point	
Earth vicinity	Mars vicinity
Em-L1	SM-L1
Em-L2	
Em-L4	
Em-L5	
SE-L2	

Table 4.5: Overview of the gateway locations in the vicinity of a Lagrange point that will be considered in this research.

With both location categories considered, a total of nine gateway locations are to be considered in the research analyses. For the sake of completeness and overview, all nine have been listed in Table 4.6. The same table gives the shorter names that will be used for these gateway locations in the remainder of this thesis work. Gateway trajectory designs will often be referred to using the short name corresponding to their location.

All gateway locations considered	
Gateway location	Short name
Em-L1	G1
Em-L2	G2
Em-L4	G3
Em-L5	G4
SE-L2	G5
SM-L1	G6
EO	G7
mO	G8
MO	G9

Table 4.6: Overview of all the gateway locations that will be considered along with the names used in this thesis work.

4.5. Gateway orbits

Now that the possible locations of the gateway have been put forward, the motion of the gateway at these locations can be discussed. Similar to the previous section, this section will also be split into two subsections. First, the considerations for the orbits around the central celestial body will be discussed. Secondly, a choice for a Lagrange-Point Orbit (LPO) family is made.

4.5.1. Central orbit

By playing with the six Kepler elements in a simple two-body problem, an endless number of different orbits can be generated. Adding perturbations further increases the complexity of this central orbit library. Careful orbit design considerations are needed to narrow down the orbit options, so that a manageable orbit library is obtained. These considerations are itemized below.

- **Kepler orbits** - For the purpose of this research, orbits can be modelled in the two-body problem. Additionally, no perturbations will be considered. As a result, only Kepler orbits need to be considered. This simplification is justified since the accuracy requirements for the concept comparisons in this feasibility study do not require detailed orbit computations.
- **Circular orbits** - For practical reasons, only circular orbits will be studied. This significantly simplifies rendezvousing with the gateway. Additionally, it cuts down the number of orbits to be considered, since it allows us to focus on three Kepler elements only: inclination, orbital radius and the longitude of the ascending node. Each will be discussed in a separate bullet point.
- **Inclination** - In order to study the effect that the inclination of the gateway orbit has on the objectives, different inclination angles will be considered. Table 4.7 lists the angles that will be considered. As can be seen, these differ for each central planet. These values were carefully selected and carry some physical meaning. The inclination angles for orbits around the Earth are associated with

the Kennedy Space Center and Kourou launch sites. The Lunar inclination angles were arbitrarily chosen to include one near-polar and one near-equatorial orbit inclination. The values for Mars correspond to the Perseverance landing location and to the top of the Exploration Zone (EZ) window.

Inclination angle i [deg]		
Earth	Moon	Mars
28.5	70.0	50.0
5.0	5.0	20.0

Table 4.7: Inclination angles to be considered in this research for each central orbit.

- **Orbital radius** - Similarly to the inclination, different orbital radii will be included. Table 4.8 lists the orbital altitudes to be considered in the research. For Earth, a value corresponding to LEO, MEO and GEO was selected; the orbital altitude for LEO is that of the ISS. The same values are used for Mars' orbit, with the exclusion of the GEO value. Two reasonable orbital altitudes were selected for the Lunar orbit.

Orbital altitude h [km]		
Earth	Moon	Mars
420	150	420
5000	300	5000
35786		

Table 4.8: Orbital altitudes to be considered in this research for each central orbit.

- **Longitude Of Ascending Node** - Since orbits with non-zero inclination angles are considered, the longitude of the ascending node (LOAN) needs to be taken into account. The LOAN is therefore varied from 0 degrees to 345 degrees in steps of 15 degrees to cover the full range of possible orbits.

The list above defines the orbits that will be considered. To illustrate, Figure 4.4 depicts Earth's central orbit library using the definitions above. In this figure, the orbits with an inclination of 28.5 degrees have been coloured blue, whereas the ones with an inclination angle of 5.0 degrees are depicted in green.

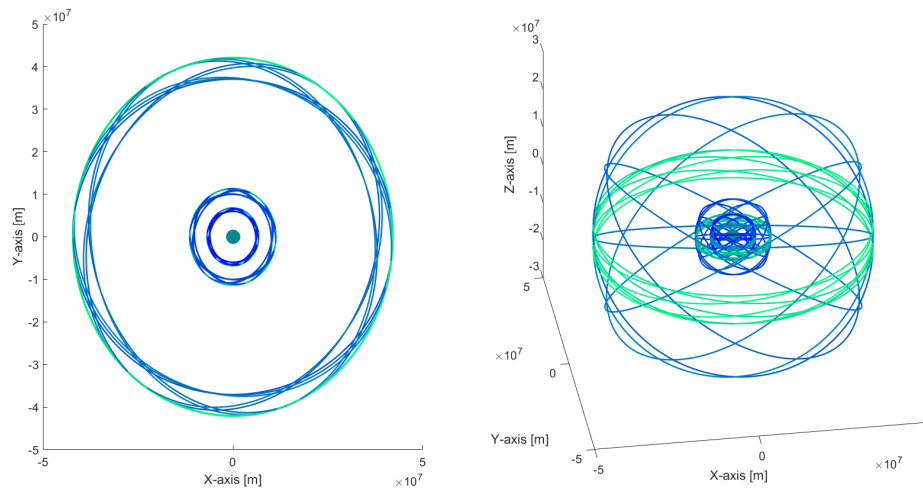


Figure 4.4: Earth central orbit library used in this research.

4.5.2. Lagrange-point orbits

As has been discussed in Section 3.3.2, LPO's can be categorized into different orbit families (i.e. horizontal Lyapunov) depending on their periodic behaviour in the XY-plane and Z-direction. Literature, for example Farquhar [43], emphasizes the benefits that Halo orbits impose over the other orbit families. As a result

of the shape of the Halo orbits, long lasting blackouts as a result of the passing of the secondary body will be avoided. This is illustrated by the drawing by Farquhar on the next page. Also, the absence of major eclipses simplifies thermal control. Furthermore, it enables the establishment of a continuous communication link in the Earth-Moon system. In general, orbit insertion and station-keeping ΔV budgets are favourable as well.

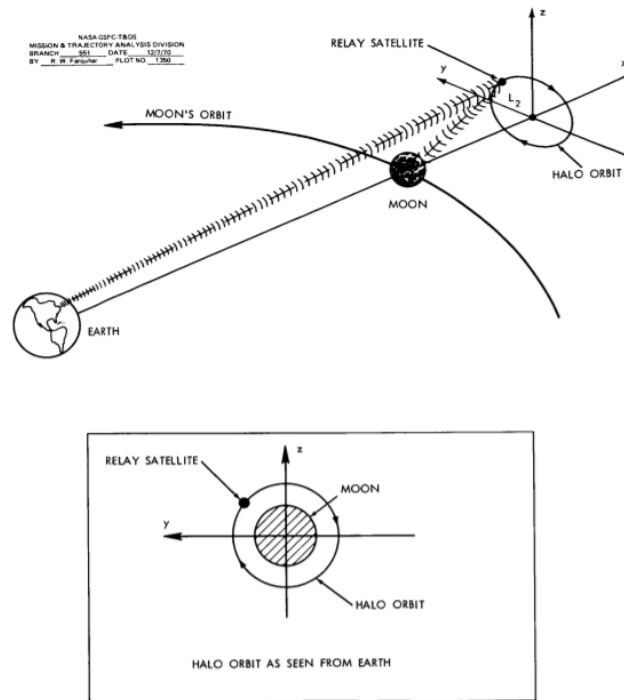


Figure 4.5: Drawing by Farquhar to illustrate benefits of Halo orbits in avoiding so-called blackouts [43].

In accordance with ESA's selection of an orbit from the Halo family for the NASA Lunar gateway, this research will therefore consider orbits from the Halo family for the LPO library used in the coming analyses. To illustrate, Figure 4.6 depicts the LPO library in the CR3BP frame for the Em-L1 location.

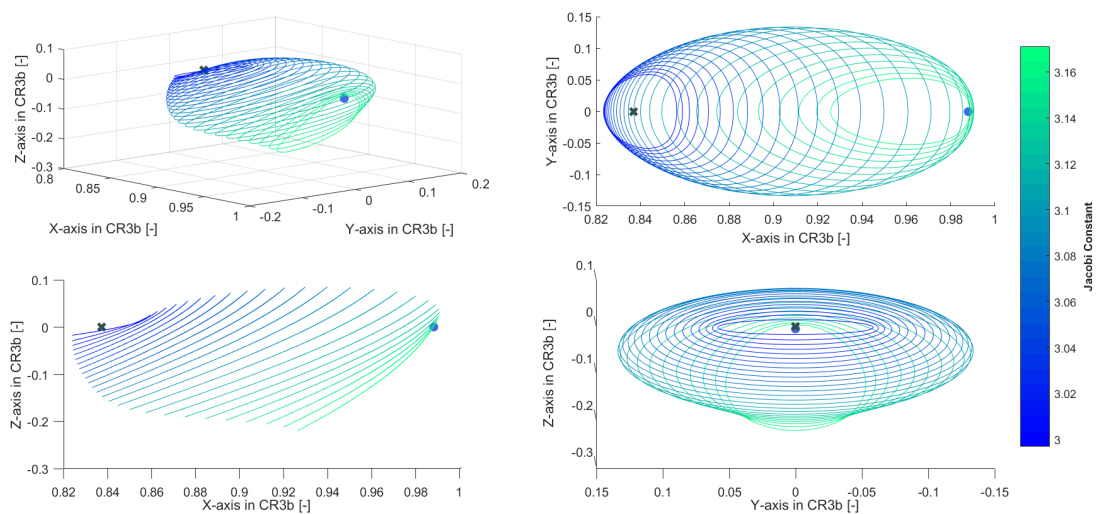


Figure 4.6: LPO library for Em-L1 location.

4.6. Transfers

Lastly, this section will cover what transfers should be considered in this research. As was done earlier, impulsive transfers and continuous transfers will be discussed in separate subsections.

4.6.1. Impulsive transfers

- **Four transfer types** - A total of four different transfer types will be considered: direct transfers, direct + DSM transfers, powered flyby transfers and powered flyby transfers + 1 DSM per leg. All will be modelled using the Lambert targeter, DSM formulation and flyby calculator discussed in Section 3.3.3. All four transfers will be implemented for both the EG- and GM-segment.
- **Three flyby bodies** - Three flyby bodies are considered: Earth, the Moon and Mars.
- **Naming trajectory options** - The four transfer types result in a wide variety of different trajectory options. The trajectory options will be named using the letters for the bodies and using 'd' to denote a DSM. A trajectory that takes the spacecraft from gateway location G1 to Mars using a direct transfer with a single DSM is denoted by 'G1dM'. The trajectory of a spacecraft departing from Earth and performing a sequence of powered flybys at the Moon and Earth to arrive at G5, with an DSM included in each leg, would be denoted by 'EdmdEdG5'.

The four impulsive transfer types have been summarized in Table 4.9 along with an example trajectory for the segment G1M.

Transfer type	Trajectory example
Direct	G1M
Direct + 1DSM	G1dM
Powered flyby	G1mEM
Powered flyby + 1DSM/leg	G1dmdEdM

Table 4.9: Impulsive transfer types to be considered in the thesis research.

A full list of all the trajectories considered for each segment is included in Appendix A.

4.6.2. Continuous-thrust transfers

In Section 4.3 it was concluded that electric propulsion is not suitable for supporting heavy crew transport to Mars. If the assumptions are made that nuclear propulsion systems will enable continuous-thrust transfers and that this technology is ready at the start of the 2030s, continuous-thrust transfers can be considered in this research. However, given the uncertainty of these assumptions, continuous-thrust transfers will only be part of the research as a bonus exercise. The results of these trajectories will only be used for extra insight but will never be used in the comparison of different gateway concepts.

That being said, a decision between the two shaping methods discussed in Section 3.3.3 needs to be made. Two arguments can be made for the selection of the hodographic shaping method:

1. **Free parameters** - The use of free parameters in the hodographic shaping method allows for more flexibility in the optimization process.
2. **Singularities** - A well-known problem of spherical shaping is that the method will not always find a feasible trajectory as a result of the conditions on its curvature. When it is unable to find a solution, the program stops, which makes it highly unsuitable for use in an optimization loop. Hodographic shaping will always find a solution, even if it is a solution that is far from optimal. This allows the hodographic shaping method to be used in an optimization loop.

The following design considerations for continuous-thrust transfers were made:

- **Hodographic shaping method** - The hodographic shaping method will be used to model the continuous-thrust transfers. The argumentation for this choice is given above.
- **Number of revolutions** - Since the transfers involve crew transportation, the TOF of the transfers cannot be too large. A maximum number of revolutions around the central body of zero was therefore set.

- **Transfer options** - Only direct transfers will be considered. Continuous-thrust trajectories involving flybys or impulsive shots are outside the scope of this research.
- **Naming trajectory options** - A continuous-thrust trajectory is denoted by the letter 'c' at the end of the trajectory name. A continuous-thrust transfer between G3 and Mars is therefore denoted by 'G3Mc'.

II

Analyses

5

Analysis A - First filter

This chapter will discuss the first experiment conducted for this thesis research, which is referred to as *Analysis A* throughout this report. Analysis A will be dissected into a number of sections. The first section (Section 5.1) will introduce the analysis and discuss its research purpose. Section 5.2 will then dive into the methodology of the analysis. This methodology was verified using several test cases, which will be discussed in Section 5.3. With the method verified, the results can be presented. This will be done in Section 5.4. The results and their implications for the following analyses can then be discussed in Section 5.5 after which the most significant conclusions are presented in Section 5.6.

5.1. Introduction

As was put forward in Section 4.4, a total of nine gateway locations will be considered in this research. Section 4.6 introduced the various transfer types to be considered, which will result in a large variety of transfer trajectory options for each gateway location. Additionally, for each gateway location numerous potential gateway orbits were defined in Section 4.5. As a result, the total number of different gateway design options is very high. It would simply be too time-consuming and too computationally challenging to perform a detailed analysis of all these designs at this stage, since this would entail performing multiple demanding trajectory optimizations for each design.

Instead, it makes sense to first try to reduce the number of different designs through a preliminary analysis. This analysis can be a simplified, stripped-down version of the analyses that will be performed to select a single trajectory design at a later stage. Although model simplifications will allow for more promptly available results, it is important to carefully design and examine the impact of such simplifications. An analysis method should be developed that allows for filtering out gateway trajectory designs that have no potential, without risking filtering out designs, which do have potential in reality but not in the simplified model. The developed methodology will be discussed in Section 5.2, following the analysis purpose statement below.

Analysis purpose statement:

Analysis A will aim to bring down the total number of feasible gateway design options by using a simplified but effective model to evaluate and compare different designs.

5.2. Analysis methods

This section will discuss the methodology used to successfully accomplish the challenge posed by the purpose statement above. It will do so by splitting the entire method in different subsections. First, in Section 5.2.1, the general method is introduced. In this section, we learn that the analysis will make use of two distinct models: the Impulsive model and the Continuous model, which refers to the mode of propulsion. Each model is then introduced separately in Sections 5.2.2 and 5.2.3, respectively. Although these sections will concern coding programs that were written using the C++ language in Tudat, discussion of code will be kept to a minimum. Instead, these sections will focus on the physics that go into the programs, the capabilities of the programs and the input variables that define the programs. If one is interested in the actual coding of these programs, the reader is referred to the GitHub repository containing all code [44].

Finally, Section 5.2.4 will cover the optimization algorithm used in this analysis and its settings. In order to improve readability, the sections below will be presented using numbered points. Each point will be a standalone characteristic of the methodology and can later be referred to using the section numbering along with its point number.

5.2.1. General method

1. **Single-objective optimization** - In this analysis, all the different trajectory options will be optimized for a single objective. The different gateway trajectory designs can then be compared based on this objective alone.
2. **Objective: minimize ΔV** - Analysis A will aim to find the most optimal trajectory in terms of ΔV budget for each trajectory option considered. In order to fairly compare results between the impulsive-thrust and continuous-thrust transfers, the ΔV outcome is used to compute the OCF using Equation 4.1.
3. **Simplification: Stationary gateways** - In Analysis A, all gateways are assumed to be stationary. Here, stationary is defined as not being in orbit. This automatically excludes the three gateway locations around a celestial body. It further places the remaining six gateway options at the exact location of their corresponding Lagrange point. The gateway locations considered in Analysis A are listed in Table 5.1.

Gateway name	Gateway location
G1	Em-L1
G2	Em-L2
G3	Em-L4
G4	Em-L5
G5	SE-L2
G6	SM-L1

Table 5.1: Naming of gateway locations studied in Analysis A.

4. **Simplification: Isolated optimization** - The Earth-Mars transfer is split into two segments: the EG- and GM-segment. In this analysis, each segment will be optimized individually. This means that the gateway arrival epoch of the optimal solution for the EG-segment might be later than the departure epoch of the solution for the GM-segment. This is visualized in Figure 5.1. Analysis B and C will use a more complex trajectory model, which carefully matches the transfer segment timing.

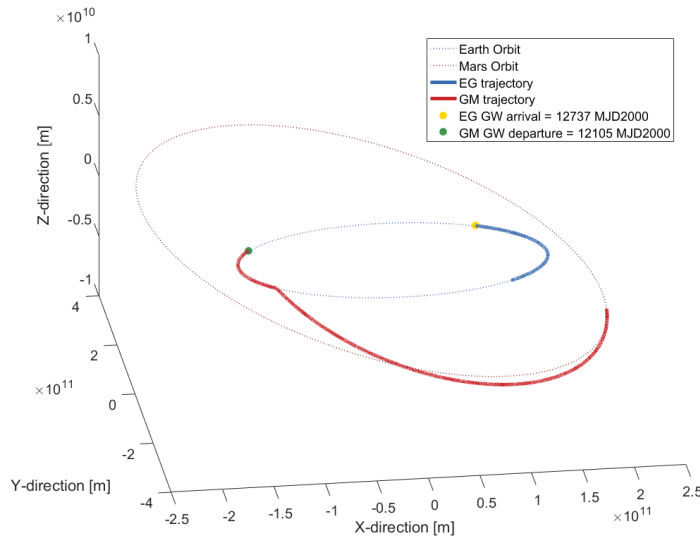


Figure 5.1: Figure illustrating the concept of the isolated segment optimization performed in Analysis A.

5. **Trajectory options** - The trajectory options to be considered in this analysis result from the combination of gateway locations, segments, thrust type and transfer type. The gateway locations and segments considered in this analysis have been introduced above. Analysis A will look at both impulsive-thrust transfers and continuous-thrust transfers, whose transfer types have been discussed in Section 4.6. Figure 5.2 provides insight into how all trajectory options are generated, using an example G3 trajectory. A full list of all trajectory options considered, can be found in Appendix A.

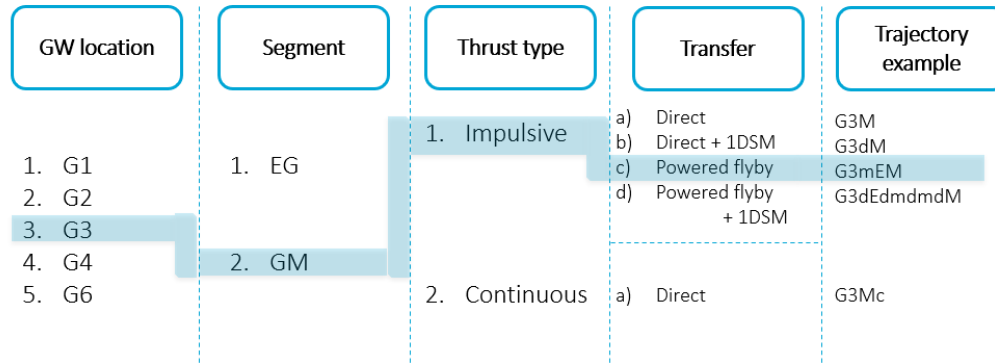


Figure 5.2: Overview of trajectory options generation for Analysis A.

The highlighted trajectory example (*G3mEM*) represents a transfer departing from the G3 location (Em-L4) that includes a sequential Lunar and Earth flyby before arriving at Mars parking orbit.

6. **TOF constraints** - Although a single-objective ΔV optimization is performed, the TOF cannot be disregarded completely. TOF constraints are therefore implemented in Analysis A. These TOF constraints are presented in Table 5.2. If a trajectory's TOF is higher than the corresponding constraint, its fitness will be penalized as to erase it.

Segment	Gateway		
	G1-4 [days]	G5 [days]	G6 [days]
EG	25	100	365
GM	365	365	100

Table 5.2: TOF constraints for each segment in Analysis A.

7. **Seeds** - To increase certainty that the global optimum was found for each trajectory, the optimization will be performed for a total of five different seed numbers. These seed numbers are used to generate quasi-random numbers in the optimization loop. The following five seed numbers were used throughout Analysis A: 123, 456, 654, 789, 987.
8. **Ephemeris settings** - The locations of all planets and all Lagrange points are computed using the most recent SPICE ephemeris data. Table 5.3 lists all SPICE files used. Analysis A, like all other analyses, uses the ECLIPJ2000 reference frame and places the Sun at its origin.

Setting	SPICE filename
Leapseconds	naif0012.tls
Main kernel	de440.bsp
Mars kernel	mar097.bsp
Jupiter kernel	jup343.bsp
Saturn kernel	sat428.bsp
Uranus kernel	ura115.bsp
Neptune kernel	nep095.bsp
Pluto kernel	plu055.bsp
Begin time	1990 JAN 01
End time	2060 JAN 01

Table 5.3: SPICE settings used in Analysis A.

9. **Program structure** - Both programs (CT and IT) share the same program structure. This structure is shown in the pseudo-code below.

Algorithm 1: General structure of programs in Analysis A.

```

Define Global parameters;
for gateway : Gateways options do
  for segment : Segment options do
    Define All trajectory options;
    for trajectory : Trajectory options do
      Define Trajectory specific parameters;
      for seed : Seed options do
        Load problem to be optimized;
        Perform Optimization;
        Save Populations and Fitness files;
      end
      Create trajectory for best Individual for seed number that resulted in best fitness;
      Save all relevant results for trajectory;
    end
  end
end

```

The two programs will be further discussed in the following two sections.

5.2.2. IT method

1. **Algorithm** - This program was built using the Lambert targeter algorithm by D. Izzo [32] to solve Lambert's problem. Section 3.3.3 has discussed both the Lambert problem and the targeter by Izzo. This targeter can solve a variety of different trajectory legs: A departure leg, a departure leg followed by a DSM, a swingby leg, a swingby followed by a DSM leg, and a capture leg.
2. **Transfer Types** - As a result, the program is capable of designing all four impulsive trajectory types: direct transfers (IT-DT), 1-DSM transfers (IT-1DSM), Multi-Gravity-Assist transfers (IT-MGA) and Multi-Gravity-Assist transfers with one DSM in each leg (IT-MGADSM). The IT-DT and IT-1DSM trajectories all consist of only two legs: a departure leg and a capture leg. Each swingby in the IT-MGA and IT-MGADSM trajectories adds another leg, either a swingby leg or a swingby+1DSM leg, respectively.
3. **Parameterization** - The trajectories without a DSM are parameterized using the initial position vector, the final position vector, and the time-of-flight (TOF) for each leg. Since the initial and final position can be extracted from the ephemeris information of the departure and arrival planet or gateway location, a leg can be characterized by a departure date and leg TOF only. Adding a leg to a trajectory, only adds a single parameter, since the departure date is the final time of the previous leg. Each DSM that is added to the trajectory, adds a total of four parameters to the

variable vector. DSMs are formulated using the velocity formulation (which was argued in Section 3.3.3). The number of parameters in the variable vector for a specific trajectory can then be expressed using Equation 5.1 below.

$$N_{param} = N_{Legs} + 4 \cdot N_{DSM} + 1 \quad (5.1)$$

Table 5.4 lists the design variables that are added for each leg type. The number of parameters for the different leg types is 2, 6, 1, 5 and 0, respectively. To illustrate, a *EdmdG1* trajectory would consist of eleven design variables; eight variables to model the two DSMs, two leg TOF's and one departure date.

N_{param}	Leg type				
	Departure	Departure + 1DSM	Swingby	Swingby + 1DSM	Capture
1	Departure date	Departure date (T_0)	Leg TOF	Leg TOF	-
2	Leg TOF	Leg TOF		TOF fraction of DSM (η)	
3		TOF fraction of DSM (η)		pericenter radius GA (r_p)	
4		excess velocity (V_∞)		rotation angle GA (β)	
5		in-plane angle (θ)		ΔV performed at GA	
6		out-of-plane angle (ϕ)			

Table 5.4: Parameterization of each leg type used in the IT program for Analysis A.

In Table 5.4, the excess velocity, in-plane angle and out-of-plane angle refer to the velocity relative to the departure planet.

- Parameter Bounds** - The trajectory parameters can take on any values within the bounds defined in the program. Three types of bounds were defined: departure date bounds, TOF bounds and DSM bounds. The TOF bounds are programmed to vary depending on the leg. This means that the upper TOF bound for a trajectory from Earth to Mars will be larger than a trajectory between Earth and the Moon for instance. The DSM bounds are dependent on the legtype (departure or swingby) as can be seen in Table 5.4 above. The pericenter radius r_p for the swingby+1DSM leg is dependent on the planet at which the Gravity Assist (GA) is performed. The departure date bounds are constant: the lower bound is placed on the 1st of January 2030 and the upper bound is defined 5 years later on the 1st of January 2035. An overview of the different bounds and their values is given in Table 5.5.

Bound type	Bound	Lower	Upper
Departure	Departure date [MJD200]	10958	12784
TOF	TOF of leg [days]	<i>Leg dependent (see Tab. 5.6)</i>	
DSM-Dep	TOF fraction DSM [-]	0.01	0.99
	Excess velocity V_∞ [m/s]	0	5000
	In-plane angle (θ) [rad]	0	2π
	Out-of-plane angle (ϕ) [rad]	$-\frac{\pi}{2}$	$\frac{\pi}{2}$
DSM-GA	TOF fraction DSM [-]	0.01	0.99
	Rotation angle GA (b_{incl})	$-\pi$	π
	Pericenter radius GA (r_p) [-]	<i>Leg dependent (see Tab. 5.7)</i>	
	ΔV performed at GA [m/s]	0	2000

Table 5.5: Bounds used for the design variables used in the IT program for Analysis A.

- Leg TOF** - As was discussed above, the values for the bounds placed on leg TOF are dependent on what trajectory the leg describes. The TOF of a leg between Earth and the Moon naturally is less than that of a transfer between the Earth and Mars. Table 5.6 shows the bounds on TOF for all legs that were considered in Analysis A. The notation of a leg is as follows: the first letter refers to the departure planet and the last letter to the arrival location. Legs that depart or arrive at a gateway, use the letter of the celestial body that is the secondary body in the corresponding three-body system. In this way, a leg between Earth and a gateway at EM-L2 has the same bounds on TOF as a leg between Earth and the Moon. The values of these bounds were inspired by problems in the GTOP library [45].

Leg	Bounds [days]	
	Lower	Upper
EE	1	100
Em	1	100
EM	100	365
mm	1	100
mE	1	100
mM	100	365
ME	100	365
Mm	100	365
MM	1	100

Table 5.6: TOF bounds for each leg considered in the IT program for Analysis A.

6. **Flyby Pericenter Radius** - As was discussed in point 3 and can be seen in Tables 5.4 and 5.5, the distance from the celestial body at which a swingby is performed is a design variable for the swingby+1DSM leg. This variable can best be expressed using a factor multiplying the radius of the target celestial body. These minimum pericenter radii were already discussed in Section 3.3.3 but have been repeated in Table 5.7 below.

Body	R_p [km]	r_{pmin} [R_p]	h_{pmin} [km]	Mission
Earth	6378	1.048	306	Galileo
Mars	3397	1.076	257	Rosetta
Moon	1737	1.01	17	-

Table 5.7: Pericenter factor bounds for the flybys considered in the IT program for Analysis A.

7. **Boundary conditions** - The program allows eccentricity (e) and semi-major axis (a) information to be inputted as to impose boundary conditions on the departure and arrival of the leg. To adhere to the boundary conditions introduced in point 8 of Section 5.2.1, the parameters in Table 5.8 were used. The eccentricity values are set to 0 for all three since this corresponds to a circular parking orbit. For circular orbits, the semi-major axis simply equals the radius of the orbit, which is the sum of the planetary radius and the orbital altitude. To account for the rendezvous boundary condition for departure from and arrival at the gateway, a trick is used. This trick sets the semi-major axis to infinity, so that the orbital velocity is zero. As a result, the spacecraft will precisely match the state of the Lagrange point at the gateway and the orbital velocity of the parking orbit at Earth and Mars.

Point	e	a [km]
Earth	0	R_E+250
Mars	0	R_M+250
Gateway	0	∞

Table 5.8: Boundary conditions used in the IT program for Analysis A.

8. **Program code** - As has been stated, all program code can be found in the author's Github repository [44]. Together with the parameter definitions in the points above, this will allow all results to be replicated.

5.2.3. CT method

1. **Algorithm** - The continuous-thrust program makes use of the hodographic shaping algorithm developed by Gondelach for his thesis in 2012 [38]. This method has been explained in Section 3.3.3. This is a shaping method, so it uses a simplified, unperturbed model to shape trajectory designs for continuous-thrust transfers.

2. **Shaping base functions** - The program makes use of a Tudat module that selects the most suitable base functions. This module is based on recommendations made by Gondelach in his research [38]. The automatic selection of base functions is essential to this research, since it would be impossible to manually select suitable base functions for each trajectory analysed in this work.
3. **Parameterization** - As has been explained in Section 3.3.3, a hodographic shaped trajectory can be characterized given the begin- and endpoint and the TOF of the trajectory. Since the begin- and endpoint locations are given for any date in the ephemeris data, only the departure date and the TOF of the leg need to be defined. Additionally, the design vector consists of five free shaping coefficients: two in the radial direction, zero in the normal direction and three in the axial direction. The next point, point 4, introduces three additional design variables that were included in the optimization.
4. **Boundary conditions** - In most research and thesis papers, the begin- and endpoint of the trajectory to be designed are simply the state vectors of the two celestial bodies that the transfer aims to connect. These trajectories are often referred to as 'rendezvous' trajectories. The departure from or arrival at a gateway can be modelled as a rendezvous since the gateways are assumed to be stationary. This, however, is not the case for the departure or arrival at Earth and Mars. Doing so would not consider the ΔV needed to escape or enter the celestial body at the beginning or end of the trajectory. In order to overcome this, some model modifications were made. As a simplification, the position vector of the spacecraft can be assumed to be the same as that of the departure and capture planet. This can be done, since the radius of the sphere of influence of the planets at focus (Earth and Mars) is negligibly small on the scale of the Solar System. The velocity vector of the spacecraft at the boundaries will be the planet's velocity vector plus the vector of the hyperbolic excess velocity (V_∞):

$$S_{s,c} \approx [x_P, y_P, z_P, \dot{x}_P + V_{\infty,x}, \dot{y}_P + V_{\infty,y}, \dot{z}_P + V_{\infty,z}] \quad (5.2)$$
 The three components of the hyperbolic velocity vector will be added to the design variables of the optimization problem. This can be done, since there is a relation between this hyperbolic excess velocity and the trajectory's ΔV . This relation will be explained in the next point. This modification adds only three design variables to the problem for each trajectory since each trajectory will either begin or end by rendezvousing the gateway, but never both.
5. **Parameter bounds** - The continuous-thrust program thus makes use of a total of ten parameters to model the trajectories to be optimized. The values that these parameters can take on were restricted by bounds. The individual parameter bounds are shown in Table 5.9.

N_p	Parameter meaning	Bound	
		lower	upper
1	Departure date [MJD2000]	10958	12784
2	Time of Flight [days]	segment dependent (Table 5.2)	
3	Free coefficient r_1 [-]	-10000	10000
4	Free coefficient r_2 [-]	-10000	10000
5	Free coefficient z_1 [-]	-10000	10000
6	Free coefficient z_2 [-]	-10000	10000
7	Free coefficient z_3 [-]	-10000	10000
8	$V_{\infty,x}$ [m/s]	-5000	5000
9	$V_{\infty,y}$ [m/s]	-5000	5000
10	$V_{\infty,z}$ [m/s]	-5000	5000

Table 5.9: Parameter bounds of the design variable used in the CT-program for Analysis A.

The continuous-thrust program makes use of the same launch window as is used in the impulsive-thrust program. Furthermore, also the same TOF limitations were put in place. The free coefficient bounds were inspired by the work done by Gondelach [38]. Finally, the bounds on hyperbolic excess velocity allow for great freedom in start- and end-conditions but are limited to realistic values.

6. **ΔV computation** - The ΔV needed to either escape the departure planet with the hyperbolic excess velocity ($V_{\infty,d}$) or be captured after arriving at the destination planet with a hyperbolic entry velocity ($V_{\infty,a}$) needs to be added to the ΔV used during the continuous-thrust transfer. This is done using the simple physics shown in equations 5.3 to 5.7.

$$\Delta V_{total} = \Delta V_d + \Delta V_{ct} + \Delta V_a \quad (5.3)$$

$$\Delta V_d = \sqrt{V_{esc,d}^2 + V_{\infty,d}^2} - V_{c,d} \quad (5.4)$$

$$\Delta V_a = \sqrt{V_{esc,a}^2 + V_{\infty,a}^2} - V_{c,a} \quad (5.5)$$

$$V_{esc} = \sqrt{\frac{2\mu_p}{R_p + h_p}} \quad (5.6)$$

$$V_{\infty} = \sqrt{V_{\infty,x}^2 + V_{\infty,y}^2 + V_{\infty,z}^2} \quad (5.7)$$

$$V_c = \sqrt{\frac{\mu_p}{R_p + h_p}} \quad (5.8)$$

The total ΔV of the transfer is the sum of the ΔV 's of the departure, the continuous-thrust transfer, and the arrival, shown in Equation 5.3. Equations 5.4 and 5.5 show how the hyperbolic excess velocity influences the ΔV budget at departure and arrival. In these equations, the velocity in parking orbit is denoted by V_c and the escape velocity in this orbit is denoted by V_{esc} . As has been discussed in Section 5.2.1, the parking orbits at Earth and at Mars are both 250 km in altitude.

7. **Number of revolutions** - Another input for the hodographic shaping algorithm is the number of full revolutions that the trajectory is allowed to make around the central body, the Sun in this case. For this analysis, the maximum number of full revolutions was set to zero. This was done to prohibit the program to try to shape trajectories that will never adhere to the TOF constraints imposed.

5.2.4. Optimization method

Since this analysis involves a single-objective optimization, a single-objective optimization algorithm is to be used. Selecting and subsequently tuning such an algorithm can be a very delicate and time-consuming process. Luckily, this thesis could rely on the work done by Musegaas for his thesis report in 2012 [5]. In this work, Musegaas researched the performance of the Differential Evolution (DE), Genetic Algorithm (GA) and Particle Swarm Optimizer (PSO) algorithms. The optimization algorithms were tuned by evaluating their performance on a total of 24 test cases. These test cases involved different variations of MGA and MGADSM transfers to Saturn. It was found that the tuned version of the DE optimizer was able to outperform all other DE algorithms encountered in literature. The models in this thesis work are based on the models by Musegaas. The test cases used by Musegaas are more complex versions of the transfer problems that will be optimized in Analysis A. As a result, the DE optimizer using the settings proposed by Musegaas is expected to provide accurate results in Analysis A. The optimization algorithm used in Analysis A is listed below.

Algorithm	F value	CR value	Strategy	Population size
DE	0.7	0.90	1 (best/1/exp)	$N_{pop} = 4.5 * N_{param}$

Table 5.10: Optimizer settings for Analysis A.

The number of generations was set to a number high enough to guarantee that the optimizer had converged to a single ΔV value. For analysis A, the number of generations was set to $750 \cdot N_{param}$. The convergence rate of the results was closely monitored in the process of producing results. Due to the high rates of convergence observed (discussed into more detail in Section 5.5), no further need for optimizer tuning was identified at this stage.

5.3. Verification

Analysis A will make use of the above-described methodology to produce the results needed to provide answers and insight concerning the analysis' purpose. However, for these results to be trustworthy, it is of utmost importance that the methods described are verified first. Three different verification steps were performed:

1. Verification of gateway locations
2. Verification of IT program
3. Verification of CT program

Each step will be covered individually in the sections that follow.

5.3.1. Gateway locations

The gateway locations in Analysis A coincide with six different Lagrange points. The states of these Lagrange points need to be formulated in the ECLIPJ2000 reference frame with the Sun at its origin. To this extent, first the locations of the Lagrange points in the CR3BP frame needed to be found. Subsequently, these locations had to be translated to locations in the Cartesian reference frame of interest. Verification was performed for both steps and will be presented separately below.

Lagrange points in CR3BP frame

Table 5.11 compares the locations found in this research with those found in literature for the Em-system. The verification step has been performed twice: once using the exact same value for the gravitational parameter μ as Van der Ham [6] and James [46] used and once using the gravitational parameter taken from the most recent SPICE files (see Table 5.3). Van der Ham and James have used $\mu = 0.012153$, whereas this thesis will use the SPICE defined value of $\mu = 0.0121506$. The μ_{lit} column in Table 5.11 verifies the methods used to locate the Lagrange points in the CR3BP frame in this thesis. The μ_{spice} column shows the locations used in this thesis work, which are slightly different as a result of the small difference in gravitational parameter used.

Em-LP	Literature				Thesis			
	Van der Ham [6]		James [46]		μ_{lit}		μ_{spice}	
	x [-]	y [-]	x [-]	y [-]	x [-]	y [-]	x [-]	y [-]
L1	0.8363	0	0.836293	0	0.83629	0	0.83692	0
L2	1.156	0	1.15617	0	1.15617	0	1.15568	0
L4	0.4878	0.866	0.487723	0.866025	0.48772	0.86603	0.48785	0.86603
L5	0.4878	-0.866	0.487723	-0.866025	0.48772	-0.86603	0.48785	-0.86603

Table 5.11: Verification of the Em- system Lagrange points in the CR3BP frame.

Table 5.12 shows the verification of the Lagrange points of interest in the SE- and SM-systems. It can be seen that the differences in the gravitational parameter in literature and in SPICE are smaller for these two systems. Using the μ_{lit} value, the literature results were reproduced.

LP	Literature		Thesis			
	Van der Ham [6]		μ_{lit}		μ_{spice}	
	x [-]	y [-]	x [-]	y [-]	x [-]	y [-]
SE-L2	1.01003	0	1.01003	0	1.01008	0
SM-L1	0.995251	0	0.99525	0	0.99525	0

Table 5.12: Verification of the remaining Lagrange points in the CR3BP frame.

Based on Tables 5.11 and 5.12, it can be concluded that the gateway locations in the CR3BP frame have been verified.

Lagrange points in Cartesian frame

The methodology to transform states from the CR3BP frame to the Cartesian Sun-centred frame, described in Section 3.3.1, was developed for this thesis specifically. Therefore, it is especially important to verify the validity of this transformation. To this extent, the states of the Lagrange points in the SE-system were computed for a full period of one year and compared to available SPICE data. The SPICE kernels were generated by Min-Kun Chung of the Navigation and Mission Design Section at JPL on August 29, 2013 [47]. For the purpose of this verification, only the results of the SE-L1 verification have been plotted below. As can be seen, the states computed in this thesis are very similar to the SPICE states. To confirm this, Figure 5.4 shows the difference in the norm of the position and velocity vector for all four Lagrange points over a period of five years. The periodic difference in velocity was researched and is the result of the use of slightly different gravitational parameters μ_1 and μ_2 in Equation 3.15. Unfortunately, the μ -values used by Chung were not documented, so that the exact results could not be replicated. Instead, the μ -values were taken from the most recent SPICE files. The differences are in the order of 10^{-13} % and 10^{-3} % for the position and velocity, respectively. This is acceptable for the purpose of this thesis.

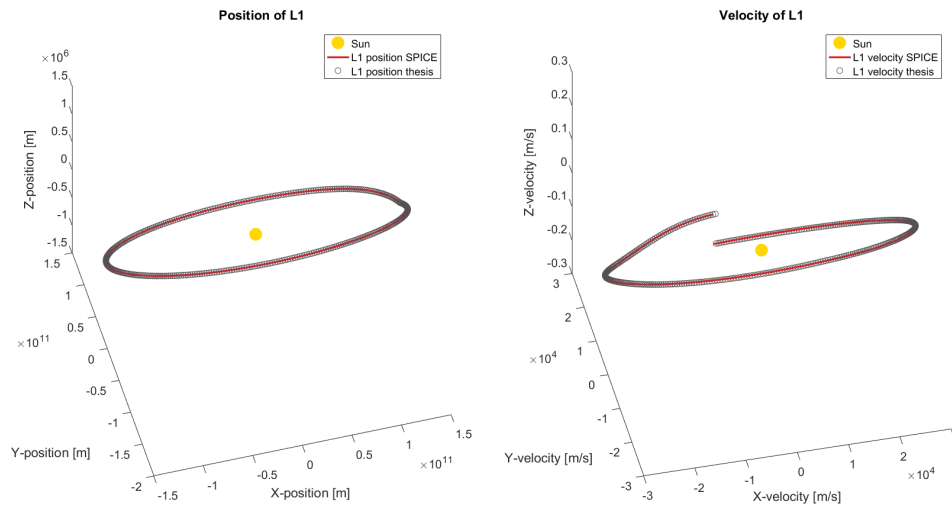


Figure 5.3: Comparison between the SE-L1 states computed in this thesis and the tabulated state of SE-L1 from the SPICE library.

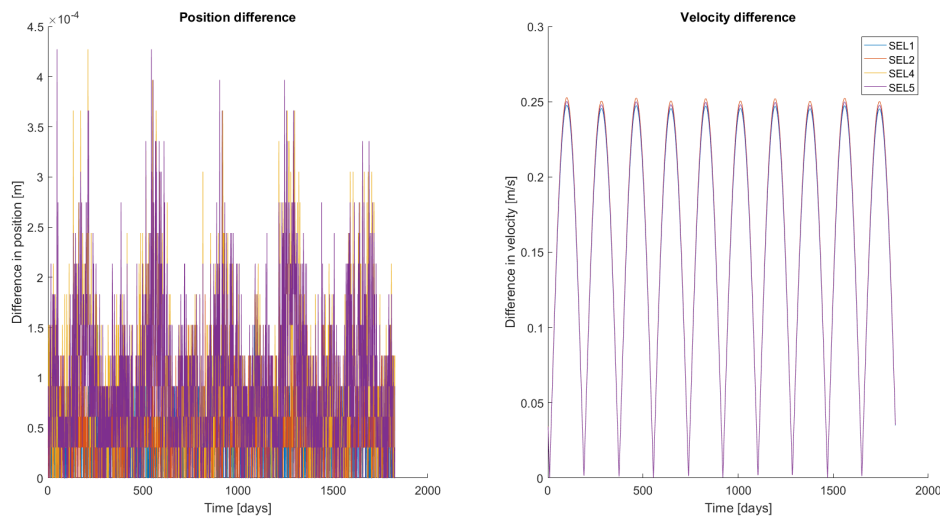


Figure 5.4: Difference between the norms of the SE-LP states computed in this thesis and the SPICE library.

Figures 5.3 and 5.4 show that the transformation between the CR3BP frame and the Cartesian Sun-centred frame is verified. This, in combination with the verification of the Lagrange-point locations in the CR3BP frame, means that the gateway locations in analysis A are correct.

5.3.2. Impulsive-thrust transfers

The impulsive-thrust program, described in Section 5.2.2, was verified using two test cases: the *EVVEJSN* powered swingby trajectory test case taken from the thesis work by Melman [7] and the Cassini2 test case (*EdVdVdEdJdS*) taken from Musegaas' work [5]. The first test case by Melman was performed to verify that trajectories without DSMs are correctly modelled by the program, whereas the second test case had to verify that DSMs are also correctly modelled. Both test cases involve complex trajectories with multiple flybys, which means two things: first, the trajectories all rely on a Lambert targeter, which would also be used for a transfer without flybys. Second, the multiple flybys result in a high number of design variables. The trajectories in Analysis A will be of lower complexity and as a result will have fewer design variables. If the test cases can be optimized successfully, it is expected that the same will be true for all trajectories in Analysis A.

Trajectories w/o DSMs

In his thesis, Melman [7] set out to design a mission from Earth to Neptune using multiple flybys. It was concluded that a trajectory with two consecutive Venus flybys followed by an Earth, Jupiter and Saturn flyby resulted in an optimum trajectory in terms of ΔV . In the notation of this thesis, the trajectory is denoted by 'EVVEJSN'. Melman considered powered flybys only. For verification purposes, the same trajectory was optimized using the same bounds on the design variables. The precise set-up of the test case and the parameter bounds can be found in the report by Melman [7]. The results obtained are compared to Melman's results in Table 5.13. A very similar optimum trajectory is found, so that the program's capability to design transfers without DSMs has been validated.

Planet	Melman			Verification		
	Date [MJD2000]	TOF [days]	ΔV [km/s]	Date [MJD2000]	TOF [days]	ΔV [km/s]
Earth	4528	Launch	1.5972	4527	Launch	1.629
Venus	4695	167	0.0010	4696	169	0
Venus	5098	403	0.0030	5098	402	0
Earth	5746	648	0.0094	5745	647	0
Jupiter	6571	825	0.4172	6610	865	0.396
Saturn	7835	1264	0.0081	7847	1237	0
Neptune	10944	3109	3.7831	10958	3111	3.775
		<u>Total TOF:</u>	<u>Total ΔV:</u>		<u>Total TOF:</u>	<u>Total ΔV:</u>
		17.57 years	5.82 km/s		17.61 years	5.80 km/s

Table 5.13: Results of the Melman test case used to verify the ability to design trajectories without DSMs.

Trajectories w/ DSMs

The Cassini2 test case is popular among researchers looking to validate or tune trajectory design programs that have flyby and DSM modelling capabilities. The problem, based on the Cassini mission, describes a transfer between Earth and Saturn using a double Venus flyby followed by a consecutive Earth and Jupiter flyby. Between the powered flybys, the spacecraft is allowed to perform a single DSM. The trajectory notation therefore is 'EdVdVdEdJdS'. In his research, Musegaas [5] made use of this test case to tune his algorithms. The test case setup was taken from Musegaas' thesis report [5] but can also be taken from the GTOP library [45]. Table 5.14 shows the outcomes of this verification step compared to Musegaas' results.

Planet	Musegaas			Verification		
	Date [MJD2000]	TOF [days]	ΔV [km/s]	Date [MJD2000]	TOF [days]	ΔV [km/s]
Earth	-785.11	Launch	3.03	-784.57	Launch	3.06
Venus	-617.77	167.34	0.57	-616.66	167.91	0.54
+DSM		$\eta_2 = 0.55$	0.39		$\eta_2 = 0.55$	0.40
Venus	-188.79	428.98	0.0	-188.02	428.64	0.0
Earth	-134.65	54.14	0.0	-134.49	53.53	0.0
Jupiter	455.28	589.93	0.0	454.14	588.63	0.0
Saturn	2655.28	2200.00	4.25	2654.14	2200.00	4.25
		<u>Total TOF:</u>	<u>Total ΔV:</u>		<u>Total TOF:</u>	<u>Total ΔV:</u>
		9.42 years	8.24		9.41 years	8.24

Table 5.14: Results of the Musegaas test case used to verify the ability to design trajectories with DSMs.

As can be seen in the table above, the results obtained in this research closely match those of the test case. It was found that the inclusion of a DSM is only beneficial when it is performed in the second leg between Venus and Venus. As a result, it was concluded that the program developed to model impulsive-thrust trajectories in this thesis is capable of producing thrust-worthy results.

The verification results in Tables 5.13 and 5.13 show the best result taken from the five seed values discussed in point 7 of Section 5.2.1. For both verification steps, the results for all five seeds showed a convergence of within 0.1% of the optimal ΔV value. Based on this, it was decided that the use five seed values should be sufficient.

5.3.3. Continuous-thrust transfers

The implementation of the hodographic shaping method was verified using an Earth-Mars transfer as a test case. The same test case was used by Gondelach [38] in his thesis work. The transfer is simplified by having the spacecraft describe a so-called 'rendezvous' transfer, which means the begin- and end-state of the spacecraft coincide with Earth's and Mars' barycenter at departure and arrival, respectively. This verification step should verify if the automatic selection of base functions is capable of producing results similar to those when manually selecting and tuning the base functions. To this extent, the produced results will be compared to the best- ΔV solutions for low-order and different high-order algorithms by Gondelach. The result comparison can be seen in Table 5.15 below. The top six solutions were produced by Gondelach, whereas the bottom solution was produced by the program used for in thesis.

V_r	V_θ	V_z	Departure [MJD2000]	TOF [days]	ΔV [km/s]	f_{max} [$10^{-4} \frac{m}{s^2}$]
CPowPow2	CPowPow2	CosR5P3CosR5P3SinR5	10025	1050	6.342	1.51
CPowCos PCos	CPowCos PSinPCos	Cos25Pow6P6Cos25	9205	1200	5.807	1.39
CPowPow2 PCos	CPowPow2 PSinPCos	CosR5P3CosR5P3SinR5	9225	1180	5.803	1.32
CPowSin05 PSinPCos	CPowSin05 PSinPCos	CosR5Pow3P3CosR5 P3SinR5	9215	1200	5.783	1.21
CPowCos PSinPCos	CPowCos PSinPCos	CosR5P3CosR5P3SinR5 P4CosR5P4SinR5	9945	1160	5.773	1.41
CPowPow2 PSin05PCos05	CPowPow2 PSin05PCos05	CosR5P3CosR5P3SinR5 P4CosR5P4SinR5	9985	1100	5.771	1.50
Thesis blackbox (automated function selection)			9252	1118	5.834	1.50

Table 5.15: Verification of continuous-thrust program using Gondelach's low- and high-order solutions on Earth-Mars transfer test case [38].

As can be seen in the Table 5.15, the results obtained using the continuous-thrust program on the test case are very similar to the results produced by Gondelach. Without extensive tuning of the optimization algorithm or the shape base functions, the program developed for this thesis is capable of producing results that match simple high-order results by Gondelach. For the purpose of this thesis, the continuous-thrust program is therefore verified.

Two aspects of the methodology of this analysis needed to be verified: The computation of the gateway locations and the trajectory design between Earth, the gateway, and Mars. Section 5.3.1 has shown that the Lagrange-point locations are correctly generated in the CR3BP frame and subsequently properly translated to the Cartesian Sun-centred frame. In this analysis, the gateway positions coincide with the Lagrange-point positions. As a result, the gateway positions have been verified. Next, Sections 5.3.2 and 5.3.3 have verified the ability to design both impulsive-thrust and continuous-thrust transfers, respectively. It can therefore be concluded that the methods used in analysis A have been verified, so that its results hold scientific value.

5.4. Results

The outcomes of the methods discussed above will be given in this section. As has been stated, the purpose of analysis A is to evaluate and compare different gateway trajectory designs with the goal of possibly filtering out gateway locations to be considered in the analysis that follows. To this extent, a table of all impulsive-thrust trajectory outcomes per segment will be shown for each gateway location (G1 to G6 in Table 5.1). The tables will give the ΔV budget and the TOF for each trajectory that was optimized. The tables will display the best results, so for the seed value that produced the lowest ΔV solution. Additionally, the tables will feature information on the accuracy of these results in the form of a convergence number between 1 and 5. A convergence number of 5 means that the optimization outcomes for all five seed numbers are within the convergence range displayed on the top of the table. Two ranges were considered: $< 0.1\%$ and $< 1\%$. To illustrate, an optimum ΔV solution of 3.510 km/s will lead to a convergence range of 3.51 m/s and 35.1 m/s for the respective ranges.

In addition to the tables, each results section will feature a figure displaying the trajectory of the best solution for each segment. This is to provide insight into the geometry of the transfers for that gateway location. No further decision-making will be made based on these figures, which is why only one trajectory for each segment is plotted. Important to note is that the scale of the Z-axis in these figures is different from that of the X- and Y-axes. This was done deliberately, as it amplifies inclination changes in the trajectories. However, as a result subtle changes in direction can seem drastic in these figures.

After the impulsive-thrust results have been presented for all six individual gateways, a seventh section is added. This section will produce the results obtained by the continuous-thrust program. Since only a single trajectory was optimized for each segment, all results can be presented in a single table and a single figure.

5.4.1. G1 (Em-L1)

G1 (Em-L1)

EG					GM				
Trajectory	ΔV [km/s]	TOF [days]	<0.1% [-/5]	<1% [-/5]	Trajectory	ΔV [m/s]	TOF [days]	<0.1% [-/5]	<1% [-/5]
EEG1	4.076	25.000	5	5	G1M	4.812	192.915	5	5
EdEdG1	4.074	24.952	5	5	G1dM	4.210	277.750	5	5
EG1	4.071	25.000	5	5	G1dEdmdM	3.978	298.148	4	5
EdG1	4.071	25.000	5	5	G1EmM	3.923	271.879	5	5
EdmdG1	3.737	25.000	5	5	G1EM	3.720	254.709	5	5
EmG1	3.510	25.000	5	5	G1dEdM	3.669	285.964	5	5
					G1mM	3.401	197.309	5	5
					G1dmdM	3.392	248.912	5	5
					G1mEM	3.169	206.234	4	5
					G1dmdEdM	3.148	289.566	2	4

Table 5.16: Optimization results for each trajectory considered for G1.

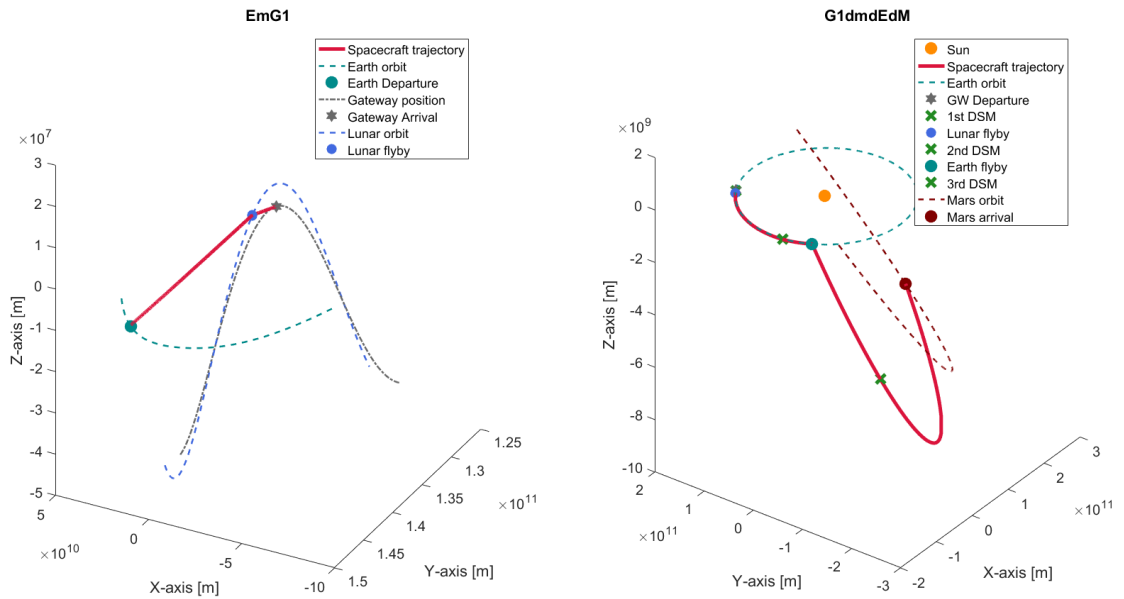


Figure 5.5: Plot of the best trajectory of each segment for G1.

5.4.2. G2 (Em-L2)

G2 (Em-L2)

EG					GM				
Trajectory	ΔV [km/s]	TOF [days]	<0.1% [-/5]	<1% [-/5]	Trajectory	ΔV [m/s]	TOF [days]	<0.1% [-/5]	<1% [-/5]
EdmdG2	4.404	25.000	5	5	G2M	4.614	191.546	5	5
EdEdG2	4.399	24.998	5	5	G2dEdmdM	4.295	297.392	2	5
EEG2	4.396	25.000	5	5	G2EmM	4.230	271.838	4	5
EG2	4.390	25.000	5	5	G2dmdM	4.052	251.764	5	5
EdG2	4.390	25.000	5	5	G2EM	4.036	255.022	5	5
EmG2	3.996	25.000	5	5	G2mM	4.026	198.573	5	5
					G2dEdM	3.978	286.269	5	5
					G2dmdEdM	3.920	316.818	5	5
					G2dM	3.877	248.588	5	5
					G2mEM	3.721	229.337	5	5

Table 5.17: Optimization results for each trajectory considered for G2.

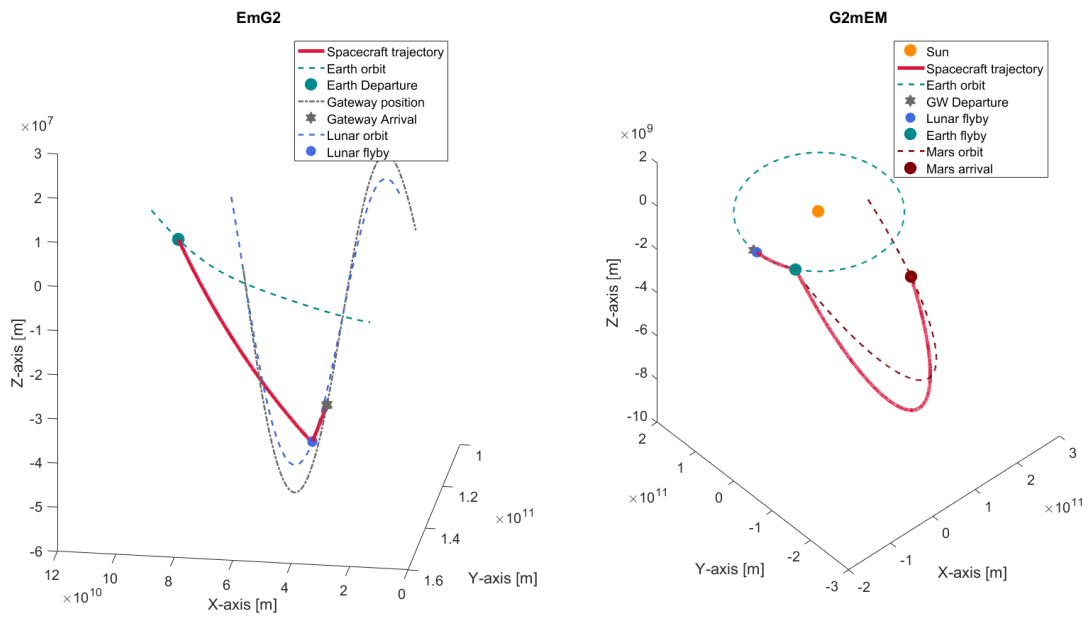


Figure 5.6: Plot of the best trajectory of each segment for G2.

5.4.3. G3 (Em-L4)

G3 (Em-L4)

EG					GM				
Trajectory	ΔV [km/s]	TOF [days]	<0.1% [-/5]	<1% [-/5]	Trajectory	ΔV [m/s]	TOF [days]	<0.1% [-/5]	<1% [-/5]
EdmdG3	4.410	25.000	5	5	G3M	4.789	190.999	5	5
EmG3	4.410	25.000	5	5	G3mM	4.230	206.333	5	5
EdEdG3	4.237	24.676	5	5	G3dEdmdM	4.129	303.657	5	5
EEG3	4.235	25.000	5	5	G3EmM	4.075	277.242	5	5
EG3	4.228	25.000	5	5	G3dmdM	4.060	253.624	5	5
EdG3	4.228	25.000	5	5	G3dM	4.027	253.263	5	5
					G3dEdM	3.858	259.878	5	5
					G3EM	3.856	231.602	5	5
					G3dmdEdM	3.761	266.368	1	5
					G3mEM	3.631	365.000	1	3

Table 5.18: Optimization results for each trajectory considered for G3.

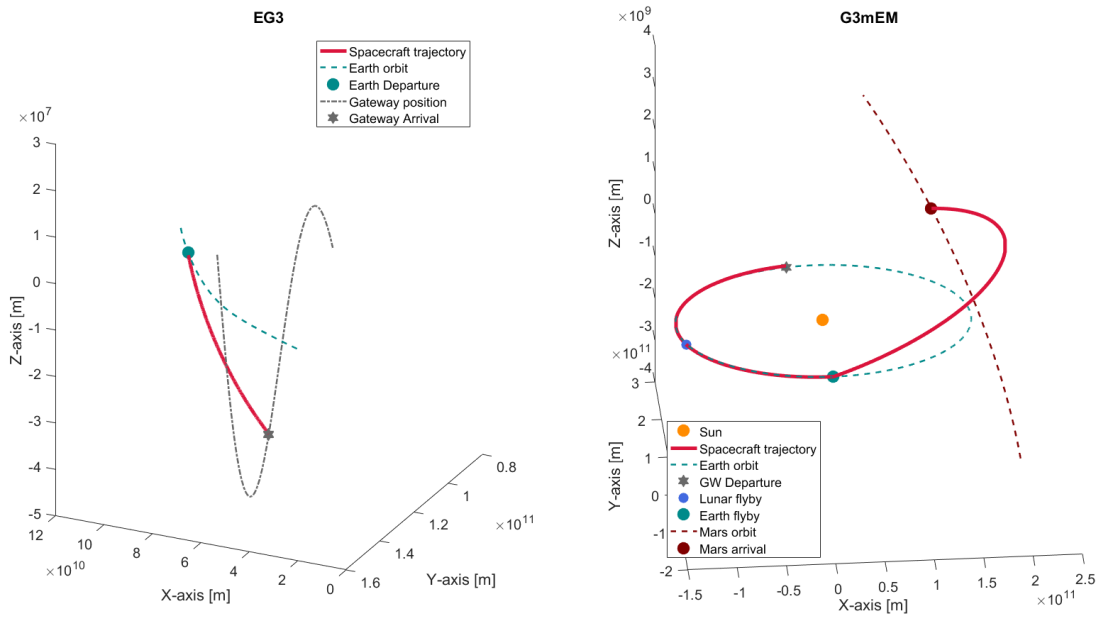


Figure 5.7: Plot of the best trajectory of each segment for G3.

5.4.4. G4 (Em-L5)

G4 (Em-L5)

EG					GM				
Trajectory	ΔV [km/s]	TOF [days]	<0.1% [-/5]	<1% [-/5]	Trajectory	ΔV [m/s]	TOF [days]	<0.1% [-/5]	<1% [-/5]
EdEdG4	4.234	24.985	5	5	G4M	4.675	193.992	5	5
EEG4	4.227	25.000	5	5	G4mM	4.522	198.031	5	5
EG4	4.227	25.000	5	5	G4dmdM	4.419	252.511	5	5
EdG4	4.227	25.000	5	5	G4dEdmdM	4.170	324.148	5	5
EdmdG4	4.221	25.000	5	5	G4EmM	4.111	266.869	5	5
EmG4	4.132	25.000	5	5	G4dM	4.035	271.550	5	5
					G4EM	3.915	250.113	5	5
					G4dEdM	3.856	281.471	5	5
					G4dmdEdM	3.759	343.322	1	5
					G4mEM	3.619	365.000	2	2

Table 5.19: Optimization results for each trajectory considered for G4.

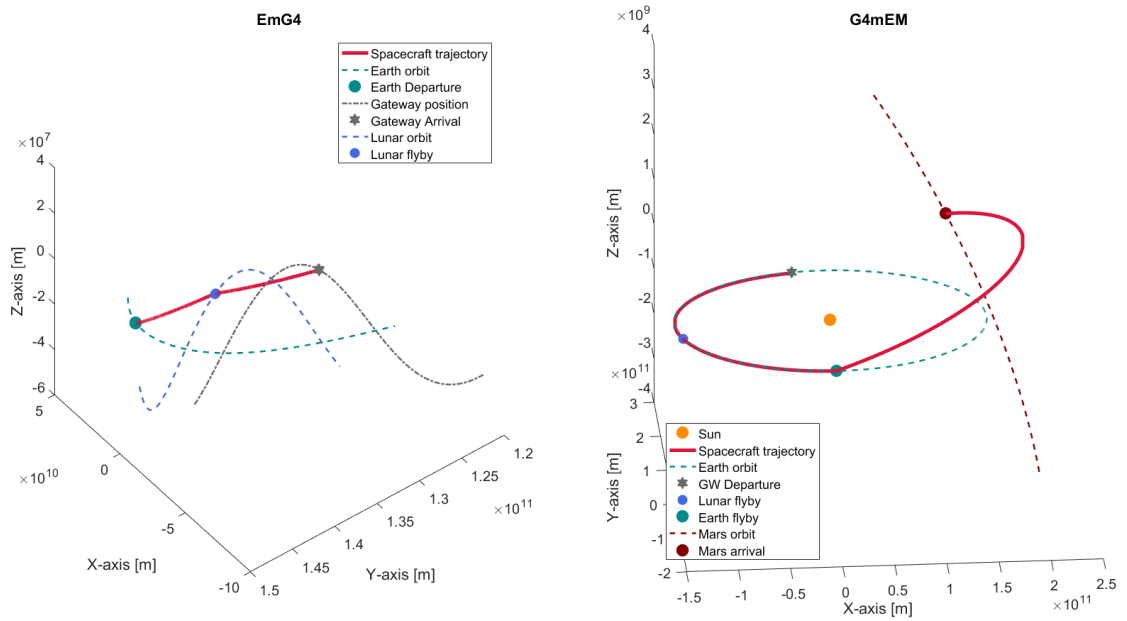


Figure 5.8: Plot of the best trajectory of each segment for G4.

5.4.5. G5 (SE-L2)

G5 (SE-L2)

EG					GM				
Trajectory	ΔV [km/s]	TOF [days]	<0.1% [-/5]	<1% [-/5]	Trajectory	ΔV [m/s]	TOF [days]	<0.1% [-/5]	<1% [-/5]
EEG5	3.456	100.000	5	5	G5M	5.143	197.189	5	5
EdmdmdG5	3.449	100.000	5	5	G5dM	4.638	253.306	5	5
EdmdEdG5	3.449	92.137	5	5	G5EEemM	4.517	292.187	5	5
EdEdG5	3.447	63.024	5	5	G5EmM	3.881	209.966	5	5
EEemG5	3.447	83.252	5	5	G5mM	3.867	245.885	5	5
EG5	3.447	61.371	5	5	G5dEdM	3.791	211.962	5	5
EdG5	3.447	61.371	5	5	G5EM	3.791	211.963	5	5
EmEG5	3.446	100.000	5	5	G5EmmM	3.700	262.178	5	5
EdEdmdG5	3.446	93.133	5	5	G5dEdmdM	3.674	278.060	5	5
EdmdG5	3.445	92.548	5	5	G5dmdM	3.645	276.062	5	5
EmG5	3.441	100.000	5	5	G5dEdmdmdM	3.582	293.384	5	5
EmmG5	3.431	100.000	5	5	G5dEdEdmdM	3.486	247.776	5	5
					G5mEEM	3.464	336.535	5	5
					G5mEmM	3.444	266.320	5	5
					G5dmdEdmdM	3.367	273.994	3	5
					G5mEM	3.226	275.443	5	5
					G5dmdEdM	3.213	280.328	4	5
					G5dEdmdEdM	3.152	249.625	5	5
					G5EmEM	3.138	261.881	5	5
					G5dmdEdEdM	2.967	285.740	5	5

Table 5.20: Optimization results for each trajectory considered for G5.

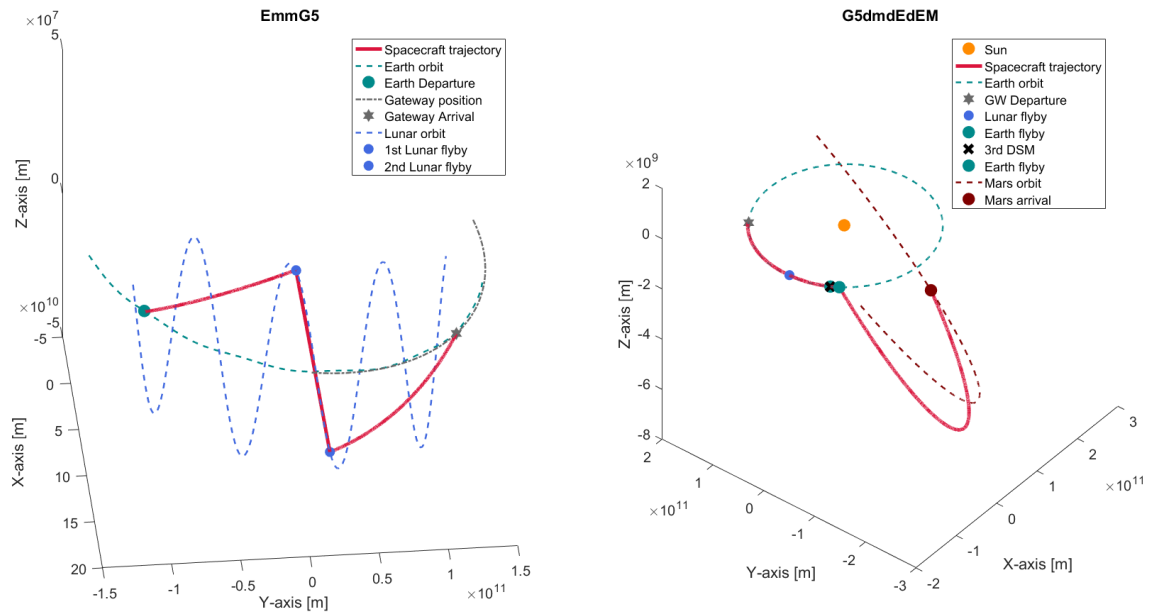


Figure 5.9: Plot of the best trajectory of each segment for G5.

5.4.6. G6 (SE-L1)

G6 (SM-L1)

EG					GM				
Trajectory	ΔV [km/s]	TOF [days]	<0.1% [-/5]	<1% [-/5]	Trajectory	ΔV [m/s]	TOF [days]	<0.1% [-/5]	<1% [-/5]
EEEmG6	6.902	365.000	5	5	G6dMdM	2.516	100.000	5	5
EEmG6	6.889	360.362	5	5	G6MM	1.932	6.596	5	5
EmEEG6	6.448	357.264	3	3	G6dM	1.931	5.598	5	5
EEG6	6.410	362.419	5	5	G6M	1.931	5.598	5	5
EEmmG6	6.407	283.113	5	5					
EEMG6	6.126	342.270	5	5					
EmG6	6.117	194.021	2	2					
EmEmG6	6.005	306.267	5	5					
EdEdmdG6	5.868	324.535	5	5					
EdmdEdmdG6	5.867	359.331	5	5					
EdmdG6	5.866	259.740	5	5					
EEmEG6	5.770	341.746	5	5					
EdmdEdG6	5.759	309.681	5	5					
EdEdG6	5.755	209.907	5	5					
EG6	5.753	208.292	5	5					
EdG6	5.753	208.292	1	5					
EmEG6	5.749	219.575	5	5					
EMG6	5.433	274.865	5	5					
EmMG6	5.350	264.358	3	5					

Table 5.21: Optimization results for each trajectory considered for G6.

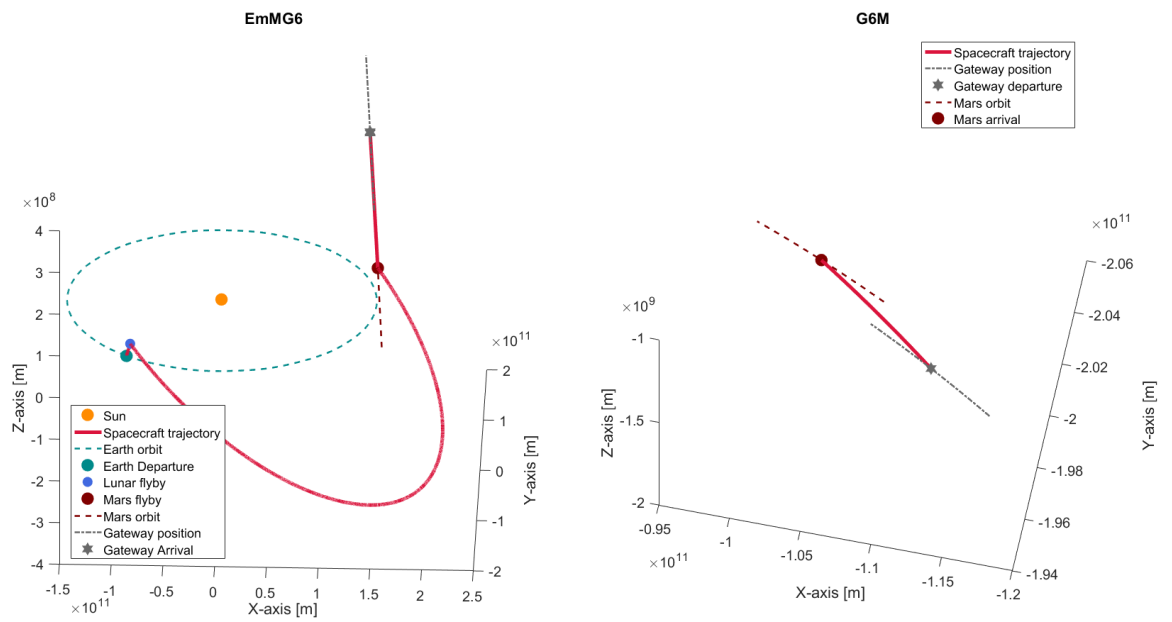


Figure 5.10: Plot of the best trajectory of each segment for G6.

5.4.7. Continuous-thrust results

		EG				GM					
Trajectory		ΔV [km/s]	TOF [days]	<0.1% [-/5]	<1% [-/5]	Trajectory		ΔV [km/s]	TOF [days]	<0.1% [-/5]	<1% [-/5]
G1	EG1c	4.241	25.000	5	5	G1Mc		5.103	290.553	5	5
G2	EG2c	4.633	25.000	4	5	G2Mc		4.900	288.894	5	5
G3	EG3c	4.431	25.000	5	5	G3Mc		4.993	296.472	5	5
G4	EG4c	4.431	25.000	5	5	G4Mc		4.929	285.950	5	5
G5	EG5c	3.522	63.824	5	5	G5Mc		5.578	365.25	5	5
G6	EG6c	7.000	292.765	1	4	G6Mc		2.821	100.000	5	5

Table 5.22: Optimization results for all continuous-thrust trajectories.

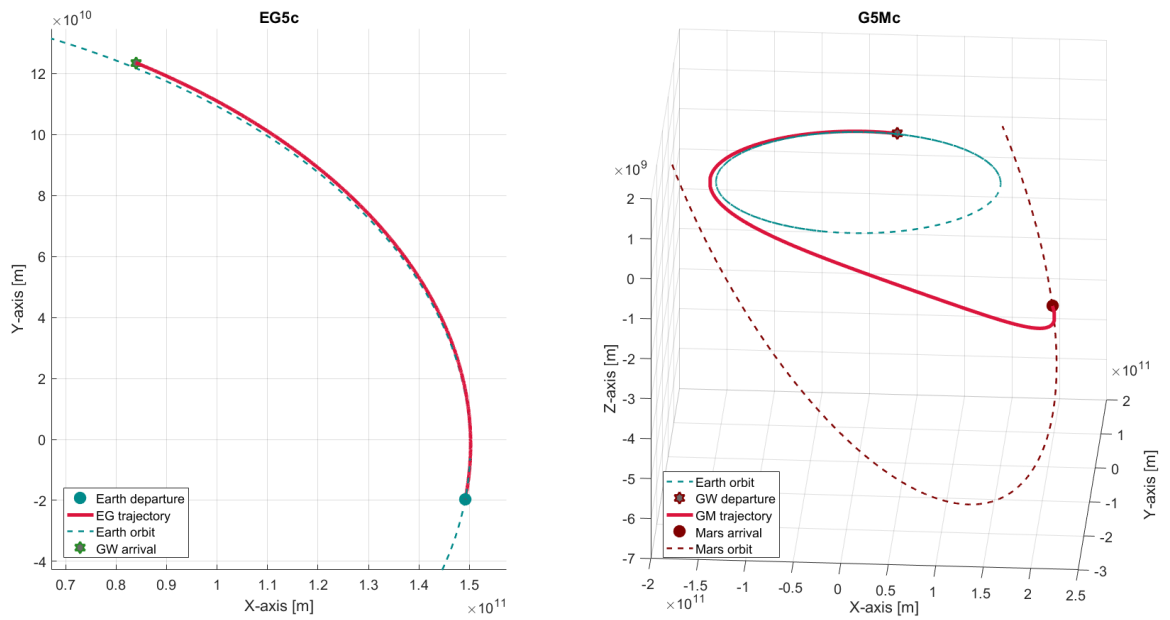


Figure 5.11: Plot of the best continuous-thrust transfer split into the two segments.

5.5. Discussion

Here the results shown in the previous sections will be discussed. The numbers and figures by themselves hold little meaning. In the discussion points below, physical, scientific, and engineering meaning will be extracted from the results of analysis A. The focus of this section lies on the results produced by the impulsive-thrust program, which will be discussed in the first subsection. The continuous-thrust results will be briefly discussed in the second subsection.

5.5.1. Impulsive-thrust

- Significance of flyby in EG segment** - It is interesting to study the role of a flyby in the EG segment of the transfer. A Lunar flyby results in a significant ΔV reduction for the G1 and G2 gateway locations, whereas the same flyby is less significant for the G3, G4 and G5 locations. The fact that G1 and G2, at Em-L1 and Em-L2 respectively, are located closer to the Moon apparently makes the inclusion of a Lunar flyby more suitable in the EG segment. Although the ΔV reduction due to the flyby of roughly 0.5 km/s and 0.4 km/s for G1 and G2 respectively is beneficial to the mission, it must be noted that it does create a certain dependency on the geometry of this specific trajectory. If in one of the analyses that follows this trajectory is deemed unfeasible, for TOF or consistency reasons for instance, the performance of these particular gateway concepts might deteriorate quickly. Interestingly, flyby transfers are preferred in the EG-segment for the G6 gateway location. A Mars flyby can apparently be effectively used to acquire the conditions beneficial for gateway rendezvous.
- Inclination change through flyby in GM segment** - It was found that the inclination change needed to go from Earth's to Mars' orbital plane can efficiently be acquired during a flyby. For the gateway locations in the vicinity of Earth, an Earth' flyby proved most suitable. Examples of this can be seen in Figures 5.5 to 5.9. For the G6 location, the inclination change of the best solution was achieved partially by a Lunar flyby and by a Mars' flyby (seen in Figure 5.10).
- Edges of TOF bounds** - In the results tables, it can be seen that a large number of the optimal transfer trajectory solutions comprise of at least one parameter at the edge of a TOF boundary. This is especially evident for the EG-segment, where the TOF of the solutions is often 25 days for the gateways located at G1 till G4 and 100 days for the G5 gateways. This behaviour makes sense since ΔV can often be decreased by increasing flight time, known as the ΔV -TOF trade-off. Although it makes sense to constrain the allowed TOF values for each segment, further research is recommended into these constraint values. This will be further discussed in Chapter 10.
- Convergence** - Looking at the convergence numbers, it is evident that the vast majority of the results are very accurate. All of the solutions in the EG segments, or GM segment for G6, have all five seed results fall in the .1% convergence range. For the longer segment, GM for G1-5 and EG G6, a few solutions score less than 5 on the .1% convergence range. Interestingly, solutions that score lower often involve a Lunar flyby followed by an Earth' flyby. No loss in accuracy is observed when the order of these flybys is reversed. This might be caused by the short orbital period of the Moon with respect to Earth, which increases the scope of trajectories that successfully use a Lunar flyby to return to Earth's vicinity. As a result, the program is more likely to converge to local optima.

Blinded by the high convergence scores, one might overlook an important sign that for some trajectories the accuracy is insufficient. This is the case for some trajectories that incorporate one or more DSMs. A trajectory with DSMs is not necessarily expected to be more efficient in terms of ΔV , but it is expected to at least score as good as the equivalent trajectory without DSMs. The ΔV of each DSM can simply be optimized to zero, which reduces the trajectory to one without DSMs. This effect can be seen by comparing most direct transfers between Earth and the gateway (i.e. *EG1* and *EdG1*). However, some trajectories with DSMs require significantly higher ΔV than their counterpart without DSMs. Significant differences in ΔV can be observed between *EdmdG2* and *EmG2* in Table 5.17 or *G6dMdM* and *G6MM* in Table 5.21. Each DSM adds an additional four parameters to be optimized. This has further complicated the optimization problem and has likely led to sub optimal results. The solution for this will be addressed in Section 5.6 Conclusions.

- Beneficial DSMs** - In contrast to the previous discussion point, inclusion of a DSM can improve a transfer in terms of ΔV required. This is true for all direct GM transfers for gateways G1 to G5, *G3dM* requires 0.762 km/s less ΔV than *G3M* for instance. Table 5.23 lists all the trajectories that significantly decrease in ΔV budget (minimum decrease of 0.3 km/s) as a result of the inclusion of one or more DSMs. The same table also indicates which manoeuvre is responsible for this improvement by renaming the trajectory in the third column.

No DSMs		With DSM(s)		Effective DSM(s)	
Trajectory	ΔV [km/s]	Trajectory	ΔV [km/s]	Trajectory	ΔV reduction [km/s]
G1M	4.812	G1dM	4.210	G1dM	0.602
G2M	4.614	G2dM	3.877	G2dM	0.737
G3M	4.789	G3dM	4.027	G3dM	0.762
G4M	4.675	G4dM	4.035	G4dM	0.640
G5M	5.143	G5dM	4.638	G5dM	0.505
G5EEmM	4.517	G5dEdEdmdM	3.486	G5dEdEdmM	1.031
G5mEEM	3.464	G5dmdEdEdM	2.967	G5mEdEM	0.497
EEG6	6.410	EdEdG6	5.755	EdEdG6	0.655

Table 5.23: List of trajectories that were improved by the inclusion of one or more DSMs.

The effect of the DSMs in each trajectory could be studied by looking at the magnitude of the impulsive burst for each individual manoeuvre. This exercise has been done for the *G5EEmM* trajectory to illustrate the process. Table 5.24 below shows the ΔV values the DSM manoeuvres and the powered flybys in the best solution for the *G5dEdEdmdM* trajectory.

Event	G5	d	E	d	E	d	m	d	M	Total
ΔV [km/s]	0.213	0.018	0	0.349	0.258	0	0	0.260	2.387	3.486

Table 5.24: Study into effect of individual DSM manoeuvres in *G5dEdEdmdM* trajectory.

As can be seen, only the second and the last DSM are actually performed. The resulting *G5EdEdmM* trajectory is plotted in Figure 5.12 for illustration purposes.

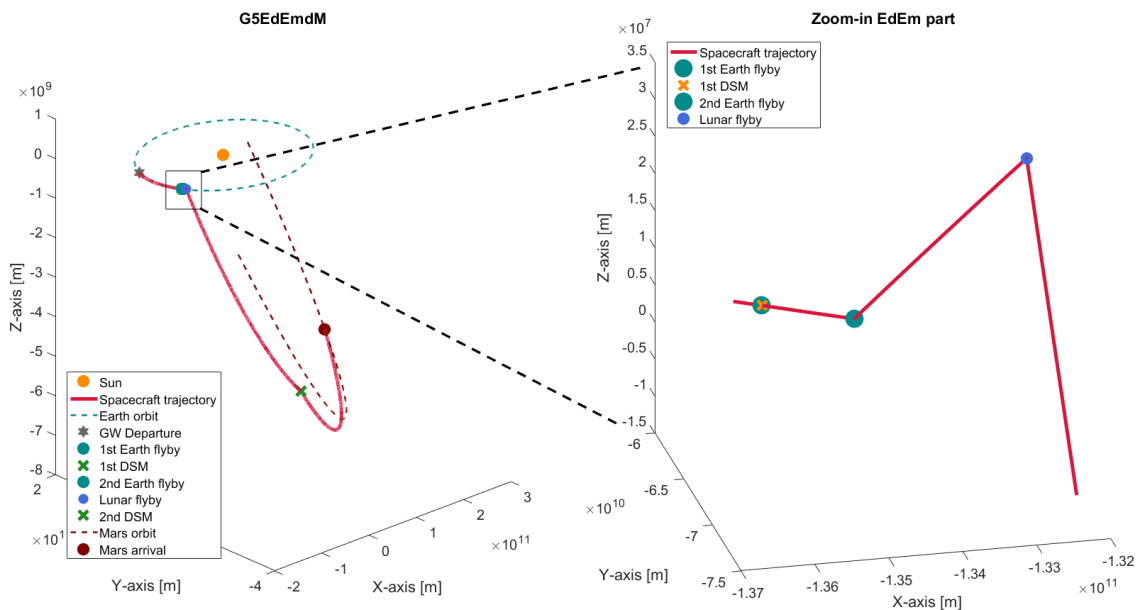


Figure 5.12: Illustration of *G5EdEdmM* trajectory showing the effective DSMs.

- **Comparison of different gateways** - It is important to address how the results of the different gateways should be compared. The most apparent comparison method is to compare the best solution for the entire transfer (EG + GM segment) of each gateway. This method, however, makes the selection process heavily dependent on a single trajectory solution. In the coming analyses, these trajectory solutions might prove to be infeasible due to their TOF or consistency characteristics. Therefore, it was decided to compare the average ΔV value of the top 3 trajectory solutions for each gateway in addition to simply the best solution. The top 3 trajectories were selected for each segment based on their ΔV requirements. For reasons discussed above, trajectories without DSMs were preferred over those with DSMs when their performance is similar. For trajectories with performance improving DSMs, Table 5.23 was used to simplify the trajectory without loss of performance. Tables 5.25 to 5.27 show the top 3 trajectory solutions for each segment of each gateway along with their performance and average performance. These tables will be used to draw conclusions in the next section.

	G1					G2				
	EG		GM		Total	EG		GM		Total
	Traj	ΔV	Traj	ΔV	ΔV	Traj	ΔV	Traj	ΔV	ΔV
Best	EmG1	3.510	G1mEM	3.169	6.679	EmG2	3.996	G2mEM	3.721	7.717
2nd	EG1	4.071	G1mM	3.401	7.472	EG2	4.390	G2dM	3.877	8.267
3rd	EEG1	4.076	G1EM	3.720	7.796	EEG2	4.396	G2EM	4.036	8.432
Average	-	3.886	-	3.430	7.316	-	4.261	-	3.878	8.139

Table 5.25: Top 3 trajectory solutions for each segment of G1 and G2 used to adequately compare gateway results.

	G3					G4				
	EG		GM		Total	EG		GM		Total
	Traj	ΔV	Traj	ΔV	ΔV	Traj	ΔV	Traj	ΔV	ΔV
Best	EG3	4.228	G3mEM	3.631	7.859	EmG4	4.132	G4mEM	3.619	7.751
2nd	EEG3	4.235	G3EM	3.856	8.091	EG4	4.227	G4EM	3.915	8.142
3rd	EmG3	4.410	G3dM	4.027	8.437	EEG4	4.227	G4dM	4.035	8.262
Average	-	4.291	-	3.838	8.129	-	4.195	-	3.856	8.052

Table 5.26: Top 3 trajectory solutions for each segment of G3 and G4 used to adequately compare gateway results.

	G5					G6				
	EG		GM		Total	EG		GM		Total
	Traj	ΔV	Traj	ΔV	ΔV	Traj	ΔV	Traj	ΔV	ΔV
Best	EmmG5	3.431	G5mEdEM	2.967	6.398	EmMG6	5.350	G6M	1.931	7.281
2nd	EmG5	3.441	G5EmEM	3.138	6.579	EMG6	5.433	G6MM	1.932	7.365
3rd	EmEG5	3.446	G5mEM	3.226	6.672	EmEG6	5.749	-	-	-
Average	-	3.439	-	3.110	6.550	-	5.511	-	1.932	7.442

Table 5.27: Top 3 trajectory solutions for each segment of G5 and G6 used to adequately compare gateway results.

It is important to note that the transfer trajectories listed in Tables 5.25 till 5.27 were selected from the Tables 5.16 until 5.21. In principle, the top 3 performing transfer trajectories were copied from these tables. However, trajectories without DSMs were preferred over trajectories with DSMs in this process when their performance is similar. In the case that the inclusion of DSMs proved significantly beneficial to the transfer trajectory's performance, only the effective DSM was included through use of Table 5.23.

5.5.2. Continuous-thrust

- **ΔV comparison between impulsive- and continuous-thrust transfers** - When comparing the ΔV requirements of the continuous-thrust transfers to the impulsive-thrust transfers, it is evident that impulsive-thrust trajectories enable more efficient transfer possibilities. This cannot solely be attributed to the inclusion of flybys in the impulsive trajectories, since direct impulsive transfers also outperform the continuous transfers. Although impulsive-thrust transfers outperform the continuous-thrust transfers in both segments, the difference is especially significant in the GM-segment (or EG-segment for G6). For this segment, the flight time is longer so that the difference in performance is accentuated.
- **Fair comparison based on OCF** - As was discussed in Section 4.2, ΔV by itself does not allow a fair comparison between transfers that make use of different propulsion systems. The same section therefore proposed the use of OCF as an additional evaluation criterion to specifically compare impulsive- and continuous-thrust transfers. Wertz [40] defined the OCF as "the ratio of the mass available in a 185-km circular orbit due East from the launch site to that at the end of mission". It can also be regarded as an inverse multiplier for the amount of payload that can be put into the mission transfer. The lower the OCF value, the more efficient the mission. Table 5.28 compares the OCF values for each continuous-thrust transfer to the best impulsive-thrust transfer for each gateway and segment. The same table also includes the mass ratio between the spacecraft mass at the end of the mission and at the start of the mission. The closer this number is to one, the more payload the mission can transport to the mission end.

		<u>Continuous</u>			<u>Impulsive</u>			
					EG			
	Trajectory	ΔV [km/s]	OCF [-]	$\frac{m_{end}}{m_{beg}}$ [-]	Trajectory	ΔV [km/s]	OCF [-]	$\frac{m_{end}}{m_{beg}}$ [-]
G1	EG1c	4.241	1.1093	0.9172	EmG1	3.510	2.5907	0.4088
G2	EG2c	4.633	1.1199	0.9099	EmG2	3.996	2.9455	0.3612
G3	EG3c	4.431	1.1144	0.9136	EG3	4.228	3.1310	0.3405
G4	EG4c	4.431	1.1144	0.9136	EmG4	4.132	3.0529	0.3489
G5	EG5c	3.522	1.0901	1.1856	EmmG5	3.431	2.5371	0.4171
G6	EG6c	7.000	0.8435	0.8670	EmMG6	5.350	4.2004	0.2558
					GM			
	Trajectory	ΔV [km/s]	OCF [-]	$\frac{m_{end}}{m_{beg}}$ [-]	Trajectory	ΔV [km/s]	OCF [-]	$\frac{m_{end}}{m_{beg}}$ [-]
G1	G1Mc	5.103	1.1327	0.9012	G1mEM	3.169	2.3668	0.4459
G2	G2Mc	4.900	1.1271	0.9049	G2mEM	3.721	2.7394	0.3874
G3	G3Mc	4.993	1.1297	0.9032	G3mEM	3.631	2.6750	0.3964
G4	G4Mc	4.929	1.1279	0.9044	G4mEM	3.619	2.6665	0.3976
G5	G5Mc	5.578	1.1457	0.8925	G5mEdEM	2.967	2.2430	0.4695
G6	G6Mc	2.821	1.0716	0.9441	G6M	1.931	1.6993	0.6113

Table 5.28: Fair comparison of continuous-thrust and impulsive-thrust transfers using OCF and mass ratio values.

As can be seen in Table 5.28, the continuous-thrust results greatly outperform the impulsive results in terms of OCF and mass ratio. This means that a mission design using a continuous-thrust transfer in the 2030s would be able to carry a significantly larger payload to Mars, since it would require a fraction of the propellant mass that impulsive transfers need. If these technologies would indeed be available in the 2030s, continuous transfers would therefore be an obvious choice in the gateway design.

5.6. Conclusions

Two significant conclusions can be drawn from the results in Analysis A. First, a selection of gateway locations to be considered in the remainder of this research will be presented. Next, a list of trajectories to be considered for these gateway locations is listed.

However, first a preliminary conclusion needs to be drawn. It was decided to disregard continuous-thrust transfers in the remainder of this research. Although continuous-thrust propulsion systems could enable very interesting transfer opportunities in terms of OCF (Table 5.28), too little certainty can be given about the characteristics of these future propulsion systems. This research intends to stay away from speculation and will therefore base its evaluation on ΔV requirements. The continuous-thrust transfers are significantly outperformed by the impulsive-thrust transfers on this evaluation criteria. The research will therefore focus on impulsive-thrust transfers and will not consider continuous-thrust transfers in the coming analyses. A recommendation for further research into the continuous-thrust transfer is given in the final chapter of this thesis report.

5.6.1. Filtering of gateway locations

The total ΔV budget for the entire Earth-to-Mars transfer for the best and the top 3 average impulsive-thrust solution is repeated for each gateway in Table 5.29 below.

GW	Best ΔV [km/s]	Average ΔV [km/s]
G5	6.398	6.550
G1	6.679	7.316
G6	7.281	7.442
G2	7.717	8.139
G4	7.751	8.052
G3	7.859	8.129

Table 5.29: Comparison of the performance of the different gateway locations.

Looking at the average performance of the gateway locations, a clear difference can be seen between the top 3 performing gateways and the bottom 3 performing gateways. Gateways G5, G1 and G6 stand out in terms of their best transfer solutions and their average performance. Of these three gateway locations, the SE-L2 location (G5; Table 5.1) is vastly superior, especially in terms of its top 3 average ΔV requirements. Naturally, these three gateways are selected and will be considered in the next analysis. This selection is especially interesting, since it includes a gateway at a Lagrange point in all three three-body systems (SE-L2, Em-L1 and SM-L1).

This would mean that the bottom three gateway locations (G2, G4 and G3) will be filtered out. However, this would mean that the gateway location chosen for the NASA Lunar gateway would not be considered in the remainder of this research. For that reason, it was decided to include the Em-L2 location (G2) in the next analysis. As a result, a total of four Lagrange-point gateway locations will be considered in Analysis B: G1, G2, G5 and G6. Figure 5.13 illustrates this selection of locations.

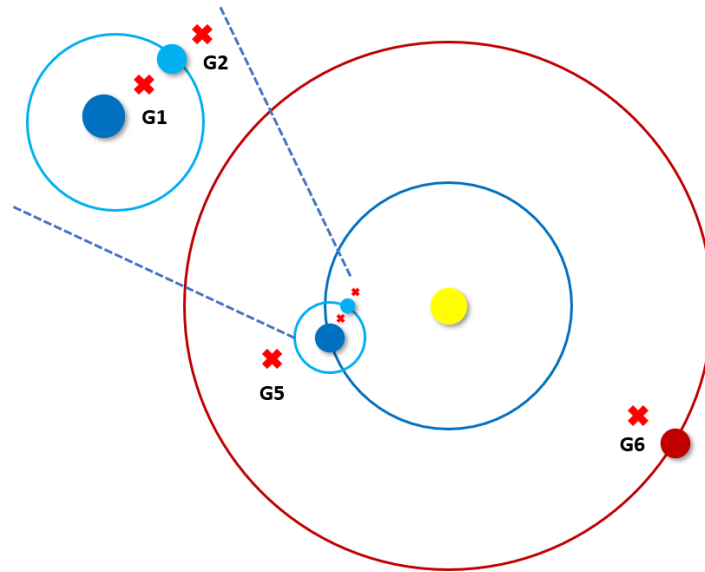


Figure 5.13: Selection of gateway locations to be considered in Analysis B.

5.6.2. Selection of trajectories

Now that a selection of gateways has been made, the scope of Analysis B can be further narrowed by limiting the trajectories to be analysed. This can be done by examining the results in Tables 5.16 to 5.21. Trajectories with DSMs will only be considered if they are proven to be effective, which can be deduced from Table 5.23. For the EG segments, however, the *EdG* trajectory will always be considered even though it does not rank among the top 3 trajectories for each gateway location. This was decided, because not having to rely on flybys will allow for a flexible and consistent transfer option between Earth and the gateway. Flexibility might be further improved by the inclusion of a DSM. As a result, the trajectories listed in Table 5.30 were selected and will thus be further analysed.

G1		G2	
EG	GM	EG	GM
EdG1	G1dM	EdG2	G2dM
EmG1	G1mM	EmG2	G2mEM
	G1mEM		

G5		G6	
EG	GM	EG	GM
EdG5	G5dM	EdG6	G6dM
EmG5	G5EM	EMG6	
	G5mEM	EmMG6	
	G5mEdEM		

Table 5.30: Trajectories selected in Analysis A to be analysed in Analysis B.

6

Analysis B - Detailed Analysis

This chapter builds upon the methodology and results presented in the previous Chapter, Chapter 5 *Analysis A*. Section 6.1 will introduce how this analysis fits into the greater research objective and will state the purpose of Analysis B. The next section will explain what methods were used to generate the desired results. These results will then be presented in Section 6.4 and will be discussed in the section that follows. Finally, conclusions will be drawn in Section 6.6.

6.1. Introduction

The work done in Analysis A has enabled a significant focus in the scope of the remaining research. Apart from eliminating a total of two gateway locations, it has also seriously brought down the number of trajectories to be considered for each selected location. Analysis A, however, did rely on several important simplifications. Most importantly, Analysis A assumed the gateway positions to be stationary at the Lagrange points and assumed each segment could be optimized individually. Although these simplifications were justified for the purpose of applying a first filter, they prevent Analysis A to be used to select the most practical gateway solution. To this extent, Analysis B will seek to more closely model reality by the implementation of a feature that models the gateway orbits and by performing segment timing. As a result, now the three central-orbit gateway locations can also be considered, which brings the number of gateways to be considered to a total of seven. Analysis B will aim to select as few gateway trajectory designs as possible, so that these can be analysed in further detail in Analysis C. A gateway design is now the combination of a gateway location, its orbit and the transfer options it supports. The purpose of Analysis B is summarized in the statement below.

Analysis purpose statement:

By modelling gateway orbits and by performing segment timing, Analysis B will aim to create insight into transfer performance regarding gateway orbits and will aim to bring down the total number of gateway trajectory designs to be considered in Analysis C.

6.2. Methodology

This section will discuss the methods used in Analysis B. First, the general method will be introduced. Here, the similarities and differences between Analysis A and B will be explained. Two major differences will then be covered individually in the next two sections. Finally, the optimization algorithm used in Analysis B will be introduced and discussed in a separate subsection.

6.2.1. General methods

1. **Most significant changes w.r.t. Analysis A** - Analysis A was based on two major simplifications: All gateways were assumed to be stationary at the Lagrange points and segments EG and GM were designed separately. Analysis B will get rid of these simplifications by implementing two new features:

- (a) **Gateway orbit model** - Gateways will be in orbit about a Lagrange point or a central celestial body. Through optimization, the most suitable gateway orbit is selected.
- (b) **Segment timing model** - The Earth-to-Mars transfer will be designed as a whole instead of two individual segments. The optimal gateway arrival and departure conditions are optimized.

These two models will be discussed separately in Sections 6.2.2 and 6.2.3.

2. **Gateways considered** - As a result of the implementation of orbit modelling capabilities, the three central-body gateway locations can now be considered. These three gateway locations were listed in Table 4.4 and depicted in Figure 4.2. As a result, a total of seven gateway locations will be included in Analysis B. All seven have been listed in Table 6.1 below, which matches the gateway location names to their actual locations.

Gateway name	Gateway location
G1	Em-L1
G2	Em-L2
G5	SE-L2
G6	SM-L1
G7	Earth orbit
G8	Lunar orbit
G9	Mars orbit

Table 6.1: Gateway locations to be researched in Analysis B.

3. **Trajectories considered** - For each gateway location above, a number of different trajectory options will be optimized. Every trajectory will start from Earth, rendezvous with the gateway, and then depart to Mars. A full transfer is therefore a combination of two segments (EG and GM) and will be denoted by $EG \times GM$. Analysis A has determined which trajectories should be considered for the Lagrange-point gateways (G1, G2, G5 and G6). These trajectories can be found in Table 5.30 of the previous chapter.

The transfer trajectory options for the 'new' CB gateways are listed in Table 6.2. The results of Analysis A were used to determine viable trajectory options for these gateway locations. Each CB gateway can be compared to the closest LP gateway. The trajectories that were proved to be efficient for that LP gateway location will likely also be suitable for the CB gateway in its vicinity. The gateways in orbit around either Earth or Mars will use direct transfer, $EG1$ and $G9M$ respectively, to connect with the central planet. This resulted in the transfer trajectory options listed in the table below.

G7		G8		G9	
EG	GM	EG	GM	EG	GM
EG7	G7dM	EdG8	G8dM	EdG9	G9M
	G7mM	EmG8	G8mM	EMG9	
	G7mEM	EEG8	G8mEM	EmMG9	
	G7EM		G8EmM	EmEG9	
	G7EmM				

Table 6.2: Trajectory options to be considered for the central-body gateway locations.

All transfer to be optimized can be found by combining the EG-trajectory with a GM-trajectory (i.e. $EdG8 \times G8mEM$). The total number of transfers that will be studied for each gateway is equal to the product of the number of EG-trajectories with the number of GM-trajectories (i.e. $3 \times 4 = 12$ for G8).

4. **Single-objective optimization of ΔV** - Similar to Analysis A, this analysis will also optimize the trajectories for a single objective. This objective, again, is the ΔV required for the transfer.
5. **Same use of TOF constraints, ephemeris settings and seeds** - In Analysis B, the TOF constraints listed in Table 5.2 are used. Furthermore, the same ephemeris settings as in Analysis A

were used, which can be found in Table 5.3. Again five seed numbers were used, but this time they were the following: 123, 234, 345, 456, 567.

In short, Analysis B will expand the gateway design process. Apart from the gateway location, the gateway orbit will also be part of the gateway design. Two additional questions will therefore be asked in Analysis B:

1. What is the optimal orbit for the gateway design?
2. What are the optimal gateway arrival and departure conditions?

In order to answer these questions, two new models were developed. These two models will be referred to as the *Gateway orbit model* (GOM) and the *Segment timing model* (STM). GOM will provide answers to the first questions, whereas STM will tackle the second question. An effort was made to minimize the number of extra design variables needed to optimize the gateway orbit and the arrival and departure conditions. This resulted in a program that only requires three additional parameters:

- Orbit ID number
- Gateway stay time
- Gateway arrival fraction

In the coming two sections, the parameters above will be introduced and their role in the models will be explained.

6.2.2. Gateway orbit model

Before being able to find the most suitable orbit for the gateway, a library of all potential orbits must be created. A library will store a large number of orbit trajectories labelled by an orbit ID number. Besides the gateway location, the content of this library of course depends on the orbit type: LPO for Lagrange-point gateways and Kepler orbits for central-body gateways. For both, the method to generate the orbit library is detailed below.

LPO library

Using the theory on LPO generation discussed in Section 3.3.2, an orbit library can be created for a selection of LPO families. As was argued in Section 4.5.2, Halo orbits will be most suitable for gateway orbits. Therefore, a library of Halo orbits was made for every Lagrange gateway location. Each orbit was labelled with an integer value, which can be related to the Jacobi constant of that orbit. Figure 6.1 shows the orbit library that was generated for gateway G1. The gateway position in the orbit is translated from the CR3BP frame to the Cartesian Sun-centred frame before it is used in the optimization.

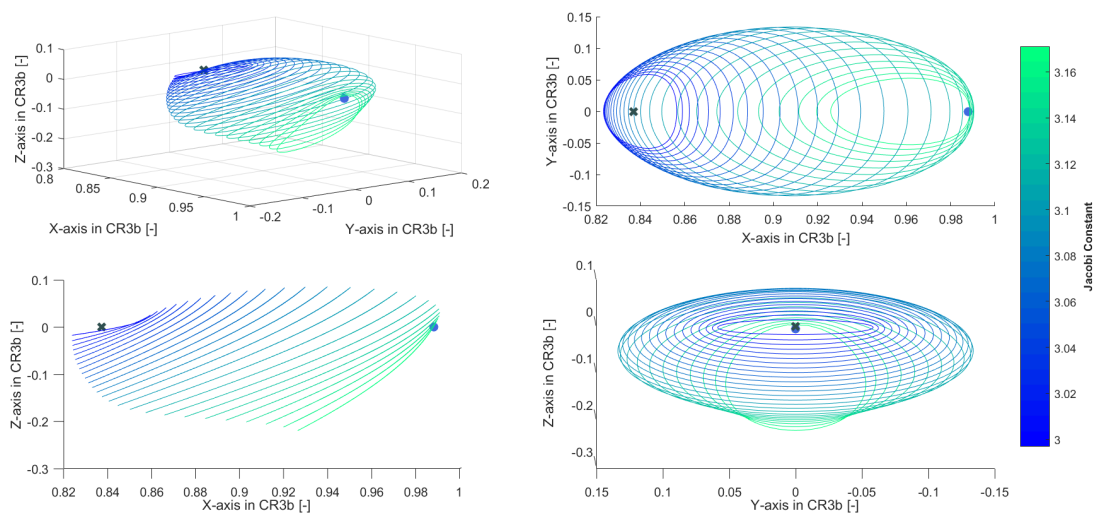


Figure 6.1: Example of an LPO orbit library generated for G1 (Em-L1), where the cross denotes the L1 position and the sphere denotes the Lunar position.

Central-orbit library

As was put forward in Section 4.5.1, only circular Kepler orbits will be considered for the central-body gateways. The orbits can be generated using a simple two-body propagator. This propagator is included in the basic Tudat toolkit and is thus described by Tudat documentation [48]. It assumes the following:

- The (initial) position and velocity of the gateway are given using Kepler elements.
- The central body is modelled as a point mass, and the gateway is modelled as having no mass.
- All perturbations are neglected.

Now this tool can be used to create an orbit library using the parameter values discussed in Section 4.5.1. Each orbit is given an orbit ID number, which corresponds to an inclination, orbital altitude, and longitude of ascending node (LOAN) value combination. Figure 6.2 shows the orbit library generated for gateway G7 and Table 6.3 shows a segment of the orbit ID number map. In order for these gateway orbits to be used in the optimization, their states have to be translated to the Sun-centred frame.

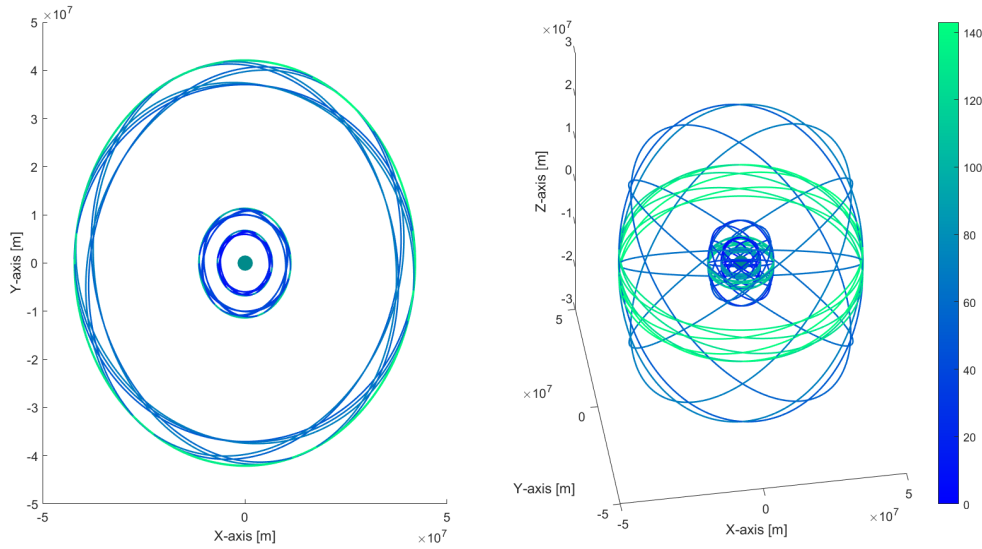


Figure 6.2: Example of a central-orbit library generated for G7 (Earth orbit), where the sphere denotes Earth's position.

orbit ID	Inclination [deg]	Altitude [km]	LOAN [deg]
0	28.5	420	0
1	28.5	420	15
2	28.5	420	30
⋮	⋮	⋮	⋮
141	5	35,786	315
142	5	35,786	330
143	5	35,786	345

Table 6.3: Part of the catalogues that maps orbit ID numbers to their orbital parameters.

For both the LPO and the central-body orbits, the orbit ID number can be fed to the optimization loop as a design variable. An optimal solution will then also include information on what orbit can best support the specific $EM \times GM$ transfer for that gateway location.

6.2.3. Segment Timing Model

In Analysis A, the transfer between Earth and Mars was divided into two segments (EG and GM). The trajectories were individually optimized for each segment. Due to this isolated optimization, the timing of the full transfer solutions was often incorrect. EG-segment solutions were allowed to have later gateway arrival dates than the gateway departure date of the GM-segment solutions. Moreover, the period between gateway arrival and departure could be arbitrarily long. Analysis B will implement a model that enables the timing of the transfer to be more in line with reality. This model will be introduced in this section.

- **Simultaneous optimization** - In Analysis B, the full Earth-to-Mars transfer will be split into three segments. Next to the EG- and GM-segments, the time spent at the gateway will also be considered as a segment. This segment will be referred to as the GW-segment. All three segments will be optimized simultaneously. As a result, the timing of the segments can be made to coincide, so that the EG-arrival date and the GM-departure date will always be sequential within a certain time bound.
- **Gateway stay time** - Between EG arrival and GM departure, the crew will occupy the gateway station. The minimum and maximum stay time was defined in Analysis B and is listed in Table 6.4 below. A minimum of one day was set to allow for preparation of the next transfer (propellant, supplies, rest). In order to research whether an elongated stay could prove beneficial to the mission, a moderately long maximum stay time of 50 days was set.

	Gateway stay time [days]
min	1
max	50

Table 6.4: Bounds on gateway stay time.

- **Orbit arrival fraction** - After completing the EG-transfer, the spacecraft will rendezvous with the gateway in orbit. The rendezvous epoch is determined by the EG departure date and TOF design variables. At the rendezvous epoch, the gateway may be positioned anywhere in its orbit. The position of the gateway in its orbit can be expressed using the orbital arrival fraction, denoted by σ_{arr} . The first state of a given orbit in the orbit library defines where $\sigma_{arr} = 0$ and where, a full orbital period later, $\sigma_{arr} = 1$. All positions in between can be expressed by a σ_{arr} -value between 0 and 1. This is illustrated for an LPO orbit and for a central-body orbit in Figure 6.3 below.

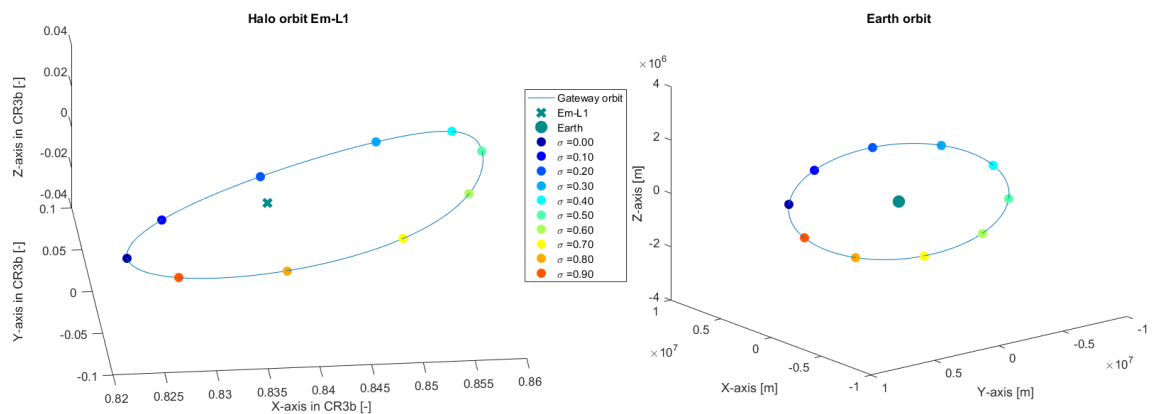


Figure 6.3: Illustration of orbit arrival fractions (σ_{arr}) for an LPO orbit ($C = 3.17102$) and for a central-body orbit ($i = 28.5^\circ$, $h = 420\text{km}$ and $LOAN = 75^\circ$).

- **Modelling gateway arrival and departure** - Using the gateway stay time (TOF_{GW}) and the orbit arrival fraction (σ_{arr}), the gateway arrival and departure states can be found. The arrival state can be retrieved from the orbit library using the orbit arrival fraction. The time of gateway departure is simply the time of gateway arrival ($T_{GW,a}$) plus the stay time (TOF_{GW}): $T_{GW,d} = T_{GW,a} + TOF_{GW}$. The departure state can then be retrieved using the orbit arrival fraction and the departure time. Both the arrival and departure states must be translated to the correct coordinate system and reference frame before optimization occurs. As a result, only three parameters are needed to model the GW-segment: Orbit ID, gateway stay time and orbit arrival fraction. This process is illustrated by Figure 6.4 for a Halo orbit around Em-L1.

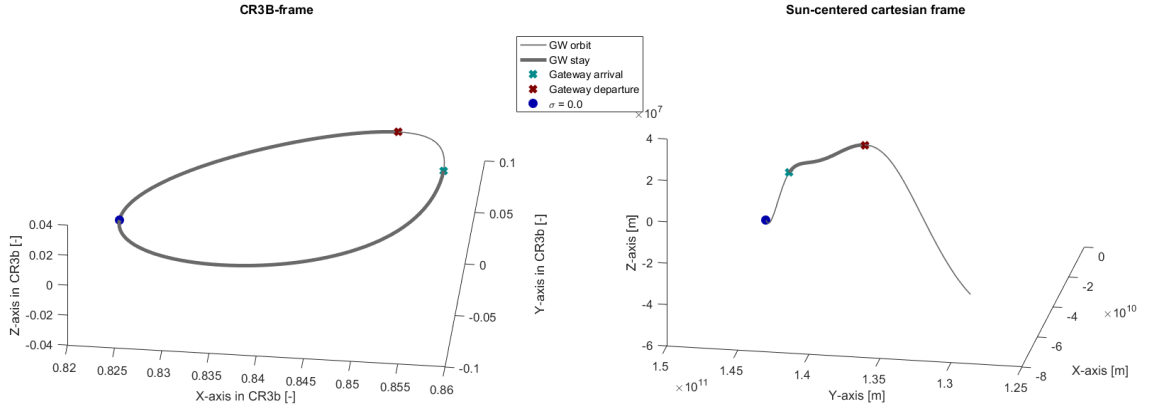


Figure 6.4: Illustration of gateway arrival and departure modelling for a Halo orbit around Em-L1 ($C = 3.17102$) and a stay time of 10 days, shown in the CR3BP- and Sun-centred frame.

By implementation of the GOM and STM models, the role a gateway orbit plays in the performance of a gateway design can be investigated. For each gateway design, a solution will be generated that consists of an orbit ID number, which corresponds to an actual orbit. Furthermore, a solution will contain information on optimal conditions for spacecraft arriving at and departing from this gateway orbit. The result section, Section 6.4, will provide further insights into these gateway orbit solutions.

6.2.4. Optimization algorithm

Similar to Analysis A, Analysis B also uses the DE optimization algorithm. In Analysis B, the optimization problem consists of many more design variables with respect to Analysis A. This is due to the inclusion of orbit optimization and because this analysis will optimize the full transfer between Earth and Mars as a whole. In order to increase the convergence rate and speed of the optimization algorithm, a simple algorithm tuning was performed. In this process, the algorithm (DE) and its strategy (best/1/exp) were fixed based on the recommendations by Musegaas [5]. The weight coefficient (F value), crossover probability (CR value) and population size (N_{pop}) were varied and the convergence results were monitored. In this process, the settings listed in Table 6.5 were selected.

Algorithm	F value	CR value	Strategy	Population size
DE	0.5	0.80	1 (best/1/exp)	$N_{pop} = 300 * N_{param}$

Table 6.5: Optimizer settings for Analysis B.

It was found that a larger population size in combination with a smaller number of generations is most effective in producing results with a high convergence rate in Analysis B. The number of generations was set to fifty times the number of parameters of one individual ($N_{Gen} = 50 \cdot N_{param}$), as this proved to be sufficiently high to allow for convergence in all transfer trajectory cases.

6.3. Verification

The methodology developed for Analysis B relies, to a large extent, on methods that have been tried and tested in Analysis A. The impulsive-thrust trajectory design has not been modified, so its verification in Section 5.3.2 still holds. New in Analysis B is the modelling of gateway orbits instead of the stationary gateway locations in Analysis A. It is essential to first verify that these orbits were generated correctly, so that the results of Analysis B can be trusted. To do so, the orbit libraries generated for Analysis B (see Section 6.2.2) need to be checked. This section will first prove the validity of the LPO's generated in Analysis B and will then do the same for the central-body orbits.

6.3.1. LPO library

The LPO's were generated using a generation scheme developed by Langemeijer [8], which was discussed in Sections 3.3.2 and 6.2.2. In his thesis report, Langemeijer did a thorough verification of the produced results through periodicity verification and eigensystem validation. As a result, his methodology was proven to be valid. If it can be proven here that the LPO library results match Langemeijer's results, the validity of the orbit generation in Analysis B is confirmed. As a test case, the Em-L1 Halo orbit family will be used. The different Halo orbits in this family can be characterized by their Jacobi constant (C) and by their dimensionless orbital period in the CR3BP frame (T). The orbit generation results can then be captured in a figure that shows both. Figure 6.5 shows this figure generated by Langemeijer.

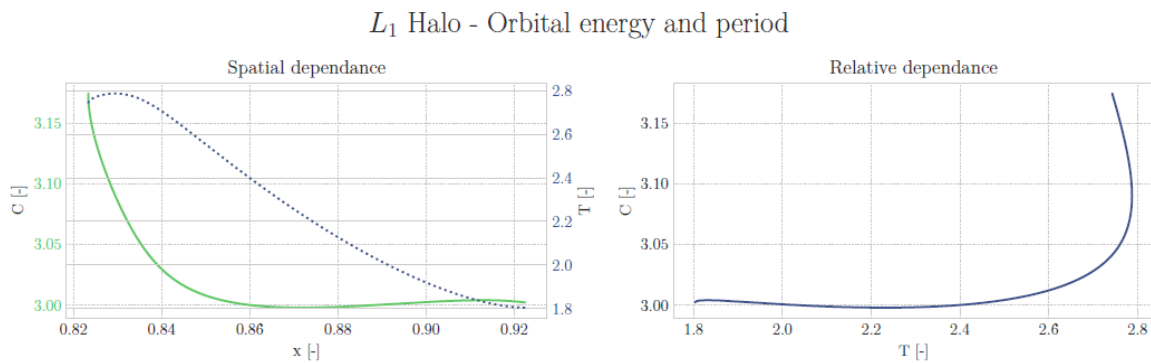


Figure 6.5: Characterisation of Em-L1 Halo orbit family by Langemeijer [8].

The same figure was made using the results of the orbit generation done for Analysis B. This figure is shown below.

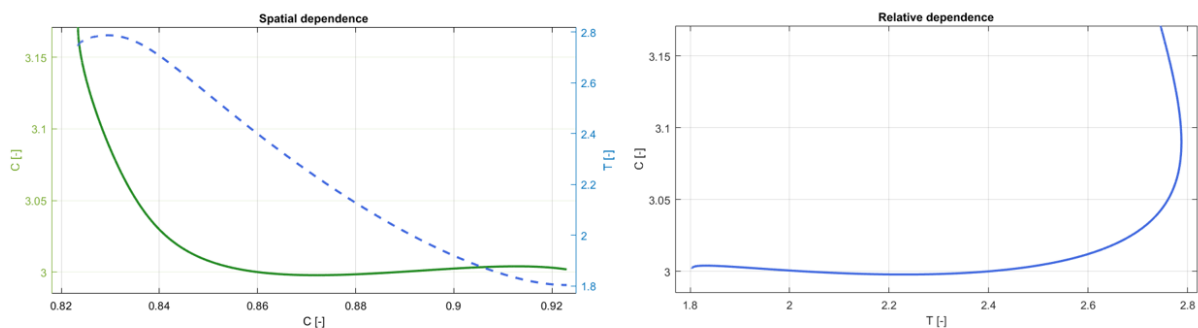


Figure 6.6: Characterisation of Em-L1 Halo orbit family using the method implemented in Analysis B.

Since the two figures are similar, it can be concluded that the orbit family generated in Analysis B is similar to the family generated by Langemeijer. Therefore, the LPO generation scheme used in Analysis B can be considered as verified.

6.3.2. Central-orbit library

As the orbits in the central-orbit libraries used in Analysis B are all circular Kepler orbits, their validation is very straightforward. The orbital velocity and the orbital period of the generated orbits can be compared with their theoretical values. These can be calculated as follows:

$$v = \sqrt{\frac{\mu}{r}} \quad (6.1)$$

$$T = 2\pi\sqrt{\frac{r^3}{\mu}} \quad (6.2)$$

Table 6.6 lists three orbits that were randomly selected for all three central bodies along with their theoretical and computed vales for their orbital velocity and orbital period. The slight difference in period is a result of the termination condition of the integrator. This difference is in the order of seconds and is therefore negligible for the purpose of this thesis. The central-orbit libraries have therefore been verified.

Earth			Computed		Theoretical	
Orbit ID	h [km]	r [km]	v [km/s]	T [h]	v [km/s]	T [h]
1	420	6791.0	7.6613	1.5486	7.6613	1.5471
100	5000	11371.0	5.9207	3.3554	5.9207	3.3520
140	35786	42157.0	3.0749	23.9284	3.0749	23.9284

Moon			Computed		Theoretical	
Orbit ID	h [km]	r [km]	v [km/s]	T [h]	v [km/s]	T [h]
1	150	1887.4	1.6117	2.0439	1.6117	2.0439
75	300	2037.4	1.5513	2.2946	1.5513	2.2923

Mars			Computed		Theoretical	
Orbit ID	h [km]	r [km]	v [km/s]	T [h]	v [km/s]	T [h]
1	420	3809.5	3.3530	1.9850	3.3530	1.9830
75	5000	8389.5	2.2594	6.4806	2.2594	6.4806

Table 6.6: Validation of the central-orbit libraries by comparison of computed and theoretical orbital velocities and periods.

6.4. Results

In this section, the results of Analysis B will be presented. This will be done in a similar manner as was done for Analysis A: for each gateway location, a table with all transfer solutions is shown. Furthermore, a figure illustrating the best transfer solution will be provided for further insight. The next section will then interpret these results.

The rest of this page is intentionally left blank, so that the result for each gateway location fit on a single page.

6.4.1. G1 (Em-L1)

Transfer	ΔV [km/s]			TOF [days]				Orbit [-]		Convergence [-/5]	
	Total	EG	GM	Total	EG	GW	GM	Orbit ID	σ_{arr}	<0.1%	<1%
EdG1 x G1dM	7.38	3.40	3.98	311	25	37	249	219	0.50	2	5
EdG1 x G1mEM	5.99	3.41	2.58	386	25	25	336	217	0.50	2	4
EdG1 x G1mM	6.94	3.40	3.54	229	25	7	197	222	0.50	3	5
EmG1 x G1dM	7.56	3.46	4.10	350	25	47	278	0	0.05	2	5
EmG1 x G1mEM	6.37	3.79	2.57	417	24	31	363	220	0.78	1	4
EmG1 x G1mM	6.84	3.47	3.37	241	21	22	197	0	0.07	5	5

Table 6.7: Transfer solutions results for the G1 gateway location (Em-L1).

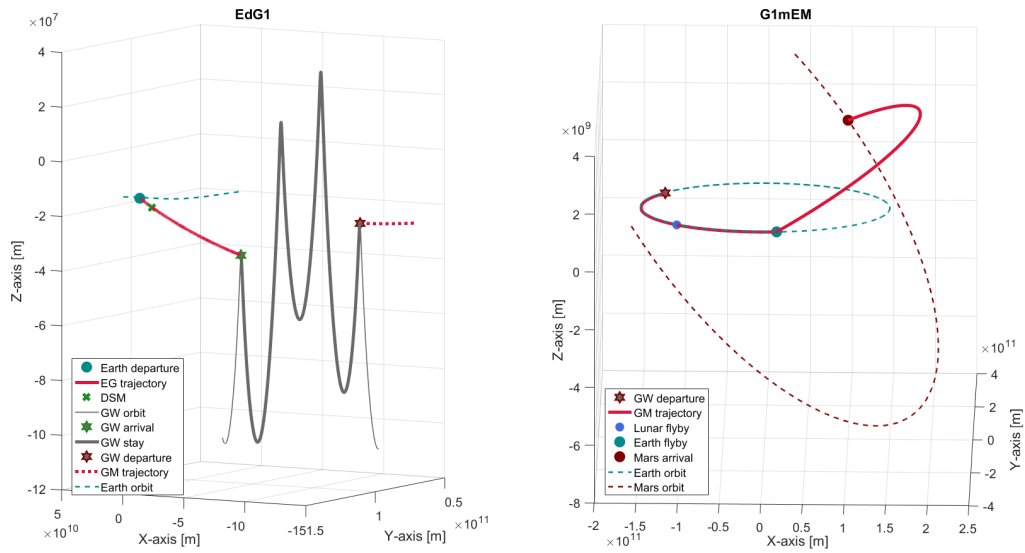


Figure 6.7: Plot of the EG and GM segment from the best transfer solution of the G1 gateway.

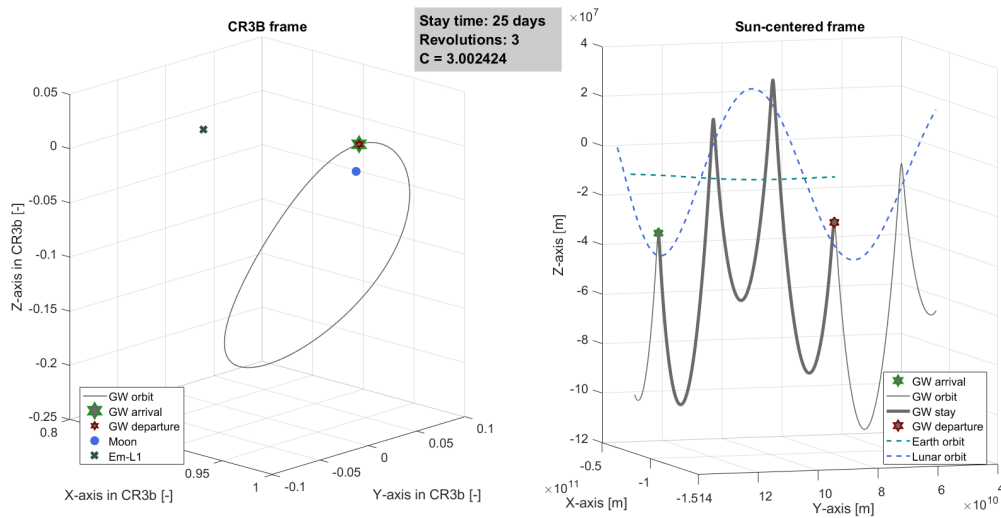


Figure 6.8: Plot of the GW segment from the best transfer solution of the G1 gateway in the CR3BP- and Sun-centered frame.

6.4.2. G2 (Em-L2)

Transfer	ΔV [km/s]			TOF [days]				Orbit [-]		Convergence [-/5]	
	Total	EG	GM	Total	EG	GW	GM	Orbit ID	σ_{arr}	<0.1%	<1%
EdG2 x G2dM	7.53	4.13	3.40	278	25	5	248	161	0.48	1	5
EdG2 x G2mEM	7.36	4.19	3.17	377	25	46	306	161	0.45	1	1
EmG2 x G2dM	7.15	3.75	3.40	322	25	50	247	161	0.24	1	5
EmG2 x G2mEM	7.14	3.76	3.38	397	25	35	337	161	0.20	3	5

Table 6.8: Transfer solutions results for the G2 gateway location (Em-L2).

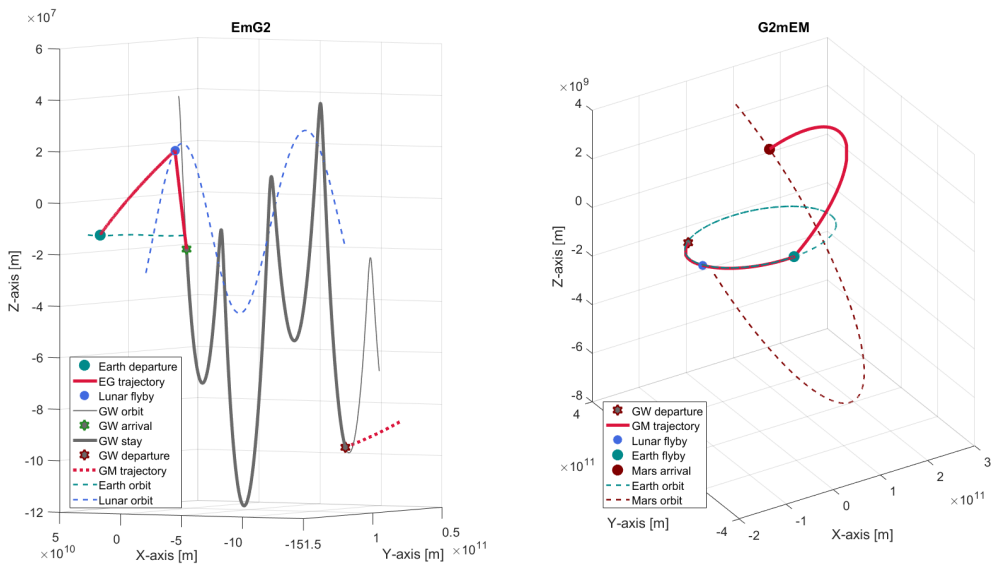


Figure 6.9: Plot of the EG and GM segment from the best transfer solution of the G2 gateway.

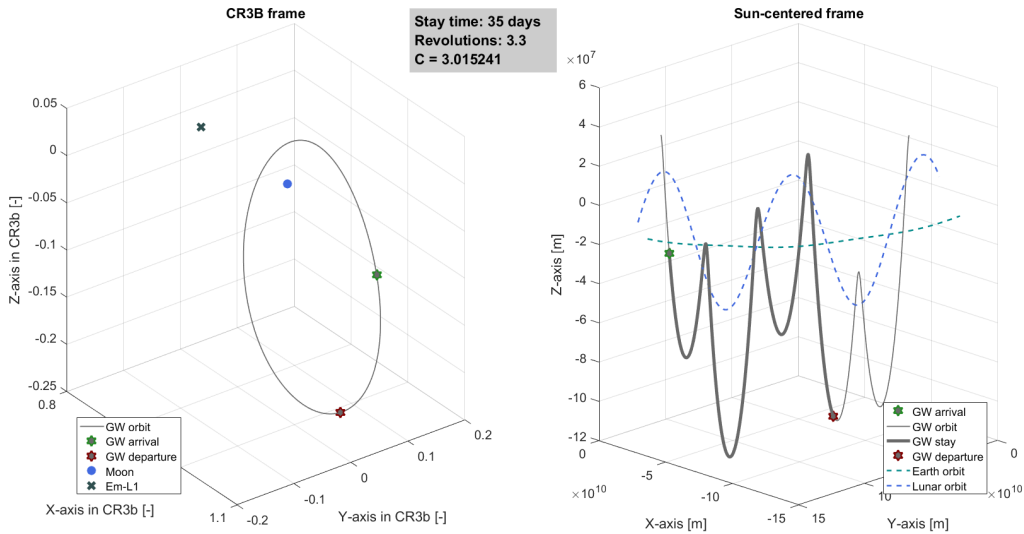


Figure 6.10: Plot of the GW segment from the best transfer solution of the G2 gateway in the CR3BP- and Sun-centered frame.

6.4.3. G5 (SE-L2)

Transfer	ΔV [km/s]			TOF [days]				Orbit [-]		Convergence [-/5]	
	Total	EG	GM	Total	EG	GW	GM	Orbit ID	σ_{arr}	<0.1%	<1%
EdG5 x G5EM	7.25	3.70	3.55	428	100	50	278	104	0.77	1	1
EdG5 x G5dM	7.66	3.64	4.02	426	100	50	276	104	0.63	5	5
EdG5 x G5mEM	6.23	3.52	2.70	481	100	50	331	0	0.28	4	5
EdG5 x G5mEdEM	5.87	3.34	2.53	515	100	50	365	0	0.38	4	4
EmG5 x G5EM	7.31	3.83	3.48	392	100	50	242	67	0.96	2	5
EmG5 x G5dM	7.64	3.64	4.00	419	100	50	269	104	0.63	5	5
EmG5 x G5mEM	6.25	3.33	2.92	507	100	50	357	0	0.40	1	5
EmG5 x G5mEdEM	6.48	3.41	3.06	507	98	50	359	0	0.31	5	5

Table 6.9: Transfer solutions results for the G5 gateway location (SE-L2).

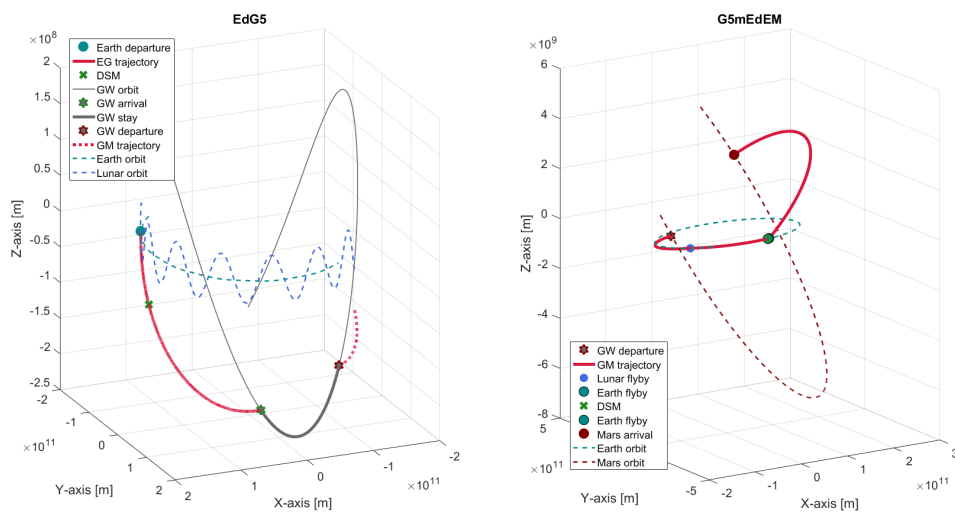


Figure 6.11: Plot of the EG and GM segment from the best transfer solution of the G5 gateway.

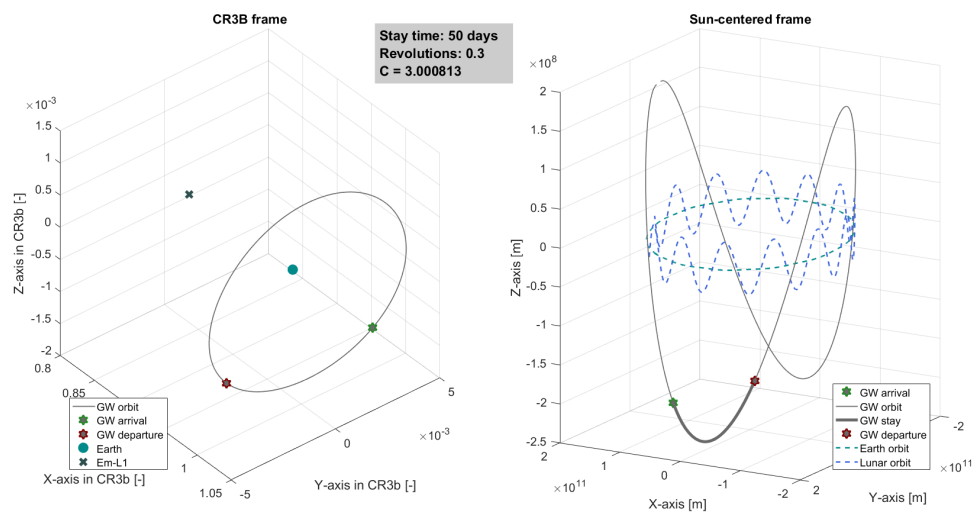


Figure 6.12: Plot of the GW segment from the best transfer solution of the G5 gateway in the CR3BP- and Sun-centered frame.

6.4.4. G6 (SM-L1)

Transfer	ΔV [km/s]			TOF [days]				Orbit [-]		Convergence [-/5]	
	Total	EG	GM	Total	EG	GW	GM	Orbit ID	σ_{arr}	<0.1%	<1%
EMG6 x G6dM	7.98	6.28	1.70	332	321	10	1	86	0.43	5	5
EdG6 x G6dM	7.23	5.53	1.70	328	326	1	1	86	0.48	2	2
EmMG6 x G6dM	8.34	5.43	2.91	294	193	1	100	55	0.66	3	3

Table 6.10: Transfer solutions results for the G6 gateway location (SM-L1).

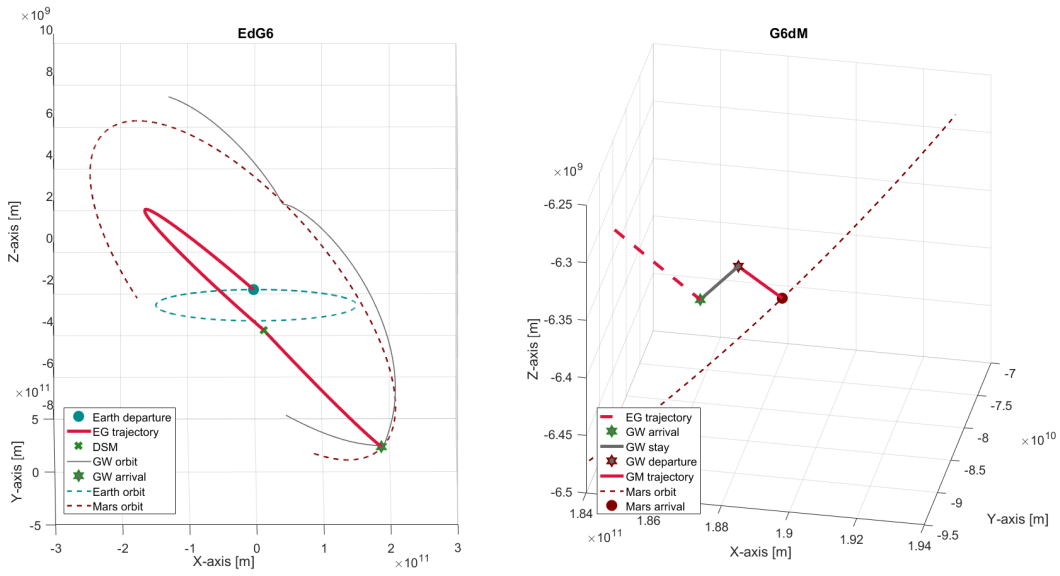


Figure 6.13: Plot of the EG and GM segment from the best transfer solution of the G6 gateway.

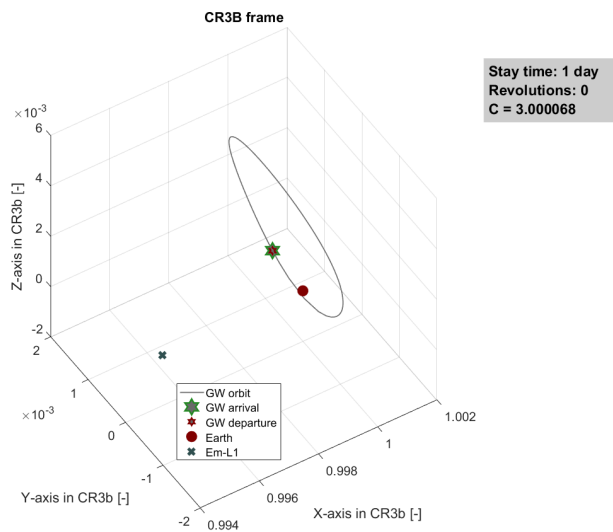


Figure 6.14: Plot of the GW segment from the best transfer solution of the G6 gateway in the CR3BP frame, Sun-centered frame disregarded due to short stay time.

6.4.5. G7 (Earth orbit)

Transfer	ΔV [km/s]			TOF [days]				Orbit [-]		Convergence [-/5]	
	Total	EG	GM	Total	EG	GW	GM	Orbit ID	σ_{arr}	<0.1%	<1%
EG7 x G7EM	9.92	4.82	5.11	354	8	46	300	52	0.75	5	5
EG7 x G7EmM	9.71	4.82	4.89	367	8	50	309	130	0.70	1	1
EG7 x G7dM	8.54	4.82	3.72	235	9	28	199	50	0.25	2	2
EG7 x G7mEM	9.44	4.82	4.62	372	9	50	313	131	0.73	1	3
EG7 x G7mM	8.81	4.82	3.99	196	9	1	186	124	0.16	1	4

Table 6.11: Transfer solutions results for the G7 gateway location (Earth orbit).

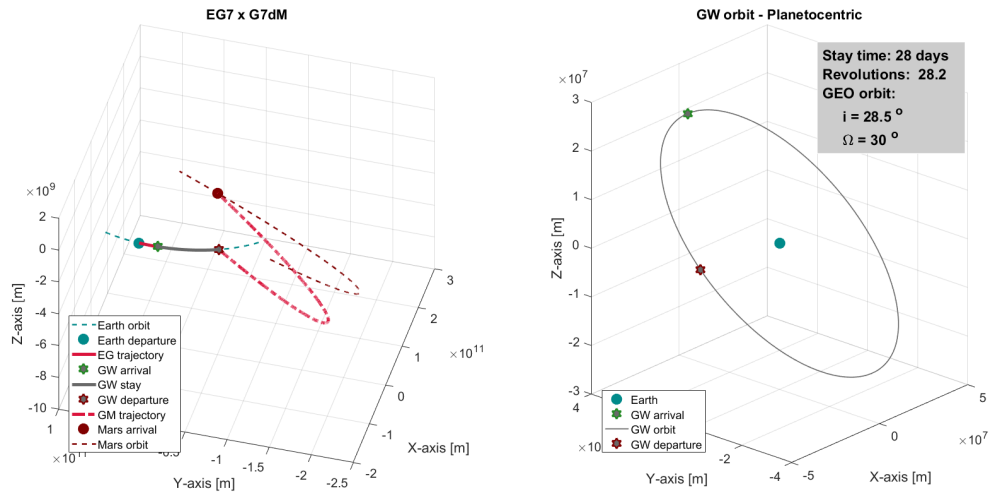


Figure 6.15: Plot of the EG and GM segments (left) and the GW segment (right) from the best transfer solution of the G7 gateway.

6.4.6. G8 (Lunar orbit)

Transfer	ΔV [km/s]			TOF [days]				Orbit [-]		Convergence [-/5]	
	Total	EG	GM	Total	EG	GW	GM	Orbit ID	σ_{arr}	<0.1%	<1%
EEG8 x G8EmM	7.59	3.92	3.67	253	20	43	190	87	0.15	1	1
EEG8 x G8dM	7.15	3.93	3.22	236	25	14	198	45	0.77	2	3
EEG8 x G8mEM	7.13	3.89	3.23	413	14	42	358	87	0.90	2	4
EEG8 x G8mM	8.00	3.89	4.11	249	11	35	203	87	0.15	2	3
EdG8 x G8EmM	7.38	3.96	3.42	249	19	40	190	84	0.16	1	1
EdG8 x G8dM	7.14	3.92	3.22	259	20	41	198	45	0.76	1	3
EdG8 x G8mEM	7.15	3.92	3.23	399	11	30	358	86	0.28	1	4
EdG8 x G8mM	8.03	3.92	4.11	220	9	8	204	86	0.10	4	5
EmG8 x G8EmM	7.73	3.92	3.81	277	21	18	238	72	0.76	1	5
EmG8 x G8dM	7.15	3.92	3.22	224	20	6	198	31	0.74	1	4
EmG8 x G8mEM	7.14	3.91	3.23	407	21	28	358	82	0.53	2	4
EmG8 x G8mM	8.02	3.91	4.11	261	21	36	204	87	0.08	4	5

Table 6.12: Transfer solutions results for the G8 gateway location (Lunar orbit).

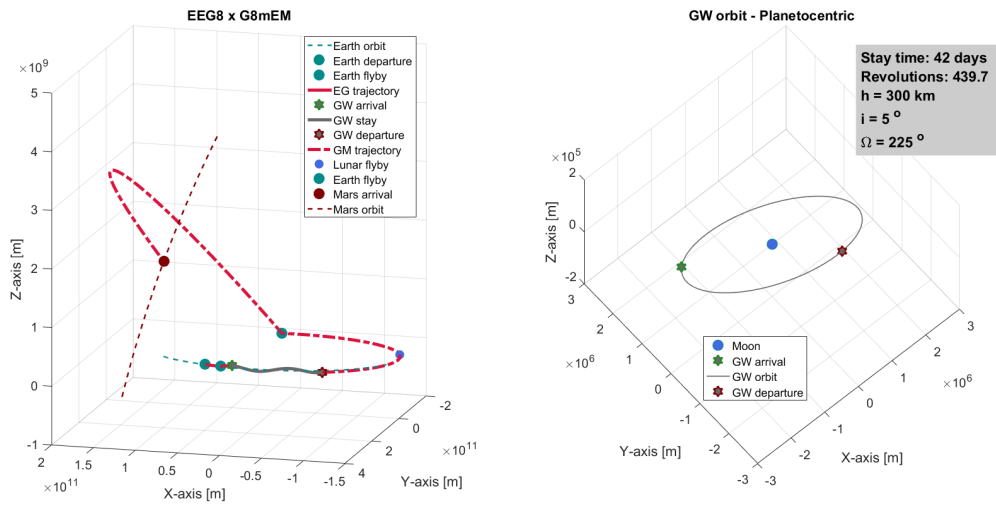


Figure 6.16: Plot of the EG and GM segments (left) and the GW segment (right) from the best transfer solution of the G8 gateway.

6.4.7. G9 (Mars orbit)

Transfer	ΔV [km/s]			TOF [days]				Orbit [-]		Convergence [-/5]	
	Total	EG	GM	Total	EG	GW	GM	Orbit ID	σ_{arr}	<0.1%	<1%
EMG9 x G9M	9.61	6.55	3.06	296	267	20	10	41	0.48	4	4
EdG9 x G9M	8.19	5.13	3.06	259	200	50	9	43	0.86	1	2
EmMG9 x G9M	9.88	6.82	3.06	312	276	27	10	30	0.00	5	5
EmEG9 x G9M	8.22	5.16	3.06	367	308	50	9	40	0.85	5	5

Table 6.13: Transfer solutions results for the G9 gateway location (Mars orbit).

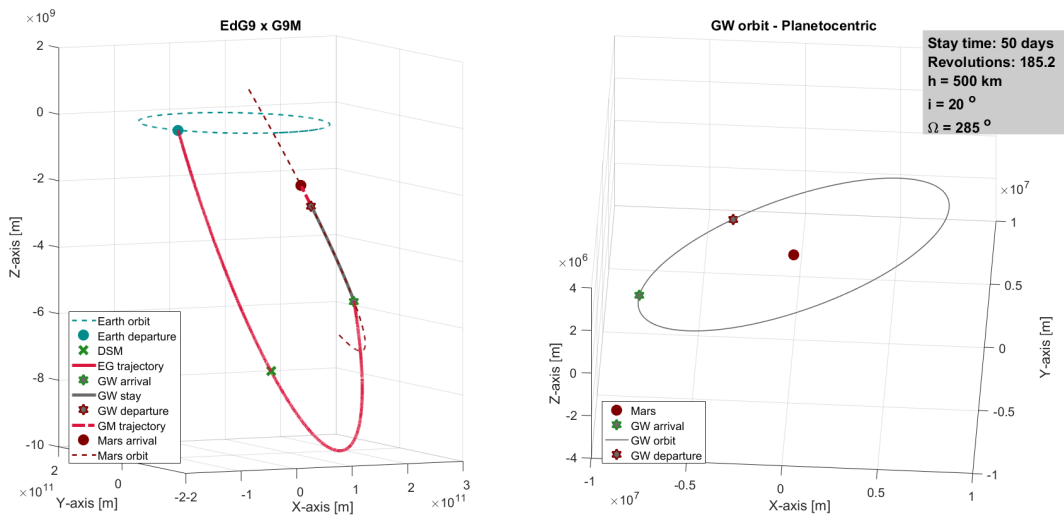


Figure 6.17: Plot of the EG and GM segments (left) and the GW segment (right) from the best transfer solution of the G9 gateway.

6.5. Discussion

This section will interpret the results shown in the previous section. It will analyse the outcomes through comparison but will also search for the physical meaning behind the numbers. As a result, several discussion points will be presented using a bulleted list to improve readability.

- **Adequate gateway comparison** - Similar to Analysis A, the results of Analysis B need an additional processing step so that they can adequately be compared among themselves and with Analysis A. Again, a table was made that lists the top 3 solutions for each gateway along with their average value for ΔV . A separate table was made for the Lagrange-point gateways and for the central-orbit gateways. Both can be found below.

G1			G2		
	Transfer	ΔV [km/s]		Transfer	ΔV [km/s]
Best	EdG1 x G1mEM	5.99		EmG2 x G2mEM	7.14
2nd	EmG1 x G1mEM	6.37		EmG2 x G2dM	7.15
3rd	EmG1 x GmM	6.84		EdG2 x G2mEM	7.36
average		6.40			7.22

G5			G6		
	Transfer	ΔV [km/s]		Transfer	ΔV [km/s]
Best	EdG5 x G5mEdEM	5.87		EdG6 x G6dM	7.23
2nd	EdG5 x G5mEM	6.23		EMG6 x G6dM	7.98
3rd	EmG5 x G5mEM	6.25		EmMG6 x G6dM	8.34
average		6.12			7.85

Table 6.14: Top 3 transfer solutions for the Lagrange-point gateways used to adequately compare gateway results.

G7			G8			G9		
	Transfer	ΔV [km/s]		Transfer	ΔV [km/s]		Transfer	ΔV [km/s]
Best	EG7 x G7dM	8.54		EEG8 x G8mEM	7.13		EdG9 x G9M	8.19
2nd	EG7 x G7mM	8.81		EdG8 x G8dM	7.14		EMG9 x G9M	9.61
3rd	EG7 x G7mEM	9.44		EmG8 x G8mEM	7.14		EmMG9 x G9M	9.88
average		8.93			7.14			9.23

Table 6.15: Top 3 transfer solutions for the central-orbit gateways used to adequately compare gateway results.

- **ΔV comparison between Analysis A and B** - Table 6.14 and Tables 5.25 till 5.27 allow comparison between the results of Analysis A and Analysis B for the Lagrange-point gateways. It can be seen that the transfer results for Analysis B are significantly lower in terms of ΔV than those in Analysis A for the G1, G2 and G5 gateway locations. Closer inspection tells us that ΔV improvements are realized in both the EG and GM segments. In contrast, the transfer solutions for the G6 gateway require more ΔV in Analysis B than in Analysis A. This increase is attributed to higher ΔV requirements in the EG segment. This behaviour was expected. With the gateways being in orbit, the spacecraft is able to maintain a higher energy level since it will lose less energy accelerating and decelerating at gateway arrival and departure. At G6, however, the spacecraft needs to accelerate to rendezvous with the gateway, before decelerating to reach Mars. This loss in energy is what makes the transfer solutions in Analysis B require more energy than in Analysis A.
- **Convergence comparison between Analysis A and B** - The convergence of the solutions is lower in Analysis B than it was in Analysis A. This is not surprising, since the number of design variables in Analysis B is much higher than in Analysis A. Not only were both EG and GM segments optimized simultaneously, but extra design variables were also added to be able to model the gateway orbits.

Despite the large expansion of design variables, most transfer solutions still show good results in the $< 1\%$ convergence range. There are some solutions that have a convergence score of 1 on both the $< 0.1\%$ and $< 1\%$ range. If one of these solutions would be selected to be analysed in Analysis C, they should first be further research using more powerful optimization settings.

- **Lagrange-point gateways vs. central-body gateways** - Tables 6.14 and 6.15 allow for a comparison between the two types of gateway locations: Lagrange-point locations and central body locations. It is evident that the Lagrange-point locations generally offer better transfer opportunities in terms of ΔV than the central-body gateway locations. The extra ΔV needed to bring the spacecraft in orbit around Earth or Mars can be spent more efficiently on reaching an outer Lagrange point. An exception is the gateway location orbiting the Moon. Due to the comparatively small mass of the Moon, orbital velocities are relatively low. As a result, less energy is lost arriving and departing from a lunar gateway than from an Earth or Mars gateway. Nevertheless, the Lagrange-point gateways G1 and G5 still offer more efficient transfer solutions.
- **Selection of extreme LPO's** - The Lagrange-point orbit libraries for each gateway consist of the range of orbit ID numbers listed in Table 6.16. This table also includes the Jacobi constants corresponding to this minimum and maximum orbit ID value.

Gateway	orbit ID		Jacobi constant	
	min	max	min	max
G1	0	256	3.171118	2.996727
G2	0	161	3.149023	3.015213
G5	0	104	3.000808	3.000216
G6	0	90	3.000187	3.000072

Table 6.16: Orbit ID ranges and corresponding Jacobi constants for the Lagrange-point Orbit libraries.

However, the transfer solutions of the Lagrange-point gateways often prefer gateway orbits at one of the extremes of the orbit library. This is, for instance, very clear for the G5 gateway location. As can be seen in Table 6.9, all but one of the G5 solutions rely on a gateway orbit at the edge of the orbit library (0 and 104). The same behaviour can be observed for most of the solutions for the other Lagrange-point gateways. The reason behind this is more easily understood by looking at a plot of the orbit library. As an example, the orbit library of the G5 gateway is plotted below, where the extremes have been highlighted.

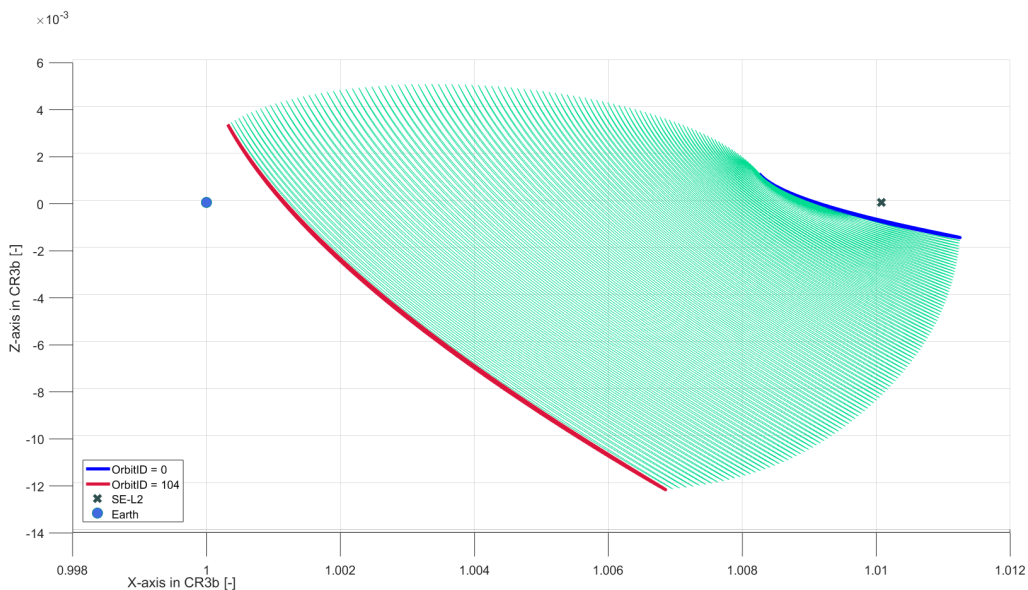


Figure 6.18: LPO library for G5 with highlighted extreme orbit ID's.

The G5 solutions that rely on a Lunar flyby after gateway departure all make use of a gateway orbit with an orbit ID of 0. This cannot be explained by looking at the position of the orbits in Figure 6.18. The lower the orbit ID, the farther away the gateway orbits from the Moon. It is explained, however, by the orbital energies. Equation 6.3, which introduced the Jacobi integral, is repeated below:

$$C = 2U - V^2 \quad (6.3)$$

Increasing (orbital) velocity adds kinetic energy to the system, which relates to a lower Jacobi constant. The transfer solutions that rely on a Lunar flyby after gateway departure use Halo orbits with higher Jacobi constants, which means they are in lower-energy orbits. The transfer solution that immediately escape the Sun-Earth system or use a high-energy Earth flyby after gateway departure use higher-energy Halo orbit with lower Jacobi constants. Using this line of thought, the gateway orbit solutions for the G1 gateway (Table 6.7) can also be better understood. When the gateway is reached after a Lunar flyby a lower-energy Halo orbit is preferred, whereas a higher-energy gateway orbit is more favourable after a direct transfer to the gateway.

- **Comparison of alternative LPO type gateways** - Although an explanation for the extreme orbit selection can be given, it does lead to a new question. What would the performance of a different gateway orbit type be? Since the LPO families are connected through bifurcation, an orbit from the vertical-Lyapunov family might be more suitable than selecting an extreme orbit from the Halo family. The vertical-Lyapunov family, with its amplitude in the Z-direction, offers many of the same advantages of the Halo orbit (discussed in Section 4.5.2). Analysis B was therefore performed one more time for the Lagrange-point gateways (G1, G2, G5 and G6) using exactly the same settings. The only difference is that now vertical-Lyapunov orbit libraries were used instead of Halo orbit libraries. The results of this extra study can be found in Tables 6.17 to 6.20.

Transfer	ΔV [km/s]			TOF [days]				Orbit [-]		Convergence [-/5]	
	Total	EG	GM	Total	EG	GW	GM	Orbit ID	σ_{arr}	<0.1%	<1%
EdG1 x G1dM	8.13	4.11	4.02	305	25	5	274	521	0.48	5	5
EdG1 x G1mEM	7.04	4.11	2.92	381	25	50	306	251	0.49	1	1
EdG1 x G1mM	7.47	4.08	3.39	250	25	28	197	320	0.96	4	5
EmG1 x G1dM	7.50	3.48	4.02	327	24	30	274	553	0.33	3	5
EmG1 x G1mEM	6.44	3.54	2.90	377	20	50	306	231	0.35	1	1
EmG1 x G1mM	6.90	3.51	3.39	246	25	24	197	359	0.38	3	5

Table 6.17: Transfer solutions results for the G1 gateway location (Em-L1) using vertical-Lyapunov gateway orbits.

Transfer	ΔV [km/s]			TOF [days]				Orbit [-]		Convergence [-/5]	
	Total	EG	GM	Total	EG	GW	GM	Orbit ID	σ_{arr}	<0.1%	<1%
EdG2 x G2dM	8.16	4.23	3.93	279	25	6	248	384	0.73	3	5
EdG2 x G2mEM	7.70	4.21	3.48	425	25	36	363	439	0.72	3	5
EmG2 x G2dM	7.83	3.89	3.93	322	25	49	248	439	0.90	1	4
EmG2 x G2mEM	7.40	3.92	3.48	393	25	44	324	439	0.39	2	3

Table 6.18: Transfer solutions results for the G2 gateway location (Em-L2) using vertical-Lyapunov gateway orbits.

Transfer	ΔV [km/s]			TOF [days]				Orbit [-]		Convergence [-/5]	
	Total	EG	GM	Total	EG	GW	GM	Orbit ID	σ_{arr}	<0.1%	<1%
EdG5 x G5EM	6.33	3.25	3.08	382	67	13	301	22	0.44	5	5
EdG5 x G5dM	8.04	3.38	4.66	436	100	50	286	8	0.53	5	5
EdG5 x G5mEM	5.93	3.25	2.67	458	72	20	365	21	0.46	4	4
EdG5 x G5mEdEM	5.48	3.26	2.22	461	70	26	364	21	0.95	2	3
EmG5 x G5EM	6.31	3.28	3.03	390	43	44	303	37	0.35	1	5
EmG5 x G5dM	8.02	3.33	4.69	450	100	50	300	9	0.49	5	5
EmG5 x G5mEM	5.89	3.29	2.60	466	80	21	365	21	0.95	2	2
EmG5 x G5mEdEM	5.51	3.28	2.85	472	81	26	365	22	0.96	4	4

Table 6.19: Transfer solutions results for the G5 gateway location (SE-L2) using vertical-Lyapunov gateway orbits.

Transfer	ΔV [km/s]			TOF [days]				Orbit [-]		Convergence [-/5]	
	Total	EG	GM	Total	EG	GW	GM	Orbit ID	σ_{arr}	<0.1%	<1%
EMG6 x G6dM	8.74	6.08	2.66	429	328	1	100	13	0.84	5	5
EdG6 x G6dM	8.33	5.64	2.69	406	305	1	100	27	0.10	4	4
EmMG6 x G6dM	8.83	6.01	2.82	297	196	1	100	11	0.76	3	3

Table 6.20: Transfer solutions results for the G6 gateway location (SM-L1) using vertical-Lyapunov gateway orbits.

These results can now be compared to the results in Tables 6.7 to 6.10. For overview purposes, this comparison is shown in Table 6.21.

<u>G1</u>	ΔV [km/s]		<u>G2</u>	ΔV [km/s]	
Trajectory	Halo	vLya	Trajectory	Halo	vLya
EdG1 x G1dM	7.38	8.13	EdG2 x G2dM	7.53	8.16
EdG1 x G1mEM	5.99	7.04	EdG2 x G2mEM	7.36	7.70
EdG1 x G1mM	6.94	7.47	EmG2 x G2dM	7.15	7.83
EmG1 x G1dM	7.56	7.50	EmG2 x G2mEM	7.14	7.40
EmG1 x G1mEM	6.37	6.44			
EmG1 x G1mM	6.84	6.90			

<u>G6</u>	ΔV [km/s]		<u>G5</u>	ΔV [km/s]	
Trajectory	Halo	vLya	Trajectory	Halo	vLya
EMG6 x G6dM	7.98	8.74	EdG5 x G5EM	7.25	6.33
EdG6 x G6dM	7.23	8.33	EdG5 x G5dM	7.66	8.04
EmMG6 x G6dM	8.34	8.83	EdG5 x G5mEM	6.23	5.93
			EdG5 x G5mEdEM	5.87	5.48
			EmG5 x G5EM	7.31	6.31
			EmG5 x G5dM	7.64	8.02
			EmG5 x G5mEM	6.25	5.89
			EmG5 x G5mEdEM	6.48	5.51

Table 6.21: Comparison of ΔV results of the different transfers per gateway between Halo- and vertical-Lyapunov gateway orbits.

The transfers in Table 6.21 that perform better in terms of ΔV using a Lyapunov gateway orbit have been made bold. As can be seen, significant improvements were made for the G5 gateway location (SE-L2) for almost all trajectory combinations. All trajectories that require a flyby in the GM-segment prefer a Lyapunov gateway orbit over a Halo gateway orbit. The result of using a different gateway orbit can best be studied by comparing Figures 6.19 and 6.20 to Figures 6.11 and 6.12. These figures show the same trajectories, but for different gateway orbit types. As is evident,

the vertical amplitude of the Lyapunov orbit is significantly larger than that of the Halo-orbit. As a result, the Lunar flyby must be used to swing back into the Earth's orbital plane, so that the two consecutive Earth flybys can be performed.

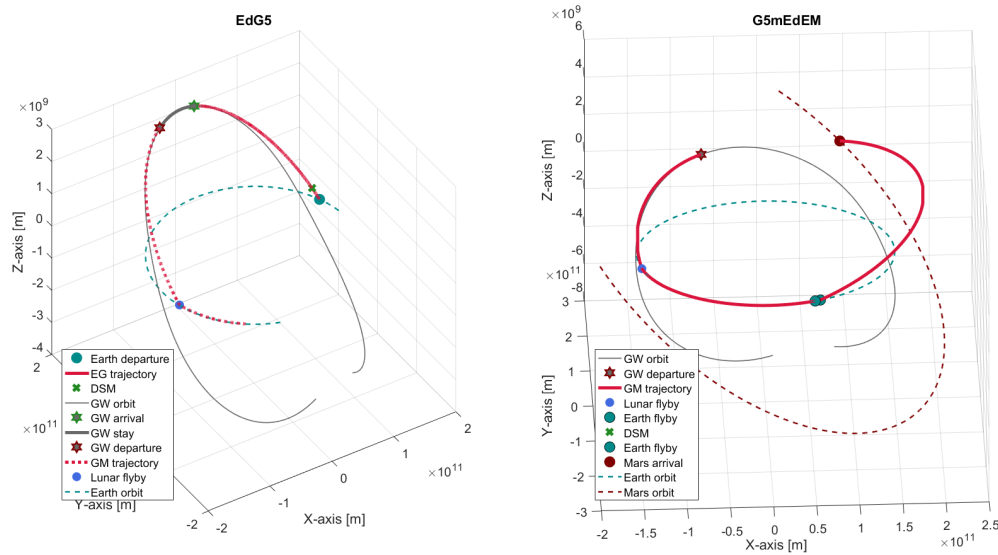


Figure 6.19: Plot of the EG and GM segment from the best transfer solution of the G5 gateway using a vertical-Lyapunov gateway orbit.

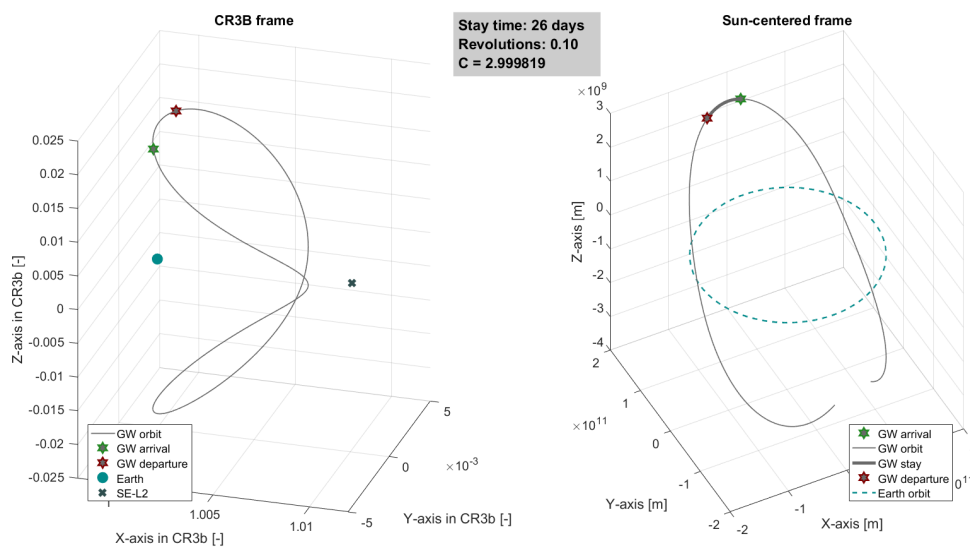


Figure 6.20: Plot of the GW segment from the best transfer solution of the G5 gateway in the CR3BP- and Sun-centred frame using a vertical-Lyapunov gateway orbit.

- Edges of GW stay time bounds** - As was the case in Analysis A, the trajectory solutions in Analysis B again favour TOF values at the edge of the bounds for, predominantly, the EG-segment. In Analysis B, this behaviour is also visible for the gateway stay time for the gateway located at G5 in a Halo orbit (Table 6.9), where the maximum stay time of 50 days is used for all trajectory options. The fact that this behavior is not visible for the gateways at G5 that are in a vertical-Lyapunov orbit suggests that the characteristics of the Halo orbit make a longer gateway stay time beneficial to minimizing total ΔV of the transfer. Further research is recommended to investigate why a longer

gateway stay time is especially effective in combination with a gateway in Halo-orbit, which will be proposed in Chapter 10.

- **Orbital parameters in central-orbit optimization** - Three Kepler elements were used to model the central-body gateway orbits: altitude h (direct relation to radius r), inclination i and longitude of ascending node (LOAN) Ω . By comparing the outcomes of the five seed values for each solution, the importance of each parameter to the solution can be studied. This is only relevant for transfer solutions with high convergence values. The seeds of multiple high-convergence transfer solutions were studied for the central-body gateways (G7, G8 and G9). Table 6.22 contains an example for each.

Seed	G7	EG7 x G7EM			G8	EEG8 x G8mEM			G9	EMG9 x G7M		
	Orbit ID	h [km]	i [$^\circ$]	Ω [$^\circ$]	Orbit ID	h [km]	i [$^\circ$]	Ω [$^\circ$]	Orbit ID	h [km]	i [$^\circ$]	Ω [$^\circ$]
123	123	35786	5.0	45	84	300	5.0	180	40	5000	20.0	240
234	71	35786	28.5	345	84	300	5.0	180	40	5000	20.0	240
345	52	35786	28.5	60	87	300	5.0	225	40	5000	20.0	240
456	120	35786	5.0	0	81	300	5.0	135	42	5000	20.0	270
567	51	35786	28.5	45	78	300	5.0	90	85	5000	50.0	195

Table 6.22: Example of seed study into significance of Kepler elements in gateway orbit modelling for each central-body orbit.

Again, Table 6.22 only shows a single transfer solution, while several were studied for each gateway. This study showed that the LOAN (Ω) is not a driving factor in gateway orbit design. Furthermore, it has shown that the inclination of the gateway orbit for the G7 gateway (Earth orbit) does not have a clear preference between 28.5 and 5.0 degrees. For the Lunar and Martian central gateway orbits (G8 and G9) the solutions do provide a clear outcome for the orbital inclination. For all three gateway configurations, there is clear convergence for a single orbital height (h) parameter. The next discussion point will go into the orbit outcomes for the central-body gateways.

- **Orbit features of central-body gateway orbits** - The results shown in Section 6.4 for the central-body gateways (G7-G9) in combination with the orbit ID information found in Appendix B create insight into preferred orbital parameters for central-body gateway orbits. Three important features could be extracted. Firstly, all gateway orbit solutions make use of the maximum allowed orbital altitude h . This means a GEO for Earth-orbiting gateways and a 300km- and 5000km-orbit for Lunar and Mars central-body gateways, respectively. It might be especially surprising that a GEO orbit is recommended, since getting into GEO from LEO is expensive. Apparently, a gateway in GEO enables more efficient interplanetary transfers compared to lower-altitude gateway orbits, so that the expensive EG-segment is compensated for. Secondly, the orbital inclination of the Lunar gateway orbit solution is dependent on the outgoing GM-transfer. All gateway solutions for the G8 gateway that contain a flyby in the GM-segment make use of a gateway orbit with a small inclination ($i = 5.0^\circ$). If a direct transfer ($G8dM$) is used, the orbital inclination of the G8 gateway orbit is high ($i = 70.0^\circ$). In order to perform a flyby, the spacecraft will need to remain in the orbital plane of the Earth and the Moon, which explains the low inclination angle of the gateway orbit. The high inclination angle in combination with a DSM can be used to account for the difference in inclination between Earth and Mars orbit for the gateway solutions that make use of a direct transfer in the GM-segment. Lastly, all Mars gateway solutions make use of the lower inclination angle ($i = 20.0^\circ$). This could be expected, since this allows for a smaller total inclination change between Earth and the gateway.

In short, an optimal central-body gateway orbit should always have a high orbital altitude. The choice for the orbital inclination of the gateway orbit is only relevant for a Lunar central gateway, as the inclination for a Mars gateway should always be 20 degrees and the choice of inclination angle for an Earth gateway is insignificant (between the 28.5° and 5.0° options).

- Meaning of σ_{arr} for arrival and departure conditions** - On first sight, the values for the arrival fraction (σ_{arr}) in Tables 6.7 till 6.13 and 6.17 till 6.20 seem to be random. However, when they are analysed into further detail it becomes evident that the σ_{arr} values are carefully selected by the optimization program. The program finds the optimal gateway arrival state through selection of the most suited arrival fraction and finds the optimal gateway departure state through tuning the combination of gateway stay time and the arrival fraction (σ_{arr}). Patterns in arrival and departure conditions become evident when plotting the arrival and departure states in a figure. An example of such an analysis will be provided below.

The results for the G1 gateway (Em-L1) in Table 6.7 show that for a *EdG1* transfer in the EG-segment, a rendezvous with the gateway can best be performed mid-orbit ($\sigma_{arr}=0.50$). The reason for this can be explored by plotting the Halo-orbit family at Em-L1 and highlighting the orbital states corresponding to $\sigma_{arr}=0.50$. This was done in Figure 6.21.

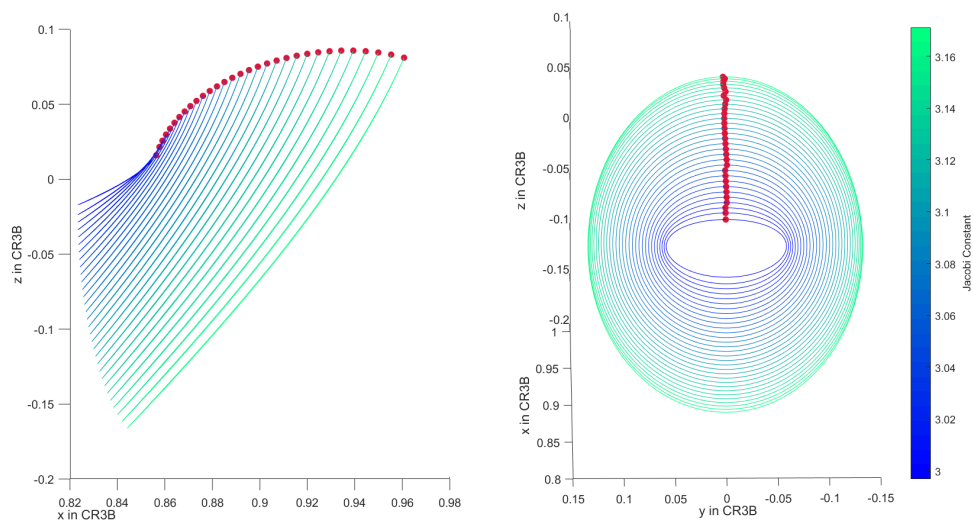


Figure 6.21: Position of $\sigma_{arr} = 0.5$ (red dots) in G1 gateway Halo orbit family

From the figure above, it is evident that the $\sigma = 0.50$ orbital state corresponds to the state that has the highest value in the Z-direction. Figure 6.22 explores the velocity state of these points.

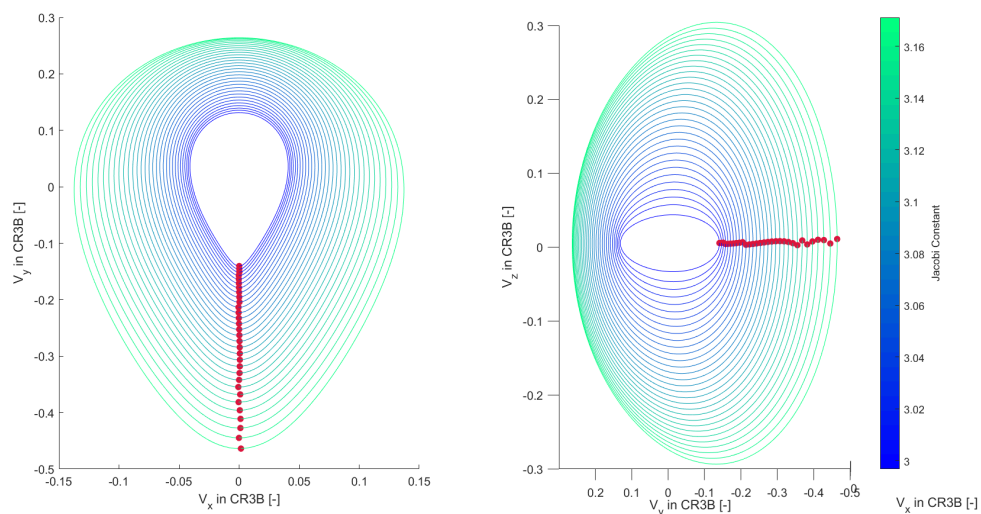


Figure 6.22: Velocity state of $\sigma_{arr} = 0.5$ (red dots) in G1 gateway Halo orbit family

Interestingly, the $\sigma_{arr} = 0.50$ arrival state corresponds to a state where the velocities in the X- and Z-directions in the CR3BP-frame are (close to) zero and the velocity in the Y-direction is at its maximum value. In the Sun-centered frame, a spacecraft at the end of the *EdG1* transfer will have a velocity in all three directions. In the CR3BP-frame however, the majority of the velocity of the incoming spacecraft will be in the Y-direction due to the geometry of the trajectory (Figure 6.7). When the orbital velocity in this direction is maximized, less ΔV needs to be spent for rendezvous with the gateway.

Furthermore, Figure 6.8 shows that the departure from the gateway matches the arrival state in the CR3BP-frame. To accomplish this, the gateway stay time was carefully selected to be an integer multiple of the gateway's orbital period. As a result, the departing spacecraft benefits from the extra velocity in the Y-direction (of the CR3BP-frame) to gain energy needed for the consecutive Lunar and Earth flyby. The gateway stay time therefore also plays an important role in establishing the optimal departure conditions. This can also be seen for other transfers. Figure 6.23 depicts the arrival and departure conditions for the *EdG1 x G1dM* transfer.

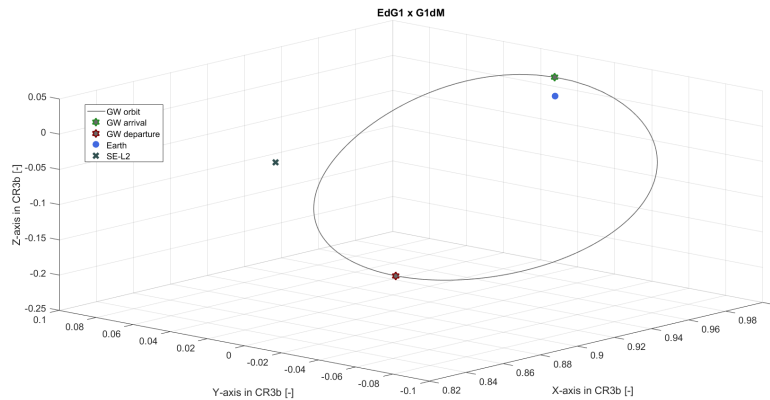


Figure 6.23: Arrival and departure state with respect to the gateway Halo orbit for the *EdG1 x G1dM* transfer

For this transfer, the most beneficial departure condition apparently is at the opposite of the discussed arrival condition. In Figure 6.22 it can be seen that the gateway will have a velocity in the opposite Y-direction as a result of the Halo orbit. This makes sense, since the direct transfer to Mars (*G1dM*) requires a decrease in heliocentric velocity.

The figures and discussions above are just one example of how the model uses the arrival fraction and gateway stay time to find optimal gateway arrival and departure conditions. These analyses can be performed for all transfer solutions and will yield insight into the physical meaning of the values for σ_{arr} and the GW stay time. For the purpose of this thesis, these analyses were not deemed crucial and will therefore not be further elaborated on.

6.6. Conclusions

Through the addition of orbit modelling and segment timing, Analysis B has realistically investigated the performance of a great number of different gateway design options. As a result, conclusions can now be drawn regarding suitable gateway locations, gateway orbit families and gateway transfer options. These conclusions will be the starting point of the final analysis, Analysis C, which will investigate a handful of gateway trajectory designs into more detail. A gateway design comprises of a gateway location, a gateway orbit, and its transfer options for the EG- and GM-segments. This conclusion section will therefore be split into these three elements. Additionally, the final subsection will list findings that do not directly influence Analysis C but are significant to gateway design in general.

6.6.1. Selecting gateway locations

A total of seven different gateway locations have been considered in this analysis. Three of these locations are the so-called central-orbit gateways and the other four are Lagrange-point gateways. These locations have been evaluated on the basis of the ΔV requirements of the Earth-to-Mars transfers they support. Locations can best be compared by looking at the average of the best three transfers and the single best transfer each location supports. These results were presented in Tables 6.14 and 6.15 and have been distilled into Table 6.23. Additionally, a bar plot is depicted in Figure 6.24, for a better overview.

GW	Best ΔV [km/s]	Average ΔV [km/s]
G5	5.48	5.63
G1	5.99	6.40
G8	7.13	7.14
G2	7.14	7.22
G6	7.23	7.85
G9	8.19	9.23
G7	8.54	8.93

Table 6.23: Comparison of the performance of the different gateway locations in Analysis B.

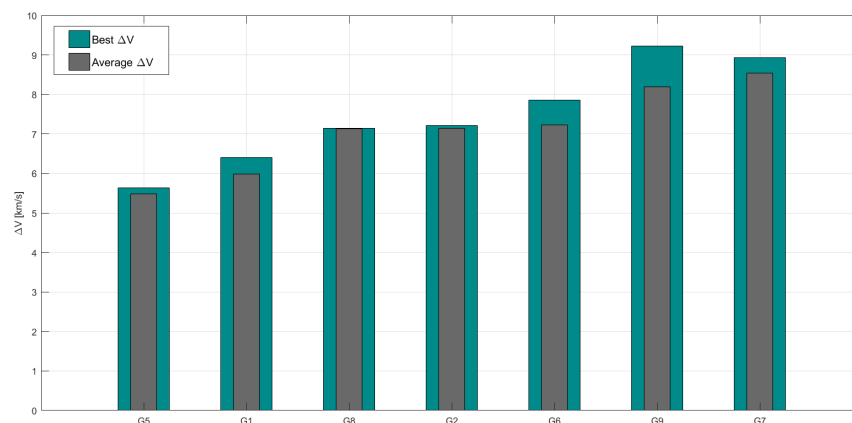


Figure 6.24: Bar plot of the results shown in Table 6.23

It must be noted that the results for gateway G5 (SE-L2) were taken from Table 6.19 using the vertical-Lyapunov orbit family. This will be further clarified in the next conclusion section.

On the basis of these results, three gateway locations can be selected to be further investigated in Analysis C: G5, G1 and G8. Besides from being the top 3 scoring gateway locations, this selection was also favoured because of its diversity. It includes a gateway at a central-body orbit and Lagrange-point gateways in two different three-body systems. The selected locations are illustrated in Figure 6.25.

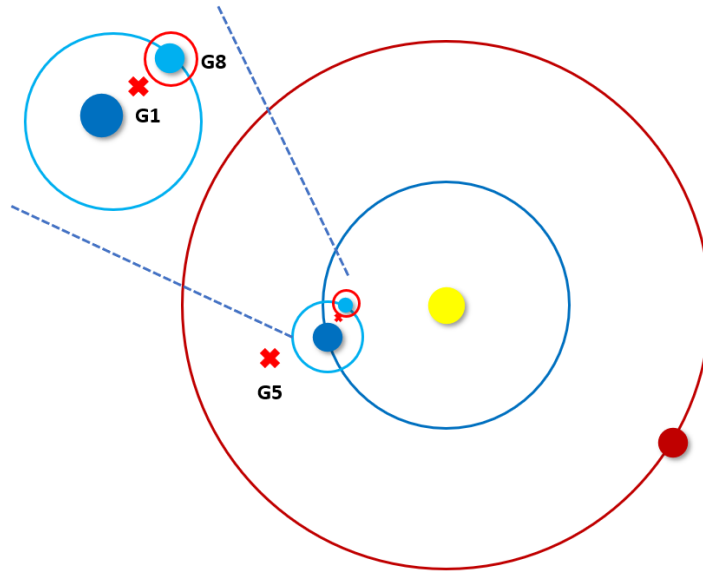


Figure 6.25: Selection of gateway locations to be considered in Analysis C.

6.6.2. Gateway orbit

Next to the location, gateway performance is heavily dependent on the orbit the gateway is in. By modelling gateway orbits and by performing segment timing, Analysis B set out to create insight into how transfer performance depends on gateway orbits. In Analysis B, a great variety of different orbits were tested for each gateway location. The design of a gateway orbit consists of two choices. First, an orbit family needs to be chosen. This is only relevant for the Lagrange-point gateways, since the central-body gateways were only tested for central orbits. Second, a specific orbit from the orbit family library is found in the optimization process. This choice of specific orbit depends on the transfer trajectories used for the EG- and GM-segments and will therefore be discussed after the next section.

The orbit family chosen for each gateway location is listed in Table 6.24 below. It was found that using a vertical-Lyapunov gateway orbit family enables significantly more efficient transfers from the G5 gateway in terms of ΔV . Despite the preference for Halo orbits in literature, it was therefore decided to use vertical-Lyapunov orbits for the G5 gateway trajectory designs, since their amplitude in the Z-direction offer the same advantages as that of Halo orbits.

Location	Orbit family
G5	Vertical-Lyapunov
G1	Halo
G8	Central

Table 6.24: Choice of gateway orbit family for each gateway location to be considered in Analysis C.

6.6.3. Transfer options

A variety of different combinations between trajectories in the EG-segment and trajectories in the GM-segment were tested in Analysis B. Their performance in terms of ΔV for the entire Earth-to-Mars transfer was listed in Tables 6.7 to 6.13 or Table 6.19 for gateway G5. Preferably, only a single trajectory for each segment is chosen per gateway to be investigated in Analysis C. This choice is dictated by the ΔV budget of the entire transfer. If the difference in ΔV between transfer options is small, the trajectories with a lower complexity were chosen (i.e. *EdG8 x GdM* was chosen over *EEG8 x G8mEM*). Extra options were added for the G1 and G5 gateway trajectory designs to increase the scope of the research. The transfer trajectories selected are listed in Table 6.25 below. This table also features the orbit ID of the gateway orbit that best supports this transfer. The table therefore features all information on the selection of gateway trajectory designs to be considered in Analysis C.

Location	Orbit family	EG options	GM options	Orbit ID
G5	Vertical-Lyapunov	EdG5	G5mEdEM G5mEM	21
G1	Halo	EdG1 EmG1	G1mEM	218
G8	Central	EdG8	G8dM	45

Table 6.25: Selection of gateway trajectory designss to be considered in Analysis C.

6.6.4. Additional findings

Next to producing results that are useful in Analysis C, Analysis B has also brought forward some significant findings. These findings, relevant to anyone who is interested in gateway trajectory designs and mission planning, are listed concisely below.

- **Significance of gateway orbit** - It was found that the orbit in which the gateway is stationed has a significant effect on the performance of the gateway design. This effect can most easily be observed when comparing the results for gateway G5 (SE-L2) using Halo- and vertical-Lyapunov orbits in Tables 6.9 and 6.19. The optimal orbit selection is dependent on the transfer trajectories that the gateway will support. Lower-energy orbits are preferred when a Lunar flyby is included in the GM-segment, for instance.
- **Difference between orbit families for LPO gateways** - Analysis B has shown that it can be very beneficial to consider different orbit families need to be considered when designing gateway orbits at Lagrange points. The two LPO families that need to be considered are Halo orbits and vertical-Lyapunov orbits because of their amplitudes in the Z-direction.
- **Performance of central-orbit gateways at focus planets** - Analysis B tested the central-body orbit gateways for the first time. The performance of gateways in orbit around Earth and around Mars was significantly worse than the performance of LPO gateways and of a gateway around the Moon.
- **Use of high-altitude central orbits** - When designing a central-orbit gateway, the use of high-altitude orbits is advised. For all three central-orbit gateway locations, all found optimal solutions consisted of the highest possible orbital altitude.

7

Analysis C - Final selection

This chapter will discuss the final analysis of this thesis. In Analysis C, a definite gateway trajectory design will be proposed based on a detailed evaluation of multiple evaluation criteria. The chapter will start with an introduction of Analysis C, which includes a purpose statement for the analysis. Next, Section 7.2 will discuss the methodology used in this analysis. Section 7.4 will then feature the results produced by these methods followed by a discussion of the results in Section 7.5. The chapter is then ended by a conclusion section in Section 7.6.

7.1. Analysis introduction

At the start of this thesis work, a total of 17 potential gateway locations had been identified. The gateway locations, combined with numerous transfer options and gateway orbit possibilities, lead to countless different gateway trajectory designs. Through the research done in Analysis A and Analysis B, the total number of potential gateway trajectory designs has been brought back to only three different designs. The filtering and selection were based on a single evaluation criterion: The ΔV budget of the Earth-to-Mars transfer supported by the gateway trajectory design. Although this evaluation criterion is very suitable for effective filtering of gateway designs, it does not take other important practical decision-making variables into considerations.

Analysis B has provided a total of three gateway trajectory designs that prove favourable in terms of the ΔV requirements of the Earth-to-Mars transfer they support. In Analysis C, these three gateway designs will be further researched on based on two extra evaluation criteria: Consistency and Time of flight (TOF). The final goal of this analysis is to propose a single gateway trajectory design for the mission that was proposed in Section 4.1. This gateway proposal will be the design that scores best when evaluated on all criteria introduced in Section 4.2. The essence of Analysis C was captured in the purpose statement below.

Analysis purpose statement:

Analysis C will aim to propose a single gateway trajectory design by evaluating the three remaining designs on their consistency and their TOF characteristics.

7.2. Methodology

Following the purpose statement above, methods were developed to test the consistency and the TOF characteristics of the three contending gateway trajectory designs. To test each, separate simulations were performed. The methodology of these two experiments will therefore be discussed separately as well. Before zooming into these, a general overview of Analysis C is given along with the settings that are shared among the two methods. This is done in the first subsection on the next page.

7.2.1. General method

As was mentioned, the two evaluation criteria are tested in two separate experiments:

- **Analysis C-I** - Consistency testing
- **Analysis C-II** - Time of Flight (TOF) study

Analysis C-I will explore the degree of consistency the three gateway trajectory designs offer. As was discussed in Section 4.2, a highly consistent design allows for frequent Earth-to-Mars travel at comparable ΔV levels. A design that lacks in consistency, is one that supports a low ΔV transfer only once every synodic period for instance. The consistency of the designs will be tested by optimization of multiple short launch windows. This method will be further explained in Section 7.2.2

Analysis C-II will investigate the TOF characteristics of the transfers supported by the three gateway trajectory designs. Section 7.2.3 will further detail how this analysis is performed.

Although these two analyses are fundamentally different, they do share some similarities. These will be listed below:

1. **Gateway designs to be considered** - In Analysis B, three gateway trajectory designs were selected to be considered in this analysis. A gateway trajectory design consists of its location, its orbit, and the transfer trajectories it should support. These elements were listed in Table 6.23 and have been repeated in Table 7.1 below.

Location	Orbit family	EG options	GM options	Orbit ID
G5	Vertical-Lyapunov	EdG5	G5mEdEM G5mEM	21
G1	Halo	EdG1 EmG1	G1mEM	218
G8	Central	EdG8	G8dM	45

Table 7.1: Selection of gateway trajectory designs to be considered in Analysis C.

2. **Gateway orbits** - In the previous analysis, the gateway orbit was optimized. In the coming two analyses, the gateway orbit is set to the orbit ID that corresponds to the solution found in Analysis B. In Table 7.2, the found orbit IDs are translated to relevant orbital parameters for each gateway design. The orbit arrival fraction (σ_{arr}) and the gateway stay time will still be optimized in both analyses. The stay time is once again bound between 1 and 50 days.

LPO gateways			
Design	Orbit family	Jacobi constant [-]	Period [days]
G5	Vertical-Lyapunov	3.000832	283.4
G1	Halo	3.002606	8.3

Central body gateway					
Design	Orbit family	h [km]	i [deg]	Ω [deg]	Period [hours]
G8	Central	300	70	315	2.3

Table 7.2: Orbits of the gateway trajectory designs considered in Analysis C.

3. **Same use of ephemeris settings and seeds** - The same ephemeris settings as in Analysis A and B were used, which can be found in Table 5.3. Furthermore, the same seed numbers as in Analysis B have been implemented: 123, 234, 345, 456, 567.

7.2.2. Analysis C-I: Consistency testing

The methodology used in this analysis will, again, be presented in the form of a numbered list to improve readability.

1. **Launch window segmentation** - The consistency of the gateway designs is tested by optimizing the transfer options for multiple smaller launch windows. As a result, the program is forced to find an optimum solution for each launch window segment instead of finding a single solution for the entire window. To this extent, the following segmentation was used: The synodic period of Earth and Mars (approximately 780 days) was split into ten segments. Each segment therefore consists of 78 days. The first launch window starts at January 1st, 2033, so that the optimal solutions found in Analysis B are included. Table 7.3 further clarifies the launch window segmentation.

Segment	MJD2000		Date [dd/mm/yyyy]	
	Begin	End	Begin	End
1	12054	12131	01-01-2033	19-03-2033
2	12132	12209	20-03-2033	05-06-2033
3	12210	12287	06-06-2033	22-08-2033
4	12288	12365	23-08-2033	08-11-2033
5	12366	12443	09-11-2033	25-01-2034
6	12444	12521	26-01-2034	13-04-2034
7	12522	12599	14-04-2034	30-06-2034
8	12600	12677	01-07-2034	16-09-2034
9	12678	12755	17-09-2034	03-12-2034
10	12756	12833	04-12-2034	19-02-2035

Table 7.3: Launch window segmentation used in Analysis C-I.

For each segment, an optimum solution will be produced. These can later be examined and compared to the other segments of the same gateway trajectory design and be used to compare the different gateway trajectory designs.

2. **Single-objective optimization of ΔV** - Similar to Analysis A and Analysis B, this analysis will also optimize the trajectories for a single objective. This objective, again, is the ΔV required for the transfer.
3. **Similar settings to Analysis B** - If no further mention is found in this chapter, one may assume that the remainder of the settings is similar to those in Analysis B. The same optimization algorithm, for instance, is used. In general, the methods used in Analysis B have been applied in Analysis C, albeit with different launch windows.

7.2.3. Analysis C-II: Testing TOF characteristics

The prior analyses have all focused on ΔV budget values to evaluate the different gateway trajectory designs. Analyses A and B have used the ΔV value to find the most efficient designs. Analysis C-I used these values to assess the practicality of the designs by looking at the consistency. The final analysis, Analysis C-II, will also concern a practical aspect of the gateway design but this time by evaluating the TOFs of the transfers that it supports.

Originally, this research set out to perform a multi-objective optimization of the ΔV and TOF values for the various gateway designs. This analysis would then produce Pareto-fronts for each design, which could be used to evaluate and compare the TOF characteristics of the various designs. Unfortunately, however, no accurate Pareto-fronts could be produced with the computational capabilities and time at hand. Even though the settings of the optimization algorithm (NSGA-II) were tuned extensively and large population sizes and number of generations were implemented, the Pareto-fronts for different seed values converged insufficiently. The failed attempt at this multi-objective optimization was documented and can be found in Appendix C. An alternative method to investigate the TOF characteristics of the gateway trajectory designs was developed and will be discussed in this section.

- **Single-objective optimization with varying TOF** - In order to acquire insights into the TOF characteristics of the different gateway trajectory designs without using a multi-objective optimization, a single-objective optimization with varying constraints on TOF can be used. Such an analysis optimizes the ΔV for different maximum TOF values. As a result, the optimal transfer in terms of ΔV is found for different TOF segments.
- **TOF constraints** - The time-of-flight constraints shown in Table 7.4 were used in Analysis C-II. The lower value of 200 days was chosen based on the TOF of the optimal direct transfer between Earth and Mars, which is roughly 200 days (the *EM*-transfer is discussed in Chapter 8). The upper value of 350 days was chosen, as flight times of over a year were deemed unrealistic.

#	TOF constraint [days]
1	200
2	250
3	300
4	350

Table 7.4: TOF constraints used in Analysis C-II.

- **Launch window setting** - The launch window used in Analysis C-II starts at January 1st, 2033, and lasts 780 days, which is one synodic period. This launch window is the same as the one used in Analysis C-I, but without the launch window segmentation.

7.3. Verification

Although the methodology of the two analyses in Analysis C is very similar to the that of the analyses before, it is important to verify the methods. For both Analysis C-I and C-II, a simple verification can be performed using the results from Analysis B. Analysis C-I is verified if the optimal solution of Analysis B is found for one of the ten launch window segments. Analysis C-II was verified by checking to see if the solution of Analysis B is found after removing the TOF constraints. Table 7.5 compares the optimal solution for each gateway transfer in Analysis B with the solution of the best launch window segment of Analysis C-I and of the solution of Analysis C-II without TOF constraints. As can be seen, the solutions closely match. Small differences between the solutions of Analysis C-I and Analysis B are explained by the non-perfect convergence, which was discussed in Section 6.5. Based on this table, the methodology and the produced results for Analysis C are considered to be verified.

Gateway transfer	Analysis	Segment	Departure date	ΔV [km/s]	TOF [days]	Stay time [days]	σ_{arr} [-]
EdG1 x G1mEM	Analysis B	N/A	12777	5.99	386	25	0.50
	Analysis C-I	10	12777	5.99	386	25	0.50
	Analysis C-II	N/A	12777	5.99	386	25	0.50
EmG1 x G1mEM	Analysis B	N/A	12745	6.37	417	31	0.78
	Analysis C-I	9	12745	6.37	417	31	0.80
	Analysis B	N/A	12745	6.37	417	31	0.78
EdG5 x G5mEdEM	Analysis B	N/A	12703	5.48	461	26	0.95
	Analysis C-I	9	12703	5.48	461	22	0.96
	Analysis B	N/A	12703	5.48	461	26	0.95
EdG5 x G5mEM	Analysis B	N/A	12703	5.93	458	20	0.46
	Analysis C-I	10	12703	5.89	459	20	0.96
	Analysis B	N/A	12703	5.93	458	20	0.46
EdG8 x G8dM	Analysis B	N/A	12094	7.14	259	41	0.76
	Analysis C-I	1	12097	7.14	258	42	0.76
	Analysis B	N/A	12094	7.14	259	41	0.76

Table 7.5: Verification of Analysis C by comparing optimal solutions of Analysis B and C.

7.4. Results

The results of Analysis C-I and Analysis C-II will be presented in this section. The section will be structured in five subsections, one for each different gateway transfer trajectory option. Each subsection will include the results from both analyses. The results of Analysis C-I, the consistency testing, are presented in the form of a table displaying the best solution for each launch window segment and in the form of a figure, which depicts the trajectories for each launch window split into the two segments. The results of Analysis C-II will be displayed in the form of a Table that lists the optimal trajectory solution for each TOF constraint and a figure showing the optimal trajectories for each constraint value split into the two segments. Most discussion and conclusion points will be drawn from the table, but the figures do improve insight into the analysis.

7.4.1. G1 (Em-L1) - *EdG1 x G1mEM*

Analysis C-I: consistency testing

Segment [-]	Departure date [MJD2000]	ΔV [km/s]	TOF [days]	Stay time [days]	σ_{arr} [-]
1	12073	6.41	287	8	0.49
2	12132	6.96	233	6	0.50
3	12211	9.51	313	6	0.51
4	12288	12.39	387	6	0.50
5	12444	16.19	440	50	0.50
6	12522	9.44	440	50	0.50
7	12600	9.09	440	50	0.49
8	12678	6.63	440	50	0.49
9	12746	6.07	416	42	0.50
10	12777	5.99	386	25	0.50

Table 7.6: Consistency testing results of the *EdG1 x G1mEM* transfer.

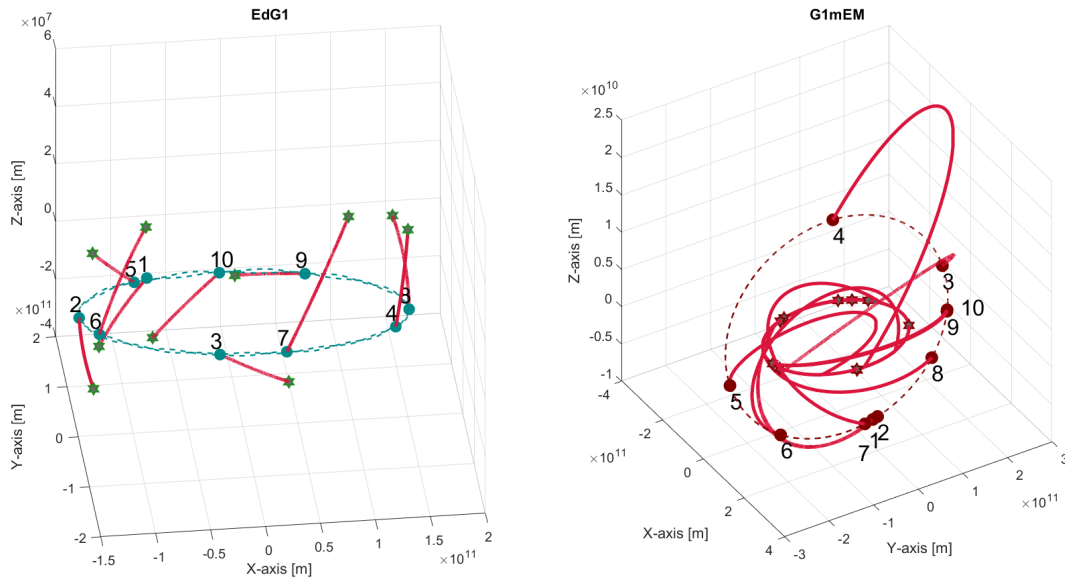


Figure 7.1: Plot of the best solutions for each launch window segment for both EG- and GM-segment of the *EdG1 x G1mEM* transfer.

Analysis C-II: Testing TOF characteristics

TOF constraint	ΔV [km/s]			TOF [days]				Orbit [-]	
	Total	EG	GM	Total	EG	GW	GM	Orbit ID	σ_{arr}
200 days	7.26	3.55	3.71	200	15	5	180	218	0.50
250 days	6.93	3.44	3.48	246	25	14	207	218	0.51
300 days	6.41	3.47	2.94	287	25	8	254	218	0.51
350 days	6.05	3.42	2.63	330	25	25	280	218	0.51

Table 7.7: TOF characteristics results of Analysis C-II for *EdG1 x G1mEM* transfer.

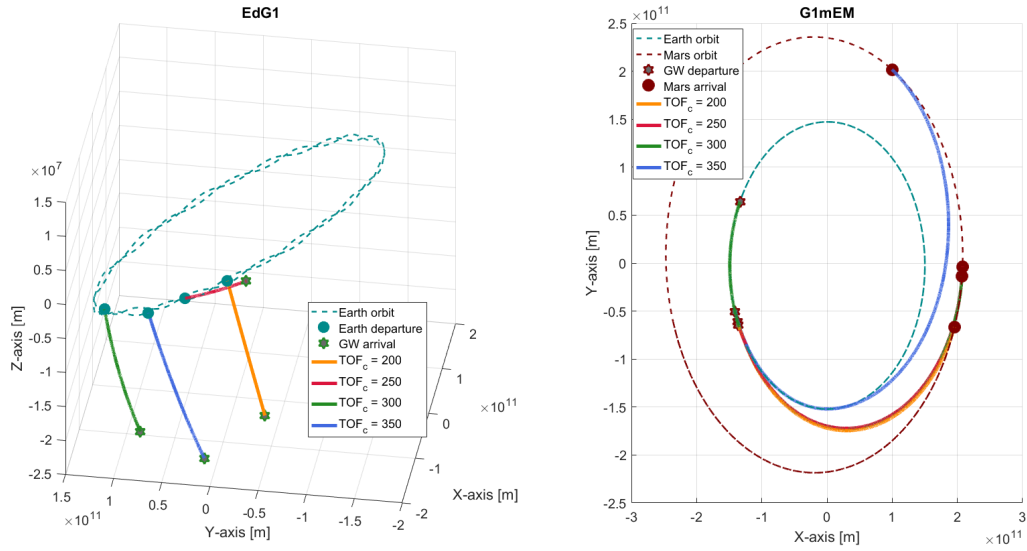


Figure 7.2: Plot of the best solutions for each TOF constraint (TOF_c) for both EG- and GM-segment of the *EdG1 x G1mEM* transfer.

7.4.2. G1 (Em-L1) - *EmG1 x G1mEM*

Analysis C-I: consistency testing

Segment [-]	Departure date [MJD2000]	ΔV [km/s]	TOF [days]	Stay time [days]	σ_{arr} [-]
1	12054	6.74	307	31	0.82
2	12132	7.28	233	3	0.79
3	12210	9.15	278	3	0.84
4	12288	12.29	365	1	0.02
5	12444	16.46	440	50	0.49
6	12522	12.07	440	50	0.49
7	12600	9.31	440	50	0.49
8	12678	6.84	440	50	0.49
9	12745	6.37	417	31	0.80
10	12795	6.40	368	6	0.77

Table 7.8: Consistency testing results of the *EmG1 x G1mEM* transfer.

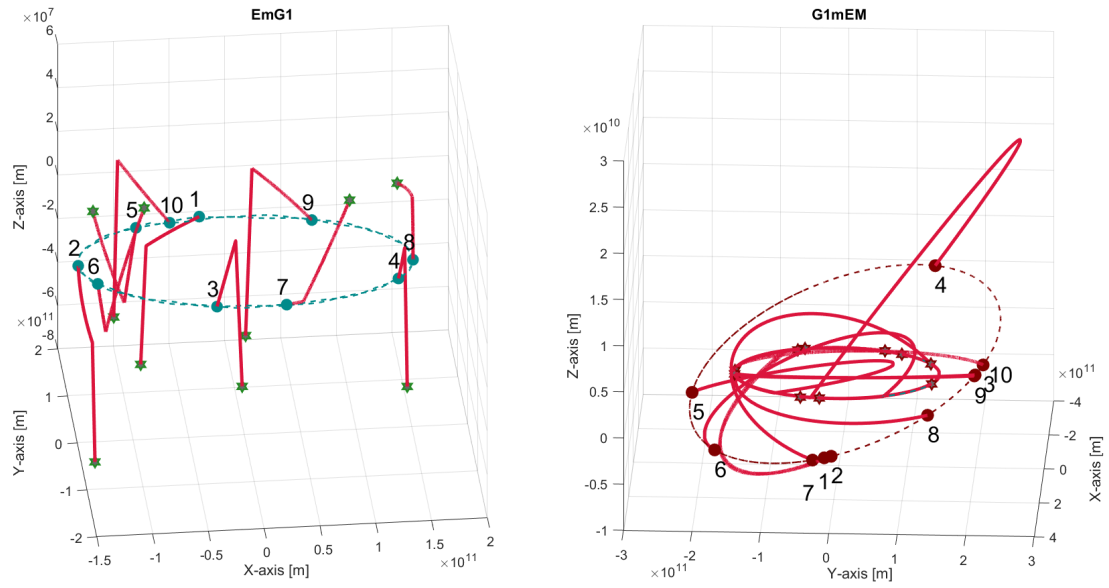


Figure 7.3: Plot of the best solutions for each launch window segment for both EG- and GM-segment of the *EmG1 x G1mEM* transfer.

Analysis C-II: Testing TOF characteristics

TOF constraint	ΔV [km/s]			TOF [days]				Orbit [-]	
	Total	EG	GM	Total	EG	GW	GM	Orbit ID	σ_{arr}
200 days	7.43	3.84	3.59	200	11	2	188	218	0.86
250 days	6.82	3.80	3.01	250	16	6	228	218	0.80
300 days	6.71	3.88	2.83	300	10	12	278	218	0.01
350 days	6.42	3.80	2.62	350	16	31	303	218	0.77

Table 7.9: TOF characteristics results of Analysis C-II for *EmG1 x G1mEM* transfer.

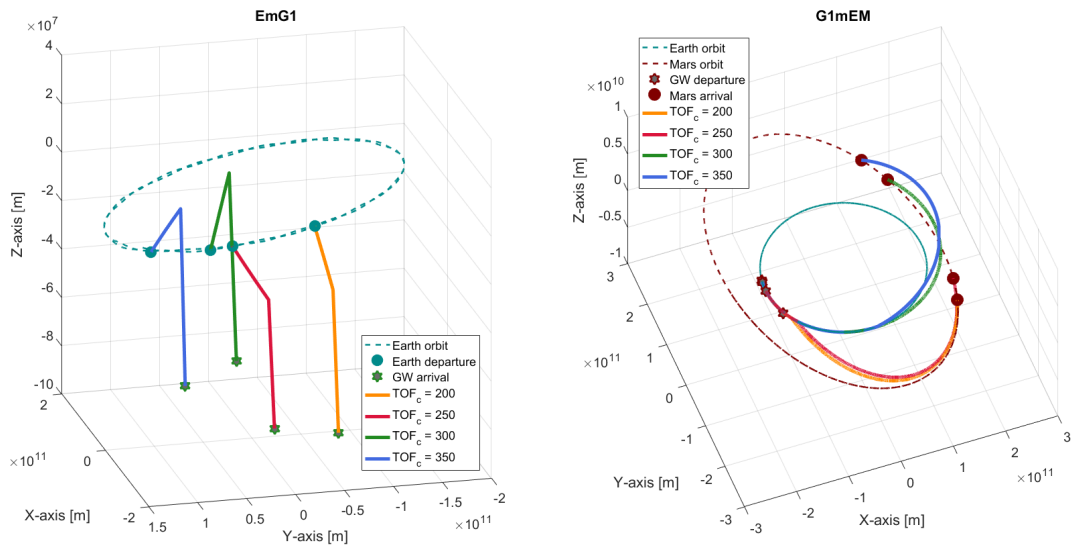


Figure 7.4: Plot of the best solutions for each TOF constraint (TOF_c) for both EG- and GM-segment of the *EmG1 x G1mEM* transfer.

7.4.3. G5 (SE-L2) - EdG5 x G5mEdEM

Analysis C-I: consistency testing

Segment [-]	Departure date [MJD2000]	ΔV [km/s]	TOF [days]	Stay time [days]	σ_{arr} [-]
1	12054	6.86	313	16	0.60
2	12132	7.93	241	1	0.69
3	12210	9.90	399	1	0.85
4	12365	10.07	508	50	0.51
5	12444	9.19	513	48	0.48
6	12522	8.24	514	49	0.91
7	12600	6.96	515	50	0.87
8	12678	5.72	487	22	0.97
9	12703	5.48	461	22	0.96
10	12756	5.91	419	50	0.97

Table 7.10: Consistency testing results of the *EdG5 x G5mEdEM* transfer.

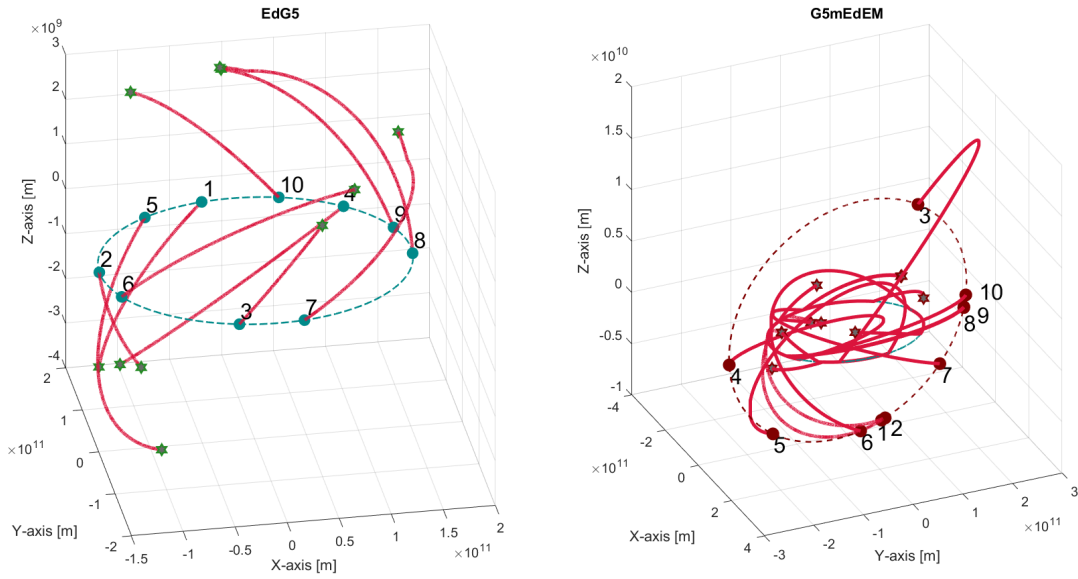


Figure 7.5: Plot of the best solutions for each launch window segment for both EG- and GM-segment of the *EdG5 x G5mEdEM* transfer.

Analysis C-II: Testing TOF characteristics

TOF constraint	ΔV [km/s]			TOF [days]				Orbit [-]	
	Total	EG	GM	Total	EG	GW	GM	Orbit ID	σ_{arr}
200 days	8.27	4.59	3.68	200	32	1	167	21	0.69
250 days	7.42	4.38	3.03	250	45	1	204	21	0.17
300 days	6.89	4.02	2.87	300	63	16	220	21	0.61
350 days	6.37	3.90	2.47	350	73	24	253	21	0.07

Table 7.11: TOF characteristics results of Analysis C-II for *EdG5 x G5mEdEM* transfer.

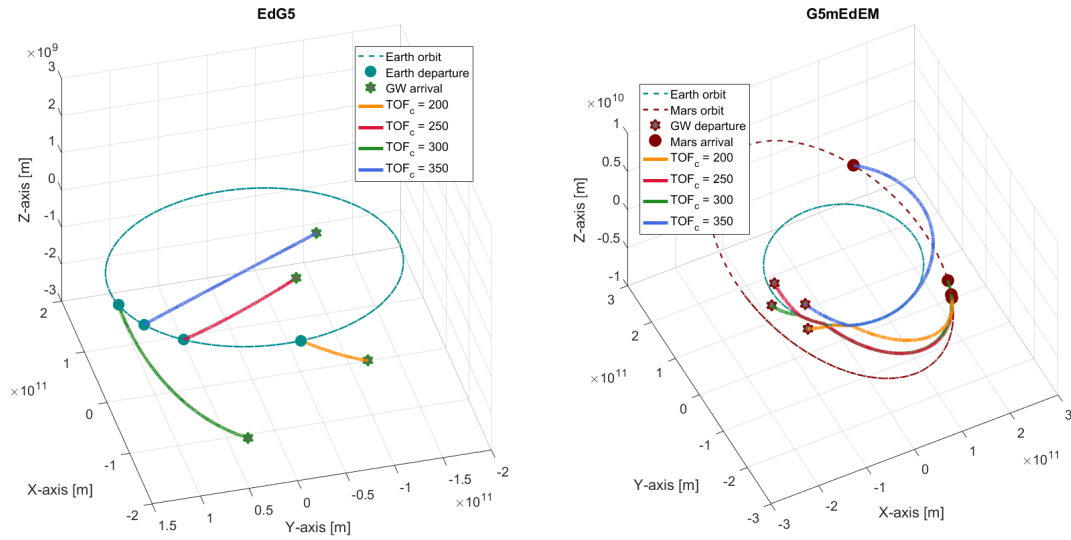


Figure 7.6: Plot of best solutions for each TOF constraint (TOF_c) for both EG- and GM-segment of the *EdG5 x G5mEdEM* transfer.

7.4.4. G5 (SE-L2) - *EdG5 x G5mEM*

Analysis C-I: consistency testing

Segment [-]	Departure date [MJD2000]	ΔV [km/s]	TOF [days]	Stay time [days]	σ_{arr} [-]
1	12054	6.93	311	21	0.10
2	12132	8.16	263	1	0.19
3	12210	10.90	313	1	0.72
4	12288	15.37	390	1	0.31
5	12444	12.87	515	50	0.52
6	12522	10.26	515	50	0.90
7	12600	7.51	515	50	0.86
8	12678	6.10	481	16	0.97
9	12703	5.89	459	20	0.96
10	12756	6.31	409	40	0.00

Table 7.12: Consistency testing results of the *EdG5 x G5mEM* transfer.

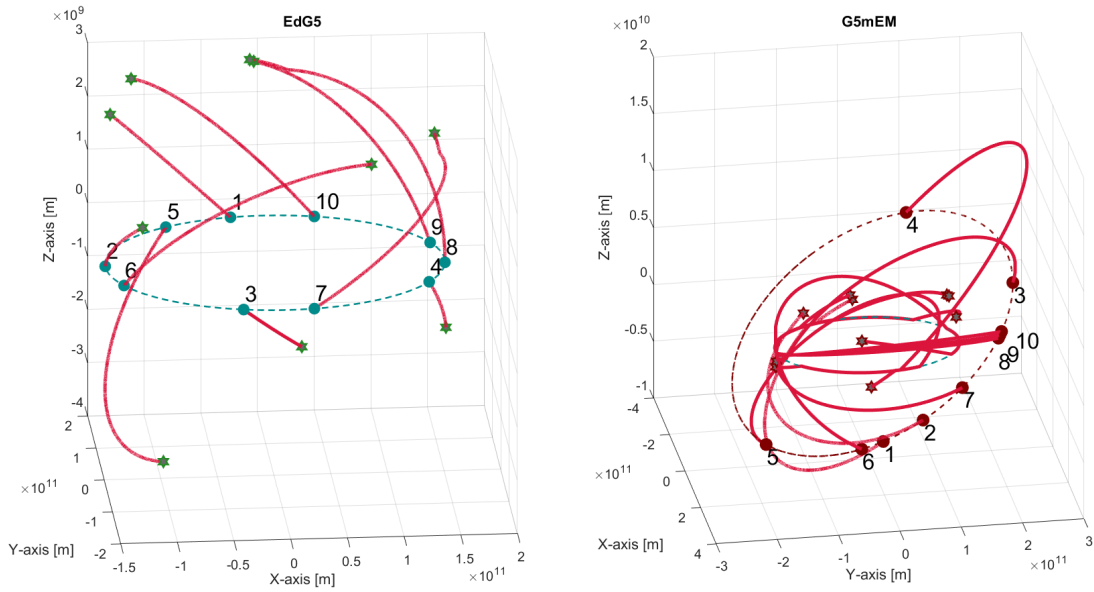


Figure 7.7: Plot of the best solutions for each launch window segment for both EG- and GM-segment of the *EdG5 x G5mEM* transfer.

Analysis C-II: Testing TOF characteristics

TOF constraint	ΔV [km/s]			TOF [days]				Orbit [-]	
	Total	EG	GM	Total	EG	GW	GM	Orbit ID	σ_{arr}
200 days	8.59	4.83	3.76	200	23	1	176	21	0.70
250 days	7.47	4.42	3.05	250	43	1	206	21	0.18
300 days	7.00	4.02	2.97	300	61	20	219	21	0.60
350 days	6.65	3.78	2.87	350	100	12	238	21	0.09

Table 7.13: TOF characteristics results of Analysis C-II for *EdG5 x G5mEM* transfer.

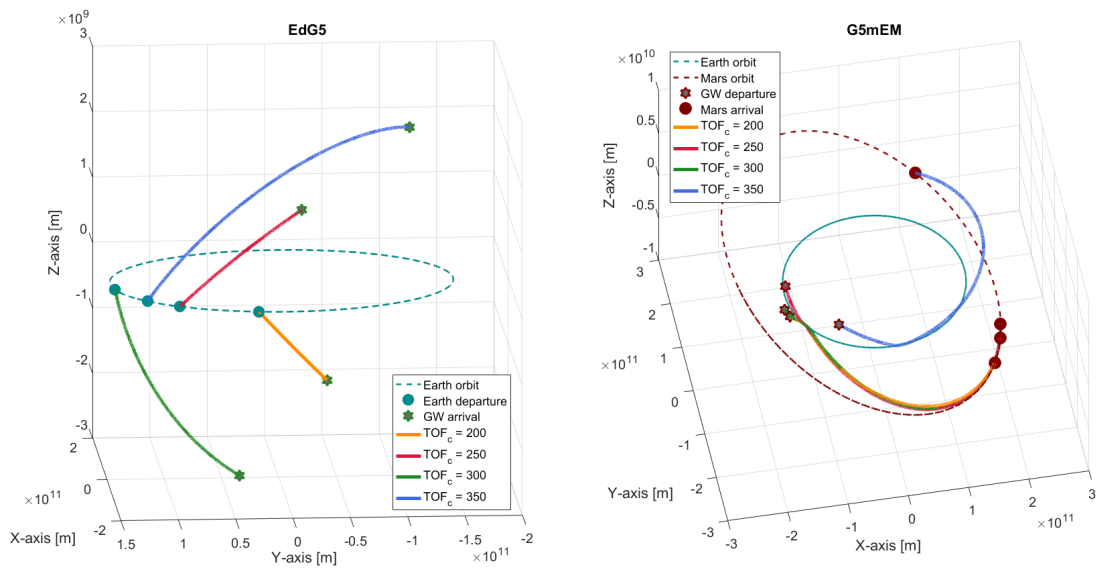


Figure 7.8: Plot of the best solutions for each TOF constraint (TOF_c) for both EG- and GM-segment of the *EdG5 x G5mEM* transfer.

7.4.5. G8 (Lunar orbit) - *EdG8 x G8dM*

Analysis C-I: consistency testing

Segment [-]	Departure date [MJD2000]	ΔV [km/s]	TOF [days]	Stay time [days]	σ_{arr} [-]
1	12097	7.14	258	42	0.76
2	12146	7.16	208	1	0.27
3	12216	9.59	393	21	0.77
4	12288	14.04	376	7	0.30
5	12444	14.91	419	43	0.26
6	12522	11.45	429	48	0.26
7	12600	10.49	435	50	0.26
8	12677	9.58	412	50	0.27
9	12756	9.07	357	44	0.76
10	12834	8.43	309	49	0.76

Table 7.14: Consistency testing results of the *EdG8 x G8dM* transfer.

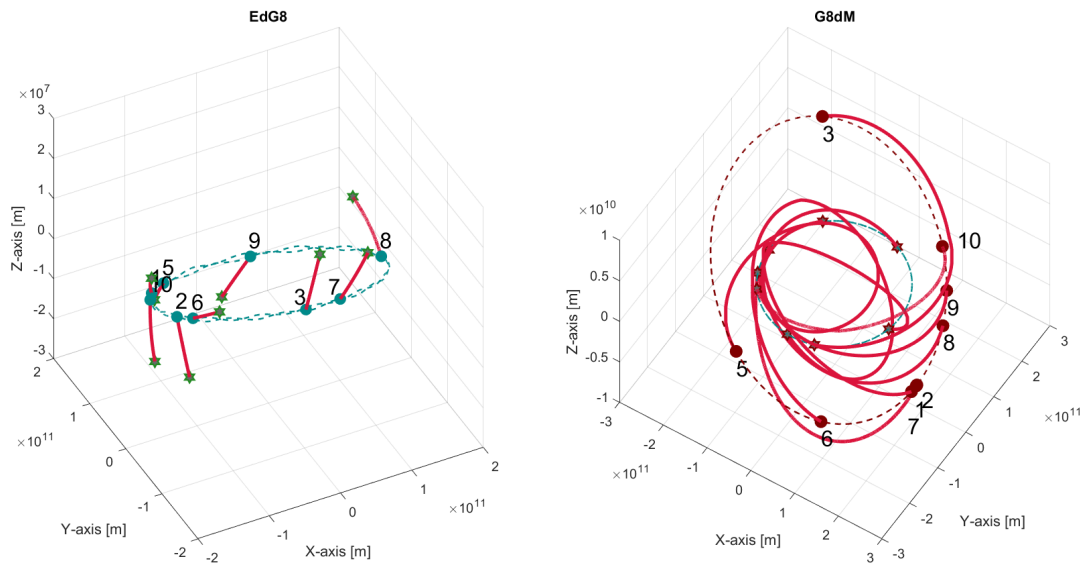


Figure 7.9: Plot of the best solutions for each launch window segment for both EG- and GM-segment of the *EdG8 x G8dM* transfer.

Analysis C-II: Testing TOF characteristics

TOF constraint	ΔV [km/s]			TOF [days]				Orbit [-]	
	Total	EG	GM	Total	EG	GW	GM	Orbit ID	σ_{arr}
200 days	7.16	3.93	3.24	200	5	2	193	45	0.27
250 days	7.14	3.92	3.22	235	23	14	198	45	0.76
300 days	7.14	3.92	3.22	226	14	14	198	45	0.76
350 days	7.14	3.92	3.22	221	8	15	198	45	0.76

Table 7.15: TOF characteristics results of Analysis C-II for *EdG8 x G8dM* transfer.

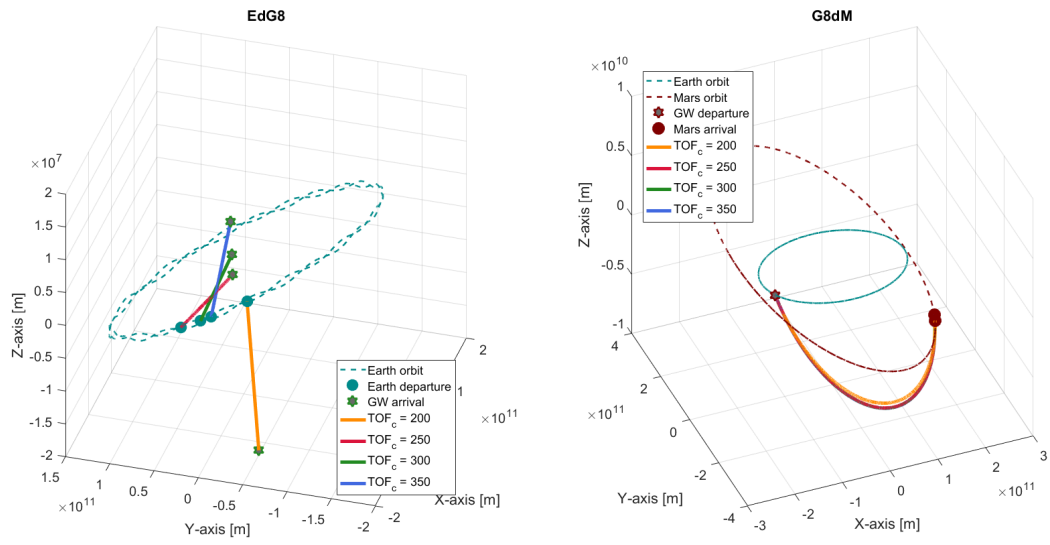


Figure 7.10: Plot of the best solutions for each TOF constraint (TOF_c) for both EG- and GM-segment of the *EdG8 x G8dM* transfer.

7.5. Discussion

The section above has presented the result of both Analysis C-I and C-II in the form of tables and figures. This section will interpret these results for Analysis C-I and Analysis C-II separately. For the sake of improving readability, this will again be done in the form of bullet points.

7.5.1. Analysis C-I

- **Comparing gateway transfers** - The consistency of the gateway transfers can be evaluated based on the information presented in Tables 7.6 till 7.14. In order to interpret these results more easily, Table 7.16 can be used. This table lists the average ΔV value of the transfers of all launch window segments. Additionally, it lists in how many of the launch window segments a transfer is possible that is below a certain ΔV budget. The average ΔV values of these subset of transfers were also computed and can be seen in the table below.

Gateway design (transfer)	Average ΔV [km/s]	# Segments w/ $\Delta V < 8 \text{ km/s}$	Average ΔV $\Delta V < 8 \text{ km/s}$	# Segments w/ $\Delta V < 7 \text{ km/s}$	Average ΔV $\Delta V < 7 \text{ km/s}$
EdG1 x G1mEM	8.87	5	6.42	5	6.42
EmG1 x G1mEM	9.30	5	6.74	4	6.60
EdG5 x G5mEdEM	7.63	6	6.48	5	6.19
EdG5 x G5mEM	9.02	5	6.54	4	6.30
EdG8 x G8dM	10.19	2	7.15	0	-

Table 7.16: Comparison of consistency of the different gateway trajectory designs analysed in Analysis C-I.

Table 7.16 shows that the LPO-gateways (G1 and G5) score similarly on consistency. These four different transfer designs allow for moderately efficient ($\Delta V < 8 \text{ km/s}$) Earth-to-Mars transfer in at least half of the launch window segments and an efficient ($\Delta V < 7 \text{ km/s}$) transfer in at least four of the ten launch windows. The gateway in Lunar orbit (G8) significantly under performs in terms of consistency. A moderately efficient transfer is only supported in two of the ten launch windows.

- **Role of position of Earth w.r.t. Mars** - When studying the consistency results (Tables 7.6 till 7.14), a certain pattern in the favourable launch window segments can be identified. For all gateway designs, the first few and last few transfer segments support more efficient transfers, whereas the launch window segments in the middle only support high- ΔV transfers. This can be explained by looking at the position of Earth and Mars during the synodic period of focus. The positions of Earth and Mars have been plotted at the start of each launch window segment in Figure 7.11.

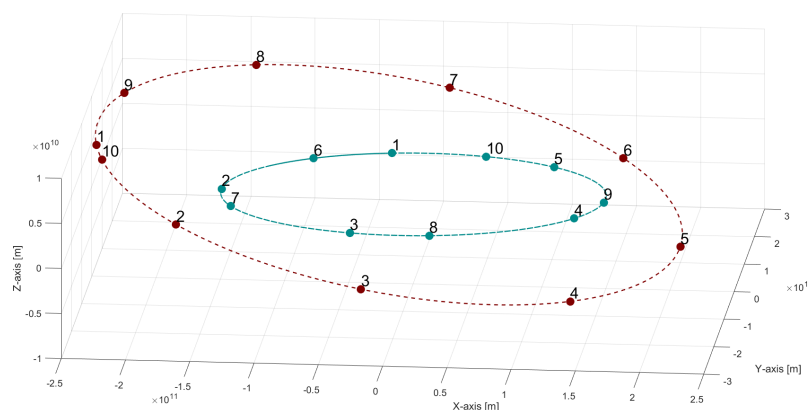


Figure 7.11: Position of Earth and Mars at the start of each launch window segment.

The high- ΔV transfers needed in launch window segments 4, 5, 6, and 7 can be explained by the fact that Mars is closely trailing Earth at the start of these segments. A transfer will therefore have to cover at least a full rotation ($\theta_t > 360^\circ$). An example of such a transfer is depicted in Figure 7.12. A significant amount of ΔV is then required to adhere to the TOF constraints.

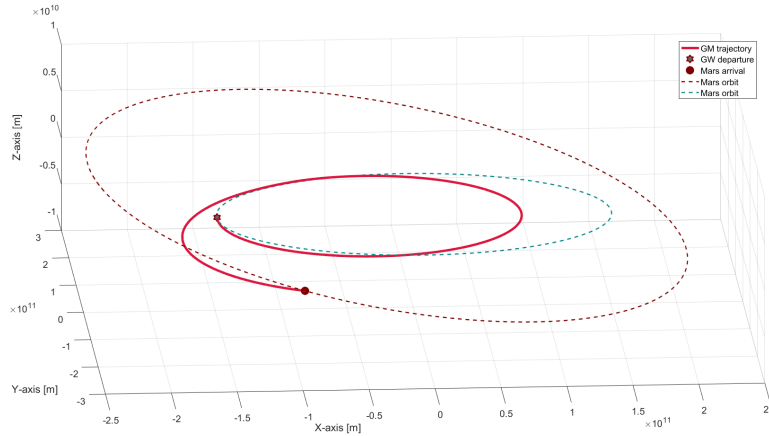


Figure 7.12: Example of a full rotation GM-transfer required in unfavourable launch window segments.

- **Role of stay time** - A pattern in stay time can be observed that is closely related to the point discussed above. In order to overcome the unfavourable geometry of the Earth-to-Mars transfer in the middle launch window segments, the stay time is either close to the minimum of a single day or close to the maximum of 50 days. This pattern is especially apparent in Table 7.12. Solutions for the first unfavourable launch window segments aim to minimize TOF in order to try to beat the unfavourable geometry. Conversely, solutions for the later unfavourable segments use an extended gateway stay time to try to wait out the unfavourable geometry as much as possible.

7.5.2. Analysis C-II

- **Trade-off between ΔV and TOF** - The results of Analysis C-II show that there is a clear trade-off between ΔV and TOF: when the TOF of the Earth-to-Mars transfer is decreased through the implementation of a constraint, the ΔV budget of the transfer increases in almost all cases. As a result, the optimal solutions found in Analysis B in terms of ΔV , have not always been found in Analysis C-II due to the TOF constraints. This is especially true for the transfers supported by the G5 gateway design at the SE-L2 point. When limiting the allowed TOF of the transfers, the G5 transfer solutions require an added ΔV budget of approximately 1 km/s.
- **Comparing gateway transfers** - The TOF characteristics of the different gateway trajectory designs can be compared by looking at Table 7.17 below, which combines the solutions of Tables 7.9 till 7.15 into a single table. Figure 7.13 then plots the content of Table 7.17 to be able to compare the TOF characteristics of the different gateway transfers even better.

Gateway design (transfer)	ΔV [km/s]			
	$TOF_c = 200$ days	$TOF_c = 250$ days	$TOF_c = 300$ days	$TOF_c = 350$ days
EdG1 x G1mEM	7.26	6.93	6.41	6.05
EmG1 x G1mEM	7.43	6.82	6.71	6.42
EdG5 x G5mEdEM	8.27	7.42	6.89	6.37
EdG5 x G5mEM	8.59	7.47	7.00	6.65
EdG8 x G8dM	7.16	7.14	7.14	7.14

Table 7.17: Comparison of the TOF characteristics of the different gateway transfers.

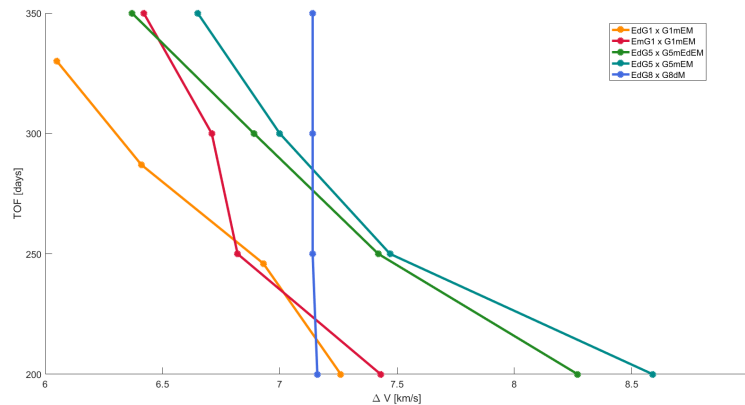


Figure 7.13: Plot showing the TOF characteristics of the different gateway transfers.

These results clearly show the differences between the three gateway trajectory designs (at G1, G5 and G8) in terms of the TOF of the transfers they support. The near-vertical line in Figure 7.13 means that the gateway in Lunar orbit is capable of supporting its optimal transfer at a TOF of close to 200 days. The G1 and G5 gateway trajectory designs are capable of supporting more efficient transfers (lower ΔV budgets), but this comes at the cost of longer flight times. Compared to the G5 (SE-L2) gateway trajectory designs, these costs are less significant for the G1 designs (EM-L1), which is why the line plots of these design can be found to the left of those corresponding to the G5 designs in Figure 7.13.

- Explanation for the differences in TOF characteristics** - The differences in TOF characteristics can be explained by the difference in gateway position. The G5 location (SE-L2) is considerably farther away from Earth than the gateways in the Earth-Moon system. As a result, the spacecraft will have to travel more distance to perform the consecutive Lunar and Earth flyby in the GM-segment, which leads to an increase in flight time. Although the distance is much smaller, the same flyby sequence in the G1 transfers also adds TOF, which explains the differences between the G8 and G1 gateway performance for small flight times. When allowing the TOF to increase, the *mE*-flyby does allow for more efficient transfers in terms of ΔV required.
- Role of segment flight times** - There is a difference in the way the different gateway trajectory designs deal with decreasing flight time constraints. The transfers using the G1 gateway (EM-L1) tend to mainly decrease the TOF of the GM-segment to adhere to stricter TOF constraints, while the EG-segment flight times remain constant. For the gateway designs at G5 (SE-L2), both EG- and GM-segments are trimmed to adhere to the TOF constraints. The gateway stay times are shortened on all occasions excluding the *EdG1 x G1mEM* design. The G8 (Lunar orbit) gateway is of course an exception since its performance is unaffected by the TOF constraints since its optimum transfer has a relatively low TOF.

7.6. Conclusions

By looking at the consistency and TOF characteristics, Analysis C was able to provide more insights into practical design criteria for the three remaining gateway trajectory designs. Based on the results of Analysis C-I and C-II, shown in Section 7.4, a final comparison of the gateway designs was made. This conclusion section will therefore start with the proposal of a single gateway trajectory design that is deemed most suitable to support the mission defined in Section 4.1. Additionally, this conclusion section will list the main findings concerning the practical evaluation of gateway trajectory designs.

7.6.1. Single gateway trajectory design proposal

A decision for a single gateway trajectory design was based on both Tables 7.16 and 7.17. As can be seen in Table 7.17, the trade-off between ΔV and TOF is better for the G1 gateways compared to the G8 and G5 gateway performances. In Table 7.16, it can be seen that the G1 and G5 gateway trajectory designs score comparably well on consistency, while the G8 gateway design significantly underperforms. When the results of the two analyses are combined, the G1 gateway design is the most promising. This design should support both the *EdG1 x G1mEM* and the *EmG1 x G1mEM* transfer, of which the first is the most efficient. The proposal for a gateway trajectory design based on the results of the three analyses in this report is summarized in Table 7.18 below.

Design aspect	Selection
Gateway location	Em-L1 point
Gateway orbit	Halo orbit: Jacobi constant: 3.002606 Orbital period: 8.3 days
Transfer	EG-segment: EdG1, EmG1 GM-segment: G1mEM

Table 7.18: gateway trajectory design proposal based on the research done in this thesis work.

7.7. Additional findings

Apart from producing results that enabled the selection of a single gateway trajectory design, Analysis C also provided further insight into the design process. These insights are listed below.

- **Influence of transfer trajectory on consistency** - Analysis C-I has shown that the consistency performance of the gateway trajectory designs is dependent on the transfer trajectory travelled by the spacecraft. When looking to improve the flexibility of a gateway trajectory design, a mission planner should explore different trajectory options.
- **Trade-off between ΔV and TOF** - The results produced by Analysis C-II were able to show that the TOF characteristics of the different gateway trajectory designs depend on the transfer trajectories and the gateway locations of the design. A mission planner is therefore advised to consider the TOF options of each gateway design from the start of the design process.

III

Conclusions

8

Discussion - evaluation of optimal gateway trajectory design

Now that an optimal gateway trajectory design was found, the performance of a gateway mission can be compared to a traditional mission that does not use a gateway as an intermediate station. Two traditional Earth-to-Mars missions will be considered: the simplest direct transfer (*EM*) and a transfer that incorporates a consecutive Lunar and Earth flyby (*EmEM*). Each will be discussed in a separate section. The final section of this chapter will use these results to evaluate the gateway concept's application to the proposed Mars mission.

8.1. Comparison to direct transfer (*EM*)

This section will compare the best ΔV trajectory, the TOF characteristics and the consistency test results of the optimal gateway trajectory design (Table 7.18) to the traditional *EM* transfer. The direct transfer (*EM*) was used for all previous Mars missions and is the likely candidate for the SpaceX Starship missions [16].

8.1.1. Best ΔV transfer

The optimal trajectory in terms of ΔV from Earth orbit to Mars orbit requires a ΔV budget of 6.08 km/s and has a TOF of 200 days. These numbers are compared to those of the proposed gateway mission in Table 8.1 below.

Mission	Departure date [MJD200]	ΔV [km/s]	TOF [days]
<i>EM</i>	12160	6.08	200
<i>EdG1 x G1mEM</i>	12778	5.99	386

Table 8.1: Comparison of optimal trajectory numbers for both the gateway and the direct (*EM*) mission.

As can be seen in the Table above, the gateway mission requires slightly less ΔV , which will result in less propellant and spacecraft mass. The optimal unconstrained gateway trajectory does take 386 days, which is considerably longer than the direct *EM* transfer. No evaluation can be made based on the figures presented in Table 8.1 alone, additional insight into the TOF characteristics are needed first. Figure 8.1 shows the trajectory of the optimal direct (*EM*) transfer compared to the optimal gateway mission trajectory.

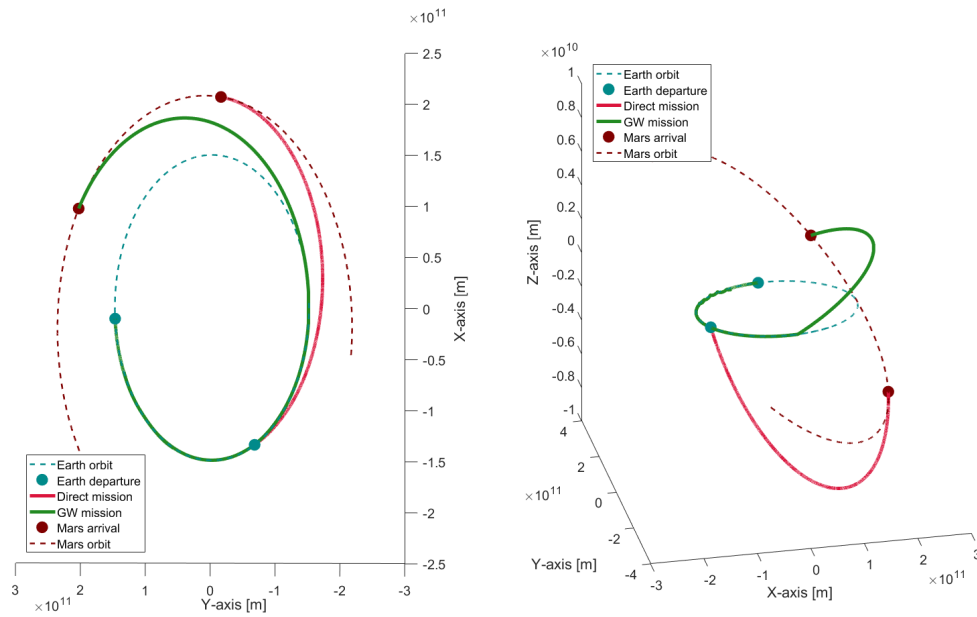


Figure 8.1: Comparison of optimal trajectory plot for both the gateway and the direct (*EM*) mission.

As can be seen in Figure 8.1 above, the direct transfer traverses less than 180 degrees around the Sun. This makes it a type-I transfer. This is not the traditional Hohmann transfer, characterized by $\Delta V = 5.59$ km/s and TOF of 259 days, since this transfer needs to account for the different orbital planes and the non-circular orbits of Earth and Mars. Due to a lack of DSMs or flybys, the inclination change has to be accounted for at launch. The difference in flight time between the gateway mission and the direct mission is explained by the difference in transfer angle traversed around the Sun. The gateway mission can have a more efficient transfer in terms of ΔV because it uses a flyby for the inclination change.

8.1.2. TOF characteristics

The TOF characteristics of both mission types were compared, and its results can be found in Table 8.2.

TOF constraint [days]	<i>Direct (EM)</i>	<i>GW (EdG1 x G1mEM)</i>
	ΔV [km/s]	ΔV [km/s]
200	6.08	7.26
250	6.08	6.93
300	6.08	6.41
350	6.08	6.05

Table 8.2: Comparison of the TOF characteristics for both the gateway and the direct (*EM*) mission.

Using the table above, it can be deduced that a direct transfer is more efficient in terms of ΔV requirements for transfers with a TOF faster than roughly a year. For an Earth-to-Mars transfer with a TOF of less than 200 days, a gateway mission would require roughly 1.2 km/s more of ΔV than a traditional direct transfer. This difference in ΔV requirements reduces for increasing TOFs. A gateway mission with a TOF of under 300 days would only require roughly 0.3 km/s of additional ΔV .

8.1.3. Consistency results

Analysis C-I was performed for the direct transfer (*EM*). Its results can be found in Table 8.3. These results can then be compared to the consistency results of the proposed gateway mission. This was done in Table 8.4. As can be seen in this table, the gateway mission design allows for more frequent transfer options against more favourable ΔV requirements. This can be explained by two factors: first, the gateway transfer trajectory incorporates two flybys, which enable course changes to overcome unfavourable geometries. Second, the flybys and the gateway stay time allow for longer transfers. As a result, the unfavourable geometries can be overcome more easily.

Segment [-]	Departure date [MJD2000]	ΔV [km/s]	TOF [days]
1	12132	6.63	197
2	12160	6.08	200
3	12210	7.24	246
4	12288	10.29	325
5	12366	16.64	365
6	12444	29.85	365
7	12600	20.20	236
8	12678	12.90	263
9	12756	9.59	262
10	12834	7.82	250

Table 8.3: Consistency testing results of the *EM* transfer.

Transfer	Average ΔV [km/s]	# Segments w/ $\Delta V < 8\text{km/s}$	Average ΔV $\Delta V < 8\text{km/s}$	# Segments w/ $\Delta V < 7\text{km/s}$	Average ΔV $\Delta V < 7\text{km/s}$
<i>EM</i>	12.72	4	6.94	2	6.36
<i>EdG1 x G1mEM</i>	8.87	5	6.42	5	6.42

Table 8.4: Comparison of the consistency performance for both the gateway and the direct (*EM*) mission.

The final section of this chapter will combine all of the results discussed above and evaluate the performance of the gateway concept with respect to the traditional direct transfer mission.

8.2. Comparison to flyby transfer (*EmEM*)

This section will compare the best ΔV trajectory, the TOF characteristics and the consistency test results of the optimal gateway trajectory design (Table 7.18) to a similar flyby transfer (*EmEM*) that does not use a gateway as intermediate station. This transfer has no flight record, nor does it appear in any of the proposed plans for future Mars missions. The subsequent Lunar and Earth flyby did appear in Mars's mission plans around the late 1990s [49]. It will be studied because it resembles the transfer of the proposed gateway mission.

8.2.1. Best ΔV transfer

The most efficient transfer requires a ΔV of 5.79 km/s between Earth orbit and Mars orbit and has a flight time duration of 330 days. It is compared to the optimal gateway mission in Table 8.5 below.

Mission	Departure date [MJD200]	ΔV [km/s]	TOF [days]
<i>EmEM</i>	12834	5.79	330
<i>EdG1 x G1mEM</i>	12778	5.99	386

Table 8.5: Comparison of optimal trajectory numbers for both the gateway and the traditional flyby (*EmEM*) mission.

A traditional flyby mission would allow for a transfer that requires 0.2 km/s less ΔV and is roughly 50 days faster than its gateway mission equivalent. This was expected since gateway arrival and departure require extra ΔV and time. This effect can best be seen in Figure 8.2, in which the two trajectories have been plotted.

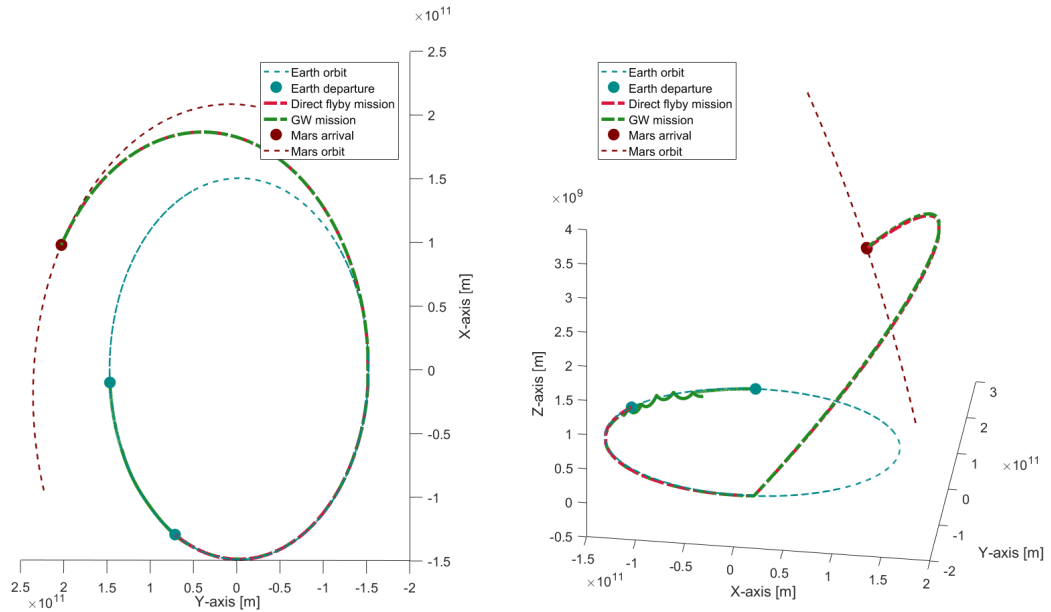


Figure 8.2: Comparison of optimal trajectory plots for both the gateway and the traditional flyby (*EmEM*) mission

Here it can be clearly seen that the interplanetary transfer trajectories are very similar. The departure from Earth vicinity seem to coincide, as well as the Earth flyby and Mars arrival. The extra mission time originates from the leg to the gateway and from the gateway stay (wrinkly green line). More insights into the TOF characteristics will be produced in the next section.

8.2.2. TOF characteristics

The results of the TOF analysis are presented in Table 8.6.

TOF constraint [days]	Direct (<i>EM</i>) ΔV [km/s]	GW (<i>EdG1 x G1mEM</i>) ΔV [km/s]
200	6.13	7.26
250	6.10	6.93
300	5.98	6.41
350	5.79	6.05

Table 8.6: Comparison of the TOF characteristics for both the gateway and the traditional flyby (*EmEM*) mission.

From the table it becomes evident that the inclusion of the intermediate gateway station adds significant ΔV requirements for shorter flight times. Due to the extra time added for the EG-segment and the gateway stay, the GM-segment needs to be trimmed more drastically for the gateway mission than for the traditional mission to adhere to the TOF constraints. As a result, more ΔV is required. This effect is of course smaller for larger flight times. A gateway mission with a TOF of under 300 days would only require roughly 0.4 km/s of additional ΔV with respect to the traditional flyby mission, whereas a mission faster than 200 days would require an extra 1.2 km/s.

8.2.3. Consistency results

Table 8.7 displays the results of the consistency testing for the traditional flyby mission (*EmEM*). These results were then compared to the consistency results of the proposed gateway mission in Table 8.8. As can be seen, the consistency performance of the flyby mission is much better than that of the traditional

direct transfer mission. Evidently, the consecutive Lunar and Earth flyby manoeuvre are the cause for the improved consistency performance. The flybys increase flexibility since they add two opportunities for course direction changes and allow for the time-of-flight to increase.

Segment [-]	Departure date [MJD2000]	ΔV [km/s]	TOF [days]
1	12054	6.10	306
2	12154	6.10	210
3	12215	7.61	375
4	12295	11.02	360
5	12444	15.57	455
6	12522	10.77	465
7	12588	8.81	458
8	12678	7.07	438
9	12756	5.83	399
10	12834	5.79	329

Table 8.7: Consistency testing results of the *EmEM* transfer.

Transfer	Average ΔV [km/s]	# Segments w/ $\Delta V < 8\text{km/s}$	Average ΔV $\Delta V < 8\text{km/s}$	# Segments w/ $\Delta V < 7\text{km/s}$	Average ΔV $\Delta V < 7\text{km/s}$
EmEM	8.47	6	6.42	4	5.95
<i>EdG1 x G1mEM</i>	8.87	5	6.42	5	6.42

Table 8.8: Consistency characteristics of the *EmEM* transfer compared to the optimal gateway mission.

As can be seen, the consistency results for the gateway mission and the traditional flyby mission are very similar. The ΔV requirements are in the advantage of the traditional flyby mission. The presence of a gateway does open up an extra opportunity in the sub-7km/s launch window. This is likely the result of the extra TOF transfer possibilities due to the EG-segment and gateway stay time.

The results of the traditional flyby (*EmEM*) transfer mission and that of the direct mission (*EM*) will be used in the next section, which will evaluate the performance of the proposed gateway mission against these traditional mission performances.

8.3. Evaluation of gateway concept

The analyses performed on the two traditional transfer missions (*EM* and *EmEM*) have provided understanding into the differences between missions that include an intermediate gateway station and missions that do not include one. Based on the results of the similar *EmEM* transfer, it can be concluded that the inclusion of a gateway in the mission design adds to the time of flight and adds to the ΔV requirements. The increase in ΔV is higher for shorter flight times than for longer flight times. When a flight time of under 200 days is desired, the increase in ΔV amounts to over 1 km/s, whereas an increase of less than roughly 0.2 km/s is required for transfer times of around a year. The inclusion of a gateway in the mission design does appear to have a positive effect on the launch opportunities, which is substantiated by the consistency test results. This effect is not significant when comparing it to the results of the traditional flyby mission (*EmEM*) and will require further research to confirm it.

Although the gateway concept will bring along an increase in flight time and in ΔV requirements as expected, one can still make a case for its use in Mars missions by referring to the benefits of the concept (Section 3.1). A gateway will facilitate a transfer between vehicles. The resulting increase in travel comfort might justify an increase in flight time. Furthermore, the gateway will act as a hub. Re-fuelling propellant at the station might allow for higher ΔV transfers. Additionally, the inclusion of an intermediate station might improve safety by opening more mission abort scenarios. This will need to be further researched. Whether these benefits justify the higher demands on ΔV and TOF requirements will have to be judged for each individual mission.

9

Conclusions

The conclusions of this thesis work can be divided into two sections. The first section will answer the research question by presenting the optimal gateway trajectory design found in this research. This is done by providing answers to the sub-questions formulated in the Introduction (Chapter 1). The second section will list the main takeaways found in the process of optimizing the gateway trajectory design. These takeaways will provide a starting point for scientists and mission designers interested in incorporating the gateway concept into future Mars missions or different mission applications.

9.1. Answer to the research question

This thesis set out to provide an answer to the following research question:

Research question *What is the optimal trajectory design for a gateway infrastructure that supports efficient and practical crew transportation between Earth and Mars?*

Through a thorough consideration of fundamental theory and through the completion of three different analyses, an answer to this question can be provided. This will be done by providing answers to each of the four sub-questions formulated in the Introduction (Chapter 1) and repeated below.

Sub-question A *What is/are the gateway location(s) of the optimal gateway design?*

The gateway location that enabled best results in terms of ΔV , consistency and TOF options is the G1 location. G1 is located at Lagrange point L1 in the Earth-moon system. An additional benefit of this location is that it is one of the closest locations to Earth that was considered in this research. This should simplify communications and its construction. Interestingly, this location showed much better performance than the location chosen by NASA for the Lunar gateway, which is Lagrange point L2 in the Earth-moon system. Both the EG- and GM-segments structurally require more ΔV for the G2 (Em-L2) location with respect to the G1 (Em-L1) location. The runner-up gateway location is the G5 location, which is Lagrange point L2 in the Sun-Earth system. This location enables Earth-to-Mars transfers with comparable ΔV and consistency performance, but with less advantageous TOF options.

Sub-question B *What is/are the gateway orbit(s) of the optimal gateway design?*

An optimal gateway at the G1 location is in a Halo orbit. The most suitable Halo orbit is characterized by a Jacobi constant of 3.002606 and an orbital period of 8.3 days. This orbit best facilitates the transfer options selected described in the answer to the next sub-question, because of its relatively high energy.

Sub-question C *What transfer trajectories should the optimal gateway design support?*

The gateway was designed to support the most efficient transfer. Many transfer options were analyzed for both the EG- and GM-segment. The most suitable transfer in terms of ΔV , TOF and consistency is the *EdG1 x G1mEM* transfer. For the EG-segment, the *EmG1* trajectory should also be considered.

Sub-question D *How does the optimal gateway design compare to a direct transfer?*

By comparison of a traditional flyby mission (*EmEM*) and the proposed gateway mission, it was found that the inclusion of a gateway in the Mars mission design both adds to the ΔV requirements and to the mission duration as was to be expected. The difference in ΔV requirements is higher for shorter TOF trajectories than for longer TOF missions. When a TOF constraint of 200 days is imposed, a gateway mission would require at least an extra 1 km/s in ΔV , whereas the difference in ΔV reduces to less than 0.2 km/s for flight times of around a year. The inclusion of a gateway does seem to improve the consistency performance, thus allowing more launch opportunities. This effect is especially significant when comparing the gateway mission to the traditional direct Mars mission (*EM*). Furthermore, the gateway concept brings along more benefits that might justify the increase in ΔV requirements. Its ability to facilitate transfers between spacecraft and re-fuelling of propellant will allow mission planners to make the case in favour of the gateway concept.

Now that all sub-questions have been answered, an answer to the main research question can be given. This research found that the optimal gateway trajectory design for an efficient and practical Mars's mission would place a gateway in a Halo orbit around the Earth-Moon Lagrange point L1, so that it can support a *EdG1 x G1mEM* and *EmG1 x G1mEM* transfer. This conclusion is summarised in Table 9.1.

Design aspect	Selection
Gateway location	Em-L1 point
Gateway orbit	Halo orbit: Jacobi constant: 3.002606 Orbital period: 8.3 days
Transfer	EG-segment: EdG1, EmG1 GM-segment: G1mEM

Table 9.1: Conclusion of gateway design process detailing the proposed gateway trajectory design.

9.2. Main takeaways for gateway trajectory design

Apart from enabling the selection of an optimal gateway trajectory design, the three analyses also provided understanding into the design process of efficient and practical gateway infrastructure. The obtained insights will be useful in future research into the application of the gateway concept to any mission type. The most significant takeaways are listed below:

- **Equilateral Lagrange points** - The equilateral Lagrange points (L4 and L5) proved unsuitable gateway locations. The ΔV requirements of transfers using these points as intermediate stations were significantly higher compared to the collinear Lagrange points.
- **Earth and Mars gateways** - This research found that gateways orbiting Earth or Mars considerably underperformed gateways positioned in orbit around the Moon or in the vicinity of a Lagrange point.
- **Favourability of continuous-thrust transfers** - Analysis A identified the great potential continuous-thrust propulsion systems have in combination with the gateway concept. Further research is required, as will be described in the next chapter.
- **Selection of Lagrange-point gateway orbits** - Mission designers should consider both the Halo and vertical-Lyapunov orbit family for the gateway orbits. It was found that often orbits at the boundaries of the orbit family are selected, due to a favourable connection between their energy state and the incoming or outgoing trajectory.
- **Central orbit altitude** - Although more ΔV is required to reach a high-altitude gateway, the total ΔV requirements of the Earth to Mars transfer are optimized for high-altitude gateway orbits (i.e. GEO) around central bodies with respect to lower orbits (i.e. LEO).
- **Gateway transfer model** - A model has been developed for this thesis that can be used to explore transfer options that include the gateway concept. This model is able to design gateway orbits and match the timing of the different transfer segments.

10

Recommendations for further research

Answering one question often leads to more questions. The same is true for this research. This chapter will put forward a list of recommendations for further research. These recommendations either involve improvements to this research or involve suggestions for research that follow up on insights obtained through the work done in this research.

- **Multi-objective analysis to obtain more insights into TOF characteristics** - This research failed to perform a useful multi-objective analysis to study the TOF characteristics in Analysis C. Limited computational capabilities and available time stood in the way of performing an accurate multi-objective optimization of the ΔV and TOF objectives. Efforts were made to tune the optimization algorithm settings (cross-over- and mutation rate) of the NSGA-II optimizer, but even for large population sizes (N_{pop}) and a large number of generations insufficiently accurate Pareto-fronts were obtained. An example of the Pareto-fronts for the *EdG1 x G1mEM* gateway transfer for five different seed values is depicted in Figure 10.1. The multi-objective optimization attempt was documented and can be found in Appendix C.

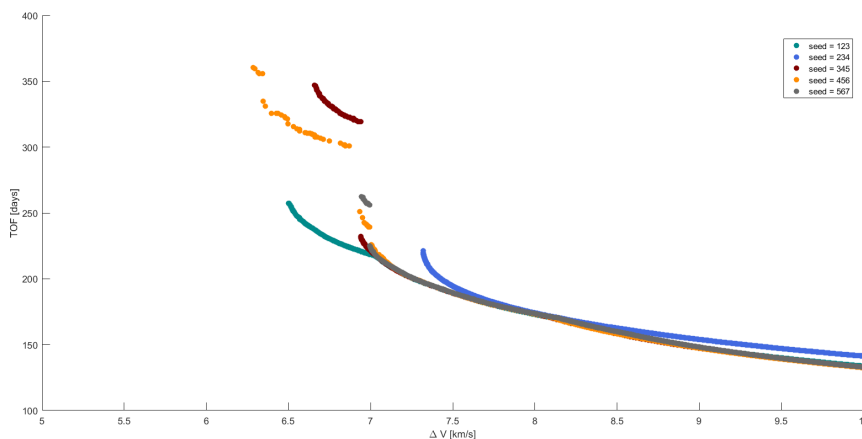


Figure 10.1: Failed attempt of multi-objective optimization of *EdG1 x G1mEM* in Analysis C.

Unfortunately, it had to be concluded that more powerful optimization tools are needed to perform an accurate multi-objective optimization of the complex gateway trajectory design problem, which consists of more than ten design variables. More powerful tools will hopefully be able to produce the Pareto-fronts for the different gateway designs. These plots will be especially useful in comparing the TOF characteristics between the different designs and between a gateway mission and a traditional mission.

- Return missions** - Further research should study return missions by including the Mars-to-Gateway segment (MG) and the Gateway-to-Earth segment (GE) for the single-gateway design. These segments are depicted in Figure 10.2. This analysis should be able to provide insights into favourable gateway design aspects to support efficient and practical return flights. The trajectories chosen for the return segments will likely not simply be the reverse order trajectories of the outward flight since their performance depends on precise flyby timing.

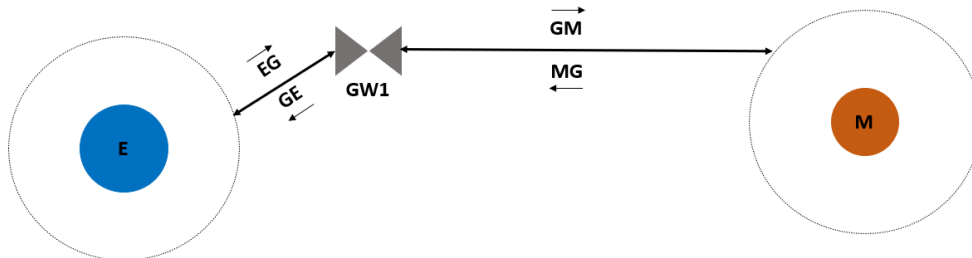


Figure 10.2: Schematic overview of the single-gateway architecture including the return segments.

- Twin-gateway design study** - Research into the application of a twin-gateway infrastructure to Earth-Mars transportation is recommended. A twin-gateway infrastructure would place one gateway in Earth's vicinity and another gateway at Mars' vicinity. This would allow for specialized and reusable spacecraft for each segment of the interplanetary transfer. It is expected that this architecture would again add to the ΔV requirements and flight duration, but it is interesting to investigate how significant this increase is. The twin-gateway mission architecture is depicted in Figure 10.3.

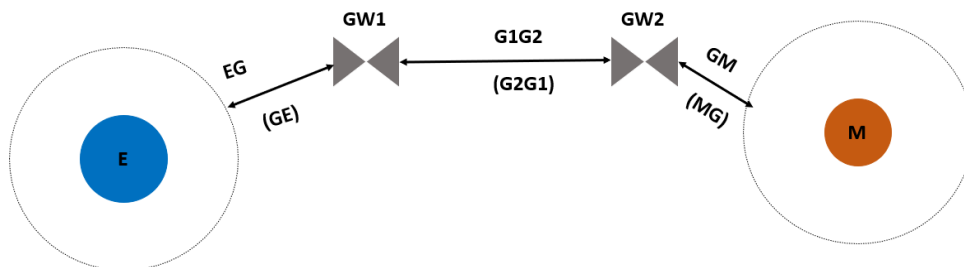


Figure 10.3: Schematic overview of the twin-gateway architecture and the resulting mission segments.

- Abort options** - Future research into mission abort options is recommended. The inclusion of a gateway in the mission design might increase mission abort opportunities since a spacecraft on an interplanetary transfer has the possibility to return to the gateway instead of the departure planet. As a result, mission safety might increase as a result of the inclusion of the intermediate station. The mission abort trajectory segments are depicted in Figure 10.4.

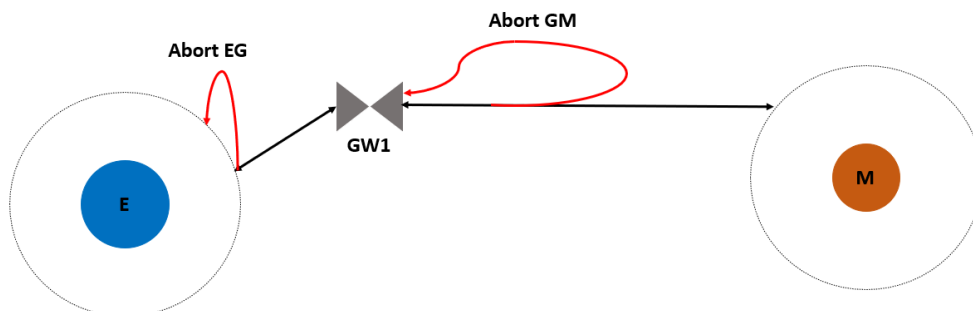


Figure 10.4: Schematic overview of the abort trajectory segments for a single-gateway one-way architecture.

- **Effect of TOF constraints** - This research made use of time of flights constraints for the different trajectory legs and the transfer segments. In some cases these constraints were based on values used in literature, but in many cases these constraints were defined for this research specifically. Even for most of the literature values, no fundamental reasoning can be given for their values except for that they are reasonable in the mission's context. At the same time, most design variables were optimized to be close to or on the constraint value. This was especially evident for the segment constraints and the gateway stay time. Subsequently, the produced results depend on the set constraints. Future research is encouraged to investigate the significance of these constraints by performing an analysis in which the constraint values are varied. If the results are found to be very sensitive to the constraint values, future research should focus on a more fundamental definition of these constraints.
- **Prioritize TOF characteristics at earlier stage** - If this research were to be performed again, it is advised to include the TOF constraints or the multi-objective optimization in an earlier stage of the analyses. In the used research design, trajectories were selected and disregarded based on their ΔV performance alone in Analysis A and B. Although unlikely, this method might have enabled trajectories to be left out that would have been very suitable because of their TOF or consistency performance. At the same time, trajectories were selected in Analysis B that later proved to be unsuitable in terms of TOF. Future research should consider performing Analysis B and C in parallel instead of in consecutive order. This, however, will increase computational load.
- **Continuous thrust propulsion systems** - Further research is encouraged into the application of continuous-thrust systems in combination with the gateway concept. The potential specific impulse and thrust levels of nuclear propulsion systems will revolutionize interplanetary space travel and open up new transfer options. When the efficiency of the propulsion systems increases, minimizing ΔV requirements becomes less stringent. Research into gateway design using continuous-thrust transfers could therefore focus more on the practical aspects of mission design: Design consistency, abort options and TOF characteristics.
- **Detailed mission design** - Now that a gateway trajectory design was selected, a detailed mission design can be made. Such a design should account for launch dates, launch vehicle(s), re-fuelling processes, spaceship characteristics, Mars surface stay, payload inventorying and other mission aspects. Furthermore, a more detailed trajectory analysis should be performed. The trajectory design process in this thesis was based on a number of assumptions and simplifications. Future research is encouraged to produce a model as close to reality as possible. This can be done by including certain perturbation forces, such as third body gravitation and solar radiation, substituting the CR3BP by a higher-fidelity model, such as the elliptic variant (ER3BP) or the four-body variant (CR4BP), and by looking into more detailed flyby modelling approaches. The resulting mission design can then be compared to other Mars mission designs, such as the SpaceX Starship program or the NASA Lunar gateway in terms of costs and flight time.

Bibliography

- [1] Lockheed Martin Corporation. *IAC2019 - Moon to Mars*. 2019. URL: <https://www.lockheedmartin.com/en-us/news/features/2019-features/moon-mars-iac.html>. (accessed: 12/07/2021).
- [2] C. Bolden. "Humans to Mars Summit". In: *Transcript from his talk at Washington University* (2013).
- [3] K. Mars. *Gateway*. 2019. URL: <https://www.nasa.gov/gateway>. (accessed: 29/09/2020).
- [4] J. Veen. "Optimizing Earth-Mars transportation using the gateway concept". In: *Literature Study, TU Delft* (2020).
- [5] P. Musegaas. "Optimization of Space Trajectories Including Multiple Gravity Assists and Deep Space Maneuvers". In: *MSc Thesis Report - TU Delft* (2012).
- [6] L. van der Ham. "Interplanetary Trajectory Design using Dynamical Systems Theory". In: *Thesis Work* (2012). URL: <https://repository.tudelft.nl/islandora/object/uuid%5C%3A98c55fe3-cd59-4c61-817e-9caa6ac835b6?collection=education>.
- [7] J. Melman. "Trajectory optimization for a mission to Neptune and Triton". In: *MSc Thesis Aerospace Engineering, TU Delft* (2007).
- [8] V. Zuccarelli. "Connecting hyperbolic invariant manifolds at variations of the Poincaré section orientation". In: *MSc Thesis Aerospace Engineering, TU Delft* (2018).
- [9] K. Landau and B. Aldrin. "Continuous Mars Habitation with a Limited Number of Cycler Vehicles". In: *Astrodynamics Specialist Conference and Exhibit* (2006).
- [10] *The Gateway Foundation*. 2019. URL: <https://gatewayspaceport.com/>. (accessed: 19/09/2019).
- [11] M. Vidmar and D. Webber. "Gateway Earth: A Pragmatic Modular Architecture For Space Access and Exploration". In: *68th International Astronautical Congress (IAC)* (September 2017).
- [12] P. Wooster et al. "Mission design options for human Mars missions". In: *Mars Informatics* (August 2007).
- [13] K. Erickson. *Solar System Explorations*. 2015. URL: <http://solarsystem.nasa.gov/planets>. (accessed: 21/09/2019).
- [14] NASA Science Mars Exploration Program. *Historical Log*. 2020. URL: <https://mars.nasa.gov/mars-exploration/missions/historical-log/>. (accessed: 13/07/2021).
- [15] NASA. "Mars Science Laboratory Launch Press Kit". In: *National Aeronautic Space Administration* (November 2011).
- [16] SpaceX and E. Musk. "Starship update." In: *SpaceX presentation slides, presented by Elon Musk* (October 2019).
- [17] SpaceX and E. Musk. "Making Life Multiplanetary." In: *SpaceX presentation slides, presented by Elon Musk* (September 2017).
- [18] NASA. "NASA's Journey to Mars: Pioneering Next Steps in Space Exploration". In: *National Aeronautic Space Administration* (October 2015).
- [19] K. Humbleton. *Deep Space Gateway to Open Opportunities for Distant Destinations*. March 2017. URL: <https://www.nasa.gov/feature/deep-space-gateway-to-open-opportunities-for-distant-destinations>. (accessed: 30/09/2019).
- [20] T. Pultarova. *Ion Thruster Prototype Breaks Records in Tests, Could Send Humans to Mars*. 2017. URL: <https://www.space.com/38444-mars-thruster-design-breaks-records.html>. (accessed: 14/09/2020).
- [21] D. Chato. "Experimentation for the Maturation of Deep Space Cryogenic Refueling Technologies". In: *Glenn Research Center* (2013).

- [22] E. Berger. *NASA agrees to work with SpaceX on orbital refueling technology*. 2019. URL: <https://arstechnica.com/science/2019/07/nasa-agrees-to-work-with-spacex-on-orbital-refueling-technology/>. (accessed: 14/09/2020).
- [23] J. Hoffman and D. Rapp. “The Mars Oxygen ISRU Experiment (MOXIE) on the Mars 2020 Rover”. In: *AIAA SPACE 2015 Conference and Exposition* (2015).
- [24] K. Wakker. *Fundamentals of Astrodynamics*. Institutional Repository, Library of Delft University of Technology, Januari 2015. ISBN: 978-94-6186-419-2.
- [25] Radu Serban et al. “Halo orbit mission correction maneuvers using optimal control”. In: *Automatica* 38.4 (2002), pp. 571–583.
- [26] N. Cornish. “The Lagrange Points”. In: *WMAP Education and Outreach* (1998).
- [27] David L Richardson. “Analytic construction of periodic orbits about the collinear points”. In: *Celestial mechanics* 22.3 (1980), pp. 241–253.
- [28] Gerard Gómez and JOSEP M Mondelo. “The dynamics around the collinear equilibrium points of the RTBP”. In: *Physica D: Nonlinear Phenomena* 157.4 (2001), pp. 283–321.
- [29] Herbert B Keller and KELLER HB. “Numerical solution of bifurcation and nonlinear eigenvalue problems.” In: (1977).
- [30] RH Gooding. “A procedure for the solution of Lambert’s orbital boundary-value problem”. In: *Celestial Mechanics and Dynamical Astronomy* 48.2 (1990), pp. 145–165.
- [31] Davide Conte. “Survey of Earth-Mars Trajectories using Lambert’s Problem and Applications”. PhD thesis. Dec. 2013. DOI: 10.13140/RG.2.2.11589.55525.
- [32] Dario Izzo. “Revisiting Lambert’s problem”. In: *Celestial Mechanics and Dynamical Astronomy* 121.1 (2015), pp. 1–15.
- [33] T.A. Leite Pinto Secretin. “Design of a Combinatorial Tool for Preliminary Space Mission Analysis, applied to the GTOC2 Problem”. In: *MSc Thesis Aerospace Engineering, TU Delft* (2012).
- [34] Jacobus W Cornelisse, HFR Schoyer, and Karel F Wakker. “Rocket propulsion and spaceflight dynamics”. In: *London: Pitman* (1979).
- [35] S. Molenaar. “Optimization of interplanetary trajectories with deep space maneuvers - Model development and application to a Uranus orbiter mission”. In: *MSc Thesis, TU Delft, The Netherlands* (2009).
- [36] Massimiliano Vasile and Paolo De Pascale. “Preliminary design of multiple gravity-assist trajectories”. English. In: *Journal of Spacecraft and Rockets* 43.4 (July 2006), pp. 794–805. ISSN: 0022-4650. DOI: 10.2514/1.17413.
- [37] Jon Sims et al. “Implementation of a low-thrust trajectory optimization algorithm for preliminary design”. In: *AIAA/AAS Astrodynamics specialist conference and exhibit*. 2006, p. 6746.
- [38] D. Gondelach. “A Hodographic-Shaping Method for Low-Thrust Trajectory Design”. In: *MSc Thesis Aerospace Engineering, TU Delft* (2012).
- [39] Daniel M Novak and Massimiliano Vasile. “Improved shaping approach to the preliminary design of low-thrust trajectories”. In: *Journal of Guidance, Control, and Dynamics* 34.1 (2011), pp. 128–147.
- [40] J R Wertz. “Orbit / Constellation, Design / Management”. In: (Jan. 2001).
- [41] K. Landau and J. Longuski. “Comparative assessment of human–Mars-mission technologies and architectures”. In: *Purdue University* (2009).
- [42] B. Drake. “Human Exploration of Mars Design Reference Architecture 5.0 Addendum”. In: *Exploration Office Document* (2009).
- [43] Robert Willard Farquhar. *The utilization of halo orbits in advanced lunar operations*. Vol. 6365. National Aeronautics and Space Administration, 1971.
- [44] J.A. Veen. *GitHub repository: Thesis - Gateway Optimizations*. <https://github.com/JasperAVeen/Thesis-Gateway-Optimizations>. 2021.
- [45] GTOP Library - ESA Advanced Concepts Team. *Cassini2*. 2013. URL: <https://www.esa.int/gsp/ACT/projects/gtop/cassini2>. (accessed: 30/05/2021).

-
- [46] J.D. Mireles James. “Celestial mechanics notes set 4: The circular restricted three body problem”. In: *Florida Atlantic University, Department of Mathematical Sciences* (2006).
- [47] C. Anton. *ReadMe Lagrange files*. 2013. URL: https://naif.jpl.nasa.gov/pub/naif/generic_kernels/spk/lagrange_point/AAREADME_Lagrange_point_SPKs.txt. (accessed: 13/07/2021).
- [48] Dominic Dirksen and Tudat team. *Tutorials and Documentation - Application Tutorials - 1. Unperturbed Earth-orbiting Satellite*. 2018. URL: <http://tudat.tudelft.nl/tutorials/application%20Walkthroughs/unperturbedEarthOrbitingSatellite.html>. (accessed: 07/06/2021).
- [49] P. Penzo. “Mission Design for Mars Missions Using the Ariane ASAP Launch Capability”. In: *AAS/IAIAA Space Flight Mechanics Meeting* (February 1999).
- [50] A. Ribeiro. “Optimal Aeroassisted Maneuvers for Orbital Transfer”. In: *MSc Thesis Aerospace Engineering, TU Delft* (2019).

A

All transfer trajectory options

The tables in this appendix chapter will list all the trajectory options that were optimized in at least one of the analyses of this research. The options are given for each gateway type and split into the two segments (EG- and GM-segment).

G1		G2		G3	
EG	GM	EG	GM	EG	GM
EG1	G1M	EG2	G2M	EG3	G3M
EdG1	G1dM	EdG2	G2dM	EdG3	G3dM
EmG1	G1mM	EmG2	G2mM	EmG3	G3mM
EEG1	G1EM	EEG2	G2EM	EEG3	G3EM
EdmdG1	G1mEM	EdmdG2	G2mEM	EdmdG3	G3mEM
EdEdG1	G1EmM	EdEdG2	G2EmM	EdEdG3	G3EmM
	G1dmdM		G2dmdM		G3dmdM
	G1dEdM		G2dEdM		G3dEdM
	G1dmdEdM		G2dmdEdM		G3dmdEdM
	G1dEdmdM		G2dEdmdM		G3dEdmdM

Table A.1: Trajectory options analyzed for the G1, G2 and G3 gateways.

G7		G8		G9	
EG	GM	EG	GM	EG	GM
EG7	G7dM	EdG8	G8dM	EdG9	G9M
	G7EM	EmG8	G8mM	EMG9	
	G7mM	EEG8	G8mEM	EmMG9	
	G7EmM		G8EmM	EmEG9	
	G7mEM				

Table A.2: Trajectory options analyzed for the G7, G8 and G9 gateways.

	G4		G5		G6
EG	GM	EG	GM	EG	GM
EG4	G4M	EG5	G5M	EG6	G6M
EdG4	G4dM	EdG5	G5dM	EdG6	G6dM
EmG4	G4mM	EmG5	G5mM	EmG6	G6MM
EEG4	G4EM	EEG5	G5EM	EEG6	G6dMdM
EdmdG4	G4mEM	EmEG5	G5mEM	EmEG6	
EdEdG4	G4EmM	EEmG5	G5EmM	EEmG6	
	G4dmdM	EmmG5	G5mEmM	EEmEG6	
	G4dEdM	EdmdG5	G5EmEM	EEmEG6	
	G4dmdEdM	EdEdG5	G5EmmM	EEmmG6	
	G4dEdmdM	EdmdEdG5	G5EEmM	EEEmG6	
		EdEdmdG5	G5mEEM	EmEEG6	
		EdmdmdG5	G5dmdM	EdmdG6	
			G5dEdM	EdEdG6	
			G5dmdEdM	EdmdEdG6	
			G5dEdmdM	EdEdmdG6	
			G5dmdEdmdM	EdEdmdEdG6	
			G5dEdmdEdM	EdEdmdEdG6	
			G5dEdmdmdM	EdEdmdmdG6	
			G5dEdEdmdM	EdEdEdmdG6	
			G5dmdEdEdM	EdmdEdEdG6	

Table A.3: Trajectory options analyzed for the G4, G5 and G6 gateways.

B

Orbit ID mapping

The tables below map the orbit ID's to the orbit parameters of the central orbit libraries for gateways G7, G8 and G9.

G7 (Earth orbit)							
Orbit ID	Inclination i [°]	Altitude [km]	LOAN Ω [°]	Orbit ID	Inclination [°]	Altitude [km]	LOAN Ω [°]
0	28.5	420	0	32	28.5	5000	120
1	28.5	420	15	33	28.5	5000	135
2	28.5	420	30	34	28.5	5000	150
3	28.5	420	45	35	28.5	5000	165
4	28.5	420	60	36	28.5	5000	180
5	28.5	420	75	37	28.5	5000	195
6	28.5	420	90	38	28.5	5000	210
7	28.5	420	105	39	28.5	5000	225
8	28.5	420	120	40	28.5	5000	240
9	28.5	420	135	41	28.5	5000	255
10	28.5	420	150	42	28.5	5000	270
11	28.5	420	165	43	28.5	5000	285
12	28.5	420	180	44	28.5	5000	300
13	28.5	420	195	45	28.5	5000	315
14	28.5	420	210	46	28.5	5000	330
15	28.5	420	225	47	28.5	5000	345
16	28.5	420	240	48	28.5	35786	0
17	28.5	420	255	49	28.5	35786	15
18	28.5	420	270	50	28.5	35786	30
19	28.5	420	285	51	28.5	35786	45
20	28.5	420	300	52	28.5	35786	60
21	28.5	420	315	53	28.5	35786	75
22	28.5	420	330	54	28.5	35786	90
23	28.5	420	345	55	28.5	35786	105
24	28.5	5000	0	56	28.5	35786	120
25	28.5	5000	15	57	28.5	35786	135
26	28.5	5000	30	58	28.5	35786	150
27	28.5	5000	45	59	28.5	35786	165
28	28.5	5000	60	60	28.5	35786	180
29	28.5	5000	75	61	28.5	35786	195
30	28.5	5000	90	62	28.5	35786	210
31	28.5	5000	105	63	28.5	35786	225

G7 (Earth orbit)							
Orbit ID	Inclination i [$^{\circ}$]	Altitude [km]	LOAN Ω [$^{\circ}$]	Orbit ID	Inclination [$^{\circ}$]	Altitude [km]	LOAN Ω [$^{\circ}$]
64	28.5	35786	240	104	5	5000	120
65	28.5	35786	255	105	5	5000	135
66	28.5	35786	270	106	5	5000	150
67	28.5	35786	285	107	5	5000	165
68	28.5	35786	300	108	5	5000	180
69	28.5	35786	315	109	5	5000	195
70	28.5	35786	330	110	5	5000	210
71	28.5	35786	345	111	5	5000	225
72	5	420	0	112	5	5000	240
73	5	420	15	113	5	5000	255
74	5	420	30	114	5	5000	270
75	5	420	45	115	5	5000	285
76	5	420	60	116	5	5000	300
77	5	420	75	117	5	5000	315
78	5	420	90	118	5	5000	330
79	5	420	105	119	5	5000	345
80	5	420	120	120	5	35786	0
81	5	420	135	121	5	35786	15
82	5	420	150	122	5	35786	30
83	5	420	165	123	5	35786	45
84	5	420	180	124	5	35786	60
85	5	420	195	125	5	35786	75
86	5	420	210	126	5	35786	90
87	5	420	225	127	5	35786	105
88	5	420	240	128	5	35786	120
89	5	420	255	129	5	35786	135
90	5	420	270	130	5	35786	150
91	5	420	285	131	5	35786	165
92	5	420	300	132	5	35786	180
93	5	420	315	133	5	35786	195
94	5	420	330	134	5	35786	210
95	5	420	345	135	5	35786	225
96	5	5000	0	136	5	35786	240
97	5	5000	15	137	5	35786	255
98	5	5000	30	138	5	35786	270
99	5	5000	45	139	5	35786	285
100	5	5000	60	140	5	35786	300
101	5	5000	75	141	5	35786	315
102	5	5000	90	142	5	35786	330
103	5	5000	105	143	5	35786	345

Table B.1: Orbit ID map of G7 orbit library (Earth orbit).

G8 (Lunar orbit)							
Orbit ID	Inclination i [$^{\circ}$]	Altitude [km]	LOAN Ω [$^{\circ}$]	Orbit ID	Inclination [$^{\circ}$]	Altitude [km]	LOAN Ω [$^{\circ}$]
0	70	150	0	48	5	150	0
1	70	150	15	49	5	150	15
2	70	150	30	50	5	150	30
3	70	150	45	51	5	150	45
4	70	150	60	52	5	150	60
5	70	150	75	53	5	150	75
6	70	150	90	54	5	150	90
7	70	150	105	55	5	150	105
8	70	150	120	56	5	150	120
9	70	150	135	57	5	150	135
10	70	150	150	58	5	150	150
11	70	150	165	59	5	150	165
12	70	150	180	60	5	150	180
13	70	150	195	61	5	150	195
14	70	150	210	62	5	150	210
15	70	150	225	63	5	150	225
16	70	150	240	64	5	150	240
17	70	150	255	65	5	150	255
18	70	150	270	66	5	150	270
19	70	150	285	67	5	150	285
20	70	150	300	68	5	150	300
21	70	150	315	69	5	150	315
22	70	150	330	70	5	150	330
23	70	150	345	71	5	150	345
24	70	300	0	72	5	300	0
25	70	300	15	73	5	300	15
26	70	300	30	74	5	300	30
27	70	300	45	75	5	300	45
28	70	300	60	76	5	300	60
29	70	300	75	77	5	300	75
30	70	300	90	78	5	300	90
31	70	300	105	79	5	300	105
32	70	300	120	80	5	300	120
33	70	300	135	81	5	300	135
34	70	300	150	82	5	300	150
35	70	300	165	83	5	300	165
36	70	300	180	84	5	300	180
37	70	300	195	85	5	300	195
38	70	300	210	86	5	300	210
39	70	300	225	87	5	300	225
40	70	300	240	88	5	300	240
41	70	300	255	89	5	300	255
42	70	300	270	90	5	300	270
43	70	300	285	91	5	300	285
44	70	300	300	92	5	300	300
45	70	300	315	93	5	300	315
46	70	300	330	94	5	300	330
47	70	300	345	95	5	300	345

Table B.2: Orbit ID map of G8 orbit library (Lunar orbit).

G9 (Mars orbit)							
Orbit ID	Inclination i [$^{\circ}$]	Altitude [km]	LOAN Ω [$^{\circ}$]	Orbit ID	Inclination [$^{\circ}$]	Altitude [km]	LOAN Ω [$^{\circ}$]
0	20	420	0	48	50	420	0
1	20	420	15	49	50	420	15
2	20	420	30	50	50	420	30
3	20	420	45	51	50	420	45
4	20	420	60	52	50	420	60
5	20	420	75	53	50	420	75
6	20	420	90	54	50	420	90
7	20	420	105	55	50	420	105
8	20	420	120	56	50	420	120
9	20	420	135	57	50	420	135
10	20	420	150	58	50	420	150
11	20	420	165	59	50	420	165
12	20	420	180	60	50	420	180
13	20	420	195	61	50	420	195
14	20	420	210	62	50	420	210
15	20	420	225	63	50	420	225
16	20	420	240	64	50	420	240
17	20	420	255	65	50	420	255
18	20	420	270	66	50	420	270
19	20	420	285	67	50	420	285
20	20	420	300	68	50	420	300
21	20	420	315	69	50	420	315
22	20	420	330	70	50	420	330
23	20	420	345	71	50	420	345
24	20	5000	0	72	50	5000	0
25	20	5000	15	73	50	5000	15
26	20	5000	30	74	50	5000	30
27	20	5000	45	75	50	5000	45
28	20	5000	60	76	50	5000	60
29	20	5000	75	77	50	5000	75
30	20	5000	90	78	50	5000	90
31	20	5000	105	79	50	5000	105
32	20	5000	120	80	50	5000	120
33	20	5000	135	81	50	5000	135
34	20	5000	150	82	50	5000	150
35	20	5000	165	83	50	5000	165
36	20	5000	180	84	50	5000	180
37	20	5000	195	85	50	5000	195
38	20	5000	210	86	50	5000	210
39	20	5000	225	87	50	5000	225
40	20	5000	240	88	50	5000	240
41	20	5000	255	89	50	5000	255
42	20	5000	270	90	50	5000	270
43	20	5000	285	91	50	5000	285
44	20	5000	300	92	50	5000	300
45	20	5000	315	93	50	5000	315
46	20	5000	330	94	50	5000	330
47	20	5000	345	95	50	5000	345

Table B.3: Orbit ID map of G9 orbit library (Mars orbit).

C

Failed attempt at multi-objective optimization

As was discussed in Section 7.2.3 of Part II and in the Chapter on the recommendation for further research (Ch. 10), an attempt was made to perform a multi-objective optimization in Analysis C-II. Unfortunately, this attempt was unsuccessful due to an insufficient convergence of the Pareto-fronts for different seed numbers. The methodology of the failed multi-objective optimization has been documented and some results were generated. Both will be presented in this Appendix chapter.

C.1. Methodology

- **Multi-objective optimization of ΔV and TOF** - Analysis C-II will perform a multi-objective optimization of two objectives: ΔV and TOF. For the multi-objective optimization to be effective, the fitness values of the objective should be the same order of magnitude. The ΔV value will therefore be expressed in metres per seconds, whilst the TOF number will be computed in hours. As a result, both numbers will have an order of magnitude of 10^4 . The optimization will produce a Pareto-front of optimal solutions.
- **Optimization algorithm: NSGA-II** - The Literature study [4] identified the NSGA-II algorithm to be the most suitable for the multi-objective applications in this research. One of the research reports that was studied was the thesis work by André Ribeiro in 2019 [50], which confirmed the selection of this algorithm. Since no research was found with a similar application for the algorithm, tuning of the algorithm settings is required. This will be done in the next bullet point.
- **Algorithm tuning** - For the single-objective optimization, the research done by Musegaas [5] proved a good starting point for the settings of the DE algorithm. For the NSGA-II algorithm, no suggested settings could be found. A tuning process, inspired by the tuning done by Ribeiro [50], was therefore performed. The following four settings were tested:
 1. Population size
 2. Seed number
 3. Cross-over rate
 4. Mutation rate

The NSGA-II algorithm was tuned by optimizing the *EdG1 x G1mEM* transfer. The results are shown in Figures C.1 and C.2 on the next page.

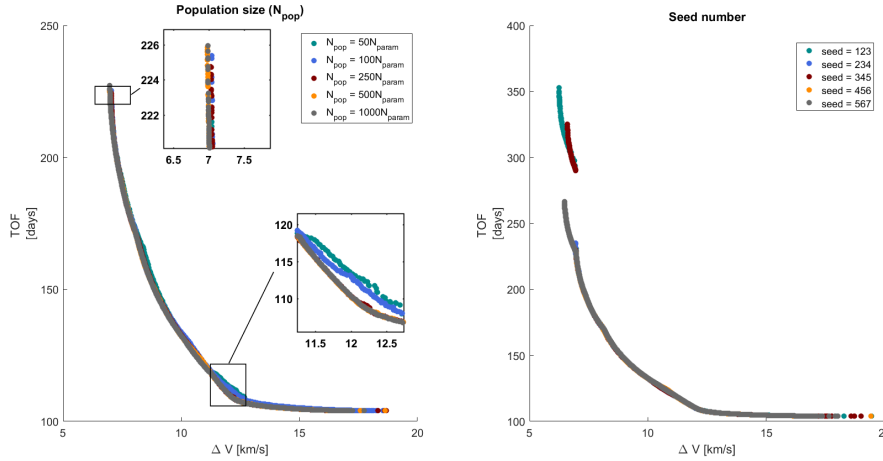


Figure C.1: Tuning the population size and seed numbers of the NSGA-II optimizer.

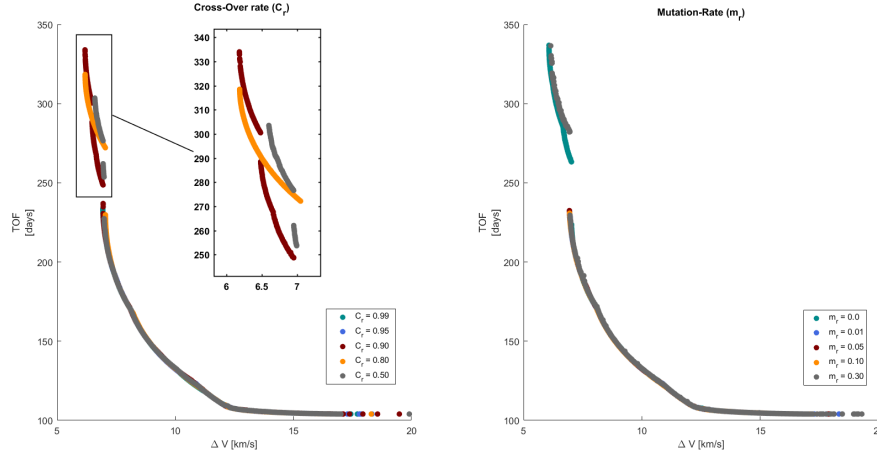


Figure C.2: Tuning the cross-over and mutation rate of the NSGA-II optimizer.

Based on these figures, the algorithm settings shown in Table C.1 were used in Analysis C-II. In order to account for the dependence on random seed value, the optimization will be performed for five different seed numbers. The resulting Pareto-fronts will be combined into a single plot.

Algorithm	C_r value	m_r value	Population size	Seeds
NSGA-II	0.90	0.0	$N_{pop} = 500 \cdot N_{param}$	123, 234, 345, 456, 567

Table C.1: Algorithm settings used for the multi-objective optimization of Analysis C-II.

- **Launch window setting** - The launch window used in Analysis C-II starts at January 1st 2033 and lasts 780 days, which is one synodic period. This launch window is the same as the one used in Analysis C-I, but without the launch window segments.
- **Box constraints on ΔV and TOF** - In order to improve the accuracy of the multi-objective optimization, the objective space of the results is boxed in. The maximum ΔV allowed is set to 10 km/s, whereas the maximum TOF is set to 350 days. Apart from improving the optimization results, these constraints also represent logical bounds on the transfer parameters. A transfer that requires a ΔV of more than 10 km/s or a has a TOF of over 350 days will never be feasible.

C.2. Results

Before deciding to abort the multi-objective analysis, some results were generated. The results of the G1 and G8 gateway are presented below. No results were generated for the G5 gateway designs. As can be seen in the figures below, the Pareto-fronts of the different seed values differ significantly. This is especially evident for the G1 gateway designs. The results for the G8 gateway design can be considered satisfactory, but are of no use without satisfactory results of the other designs.

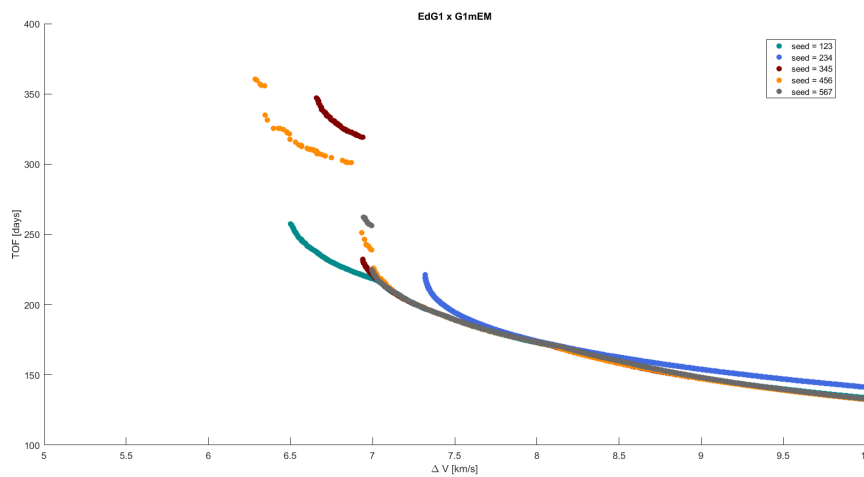


Figure C.3: Pareto-fronts for different seed values of the multi-objective optimization of the *EdG1 x G1mEM* gateway design.

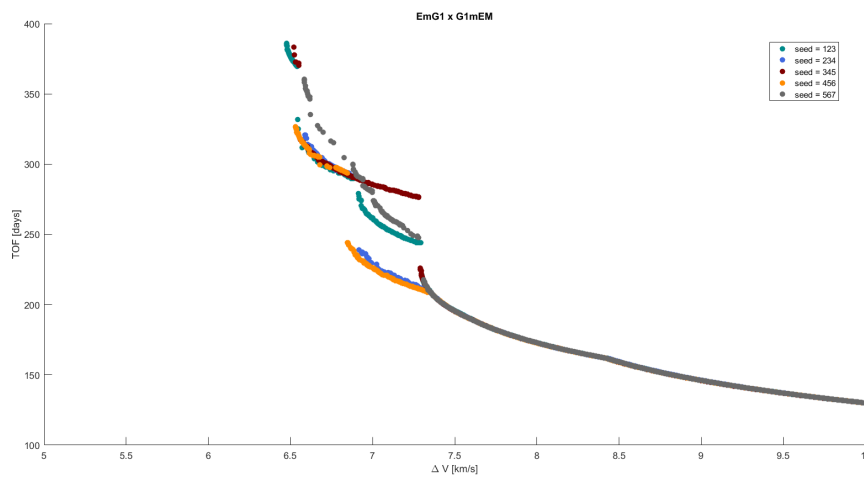


Figure C.4: Pareto-fronts for different seed values of the multi-objective optimization of the *EmG1 x G1mEM* gateway design.

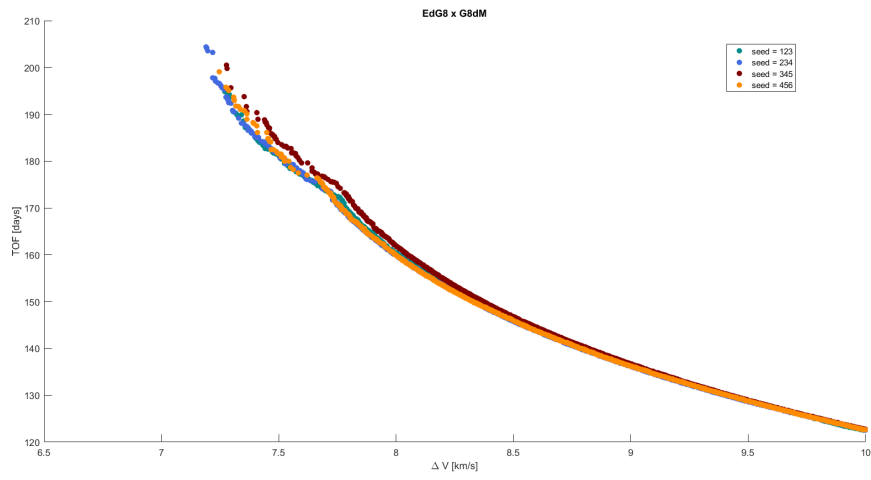


Figure C.5: Pareto-fronts for different seed values of the multi-objective optimization of the *EdG8 x G8dM* gateway design.